Ultrafast relaxation after photoexcitation of the dyes DCM and LDS-750 in solution

Dissertation

zur Erlangung des akademischen Grades

doctor rerum naturalium

(Dr. rer. nat)

im Fach Chemie

eingereicht an der

Mathematisch-Naturwissenschaftlichen Fakultät I

der Humboldt-Universität zu Berlin

von

Nina Eilers-König

geb. 13.12.1968 in Bielefeld

Präsident der Humboldt-Universität zu Berlin : Prof. Dr. Dr. h.c. H. Meyer

Dekan der Mathematisch-Naturwissenschaftlichen Fakultät : Prof. Dr. J.P. Rabe

Gutachter:
1. Prof. Dr. Nikolaus P. Ernsting
2. Prof. Dr. Thomas Elsässer (Max-Born-Institut, Berlin-Adlershof)
3. Prof. Dr. Wolfgang Rettig

Sadness flies on the wings of morning and

out of the heart of darkness comes light.

Giradoux

...On a river of crystal light,

Into a sea of dew.

Eugene Field

I see a black light

Victor Hugo (last words)

(after [Young])

Hiermit versichere ich, die vorliegende Arbeit selbständig und ohne unerlaubte Hilfe angefertigt zu haben.

Zusammenfassung

Die Relaxation der Styryl-Farbstoffe DCM und LDS-750 nach Photoanregung in flüssiger Phase wurde mittels optischer Spektroskopie, unter Anwendung der Breitband-Pump-Probe-Technik, untersucht. Zur Charakterisierung der Relaxation von DCM im elektronischen Grundzustand außerhalb des thermischen Gleichgewichts wurde außerdem die Breitband-Dump-Probe-Technik (stimuliertes Emissionspumpen) eingesetzt.

Das Donor-Akzeptor substituierte Stilbenderivat DCM zeigt im elektronisch angeregten Zustand eine im roten Spektralbereich verzögert anwachsende Emission. Sie ist zur direkt nach der Anregung beobachteten Emissionsbande bathochrom verschoben. Für ihren verzögerten Anstieg wurde eine annähernd von der Anregungsenergie und von der Lösungsmittelumgebung unabhängige Zeitkonstante von 0.23 ($\pm$ 0.04) ps gefunden. Die beobachtete Abhängigkeit des Anteils der verzögert anwachsenden Emission von der Anregungsintensität wurde auf 2-Photonen-Anregung in höhere elektronische Zustände und Schwingungsrelaxation im S_1 nach schneller innerer Konversion zurückgeführt.

Im elektronischen Grundzustand tritt nach stimuliertem Emissionspumpen Absorption rotverschoben zum stationären Absorptionsspektrum auf. Zu der zunächst beobachteten Absorptionsbande bildet sich hyposochrom verschoben eine weitere Absorptionsbande aus. Eine Zeitkonstante von 0.28 ($\pm$ 0.07) ps wurde für ihren langsamen Anstieg und den Abfall der ersten Absorptionsbande ermittelt.

Diese beiden Relaxationen gehen jeweils mit einer abgeschätzten Änderung des Dipolmomentes von maximal 2_D in S_1 und maximal 4.4 D in S_0 einher, so daß sie als Konformationsänderung mit nur geringer Ladungsverschiebung charakterisiert wurden. Die weitere spektrale Entwicklung in polarer Lösungsmittelumgebung wird sowohl im elektronischen Grundzustand wie auch im angeregten Zustand vor allem von der Solvatation bestimmt.

Für das ionische Polymethin LDS-750 wurden nach optischer Anregung solvensabhängige Kinetiken beobachtet, die sich durch Annahme dreier möglicher Konformationen im S_1 erklären lassen. In diesem Bild erfolgt die Gleichgewichtseinstellung zwischen dem durch Photoanregung erzeugten Konformer A und dem nicht fluoreszierenden Konformer B sehr schnell auf der Zeitskala der Inertialbewegung der Lösungsmittelmoleküle. Auf einer Pikosekunden-Zeitskala wird die Konformation C mit dem höchsten Dipolmoment durch die diffusive Reorientierung der Lösungsmittelmoleküle stabilisiert, so daß sie eine energetisch günstigere Lage gegenüber den anderen beiden Konformationen einnimmt. Die Pikosekunden-Relaxation von LDS-750 nach Photoanregung wurde demnach als Ladungstransfer-Reaktion gedeutet, während die schnelle Reaktion wahrscheinlich zu einem Intermediat der Isomerisierung führt.

Contents

1 Introduction

Chemical reactions in solution are of fundamental interest not only for industrial purposes, but also to achieve a deeper understanding of the processes involved in the metabolism of living organisms. Despite the complexity of such reactions, it is useful to consider only one or a few coordinates of motion as the most important ones in determining the reaction rate [Frau 85]. In this reduced approach, *interaction of the solute with the surrounding solvent molecules* may influence its reaction dynamics in two ways: by statically modifying the potential energy of the reactant and product states and/or by providing dissipation to the movement along the reaction coordinate. The second, dynamical effect is termed solvent friction and can be pictured as the action of the solvent as a heat bath, or as a viscoelastic medium hindering large-amplitude nuclear motion. A dipolar solvent may also function as a dielectric with a finite response time in adapting to changes in charge distribution connected with the reaction coordinate. Investigations of pure solvent dynamics have led to a more detailed molecular view of the relaxation mechanisms for the latter case [Flem 96].

The progress in laser technology leading to the generation of *femtosecond light pulses* has provided a means of investigating even very fast unimolecular reactions in real time. The relaxation of a chromophore after photon absorption can, for example, be followed by monitoring the fluorescence (fluorescence upconversion technique), the resonance Raman scattering, or phase coherences in the generated electronic superposition states (photon echo techniques). Another possibility to explore its relaxation dynamics is to detect the absorption and stimulated emission of the photoexcited molecule. This can conveniently be done with the pump- (supercontinuum) probe technique, combining high temporal resolution with detection over an extended spectral range [Shank 82, Bing 95]. Here, a femtosecond pulse spectrally centered within the ground state UV or visible absorption band of the molecule to be investigated is used to excite the sample electronically; the solute's transient absorption and stimulated emission is subsequently interrogated by a spectrally broad (continuum) probe pulse (Figure 1-1).

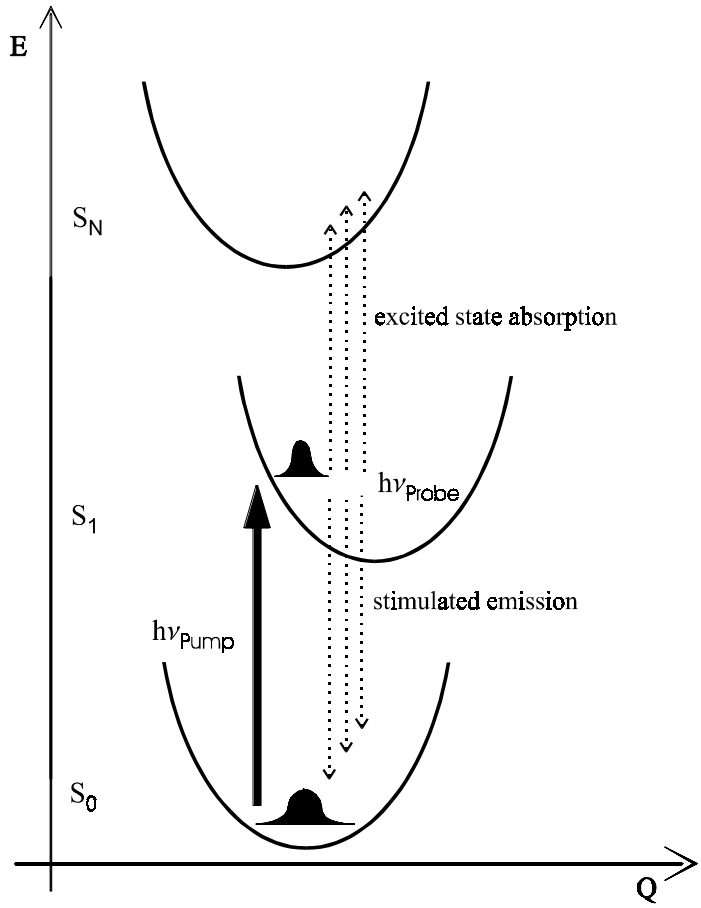

Figure 1-1 : Scheme of the pump-probe technique. Q may denote an intramolecular coordinate or the solvent configuration.

The intensity of the probe pulse is detected with and without the sample by two photodiode arrays. The temporal resolution is provided by the mechanical variation of the optical path difference between the pump and probe pulses, the instrumental response function in the time domain being determined by the temporal overlap of the intensity shape of the light pulses. The *Franck-Condon* principle states that optical electronic excitation is much faster than nuclear movement (vertical arrows in Figure 1-1 and Figure 1-2). Therefore, upon electronic excitation the nuclear intramolecular and solvent degrees of freedom maintain the equilibrium values of the electronic ground state. Their "relaxation" to the excited state equilibrium values can subsequently be followed from the solute's transient absorption and stimulated emission spectrum. Since the absorption spectrum of the solute is inhomogeneously broadened by different configurations of solvent molecules, the pump pulse selects only a sub-ensemble of the distribution of solvent configurations around the solute (spectral hole-burning). This technique has been modified to investigate not only

excited state dynamics, but also to produce information on the non-thermalized electronic ground state [Ang 89, Zhong 96, Gai 97, Kov 98]. For this purpose, a third light pulse spectrally centered in the emission band of the investigated compound is applied about 100 ps after the first pulse. It projects (dumps) a sub-ensemble of the relaxed distribution of solute molecules back into the electronic ground state. Delayed with respect to this dump or stimulated emission pumping (SEP) pulse, the absorption characteristics of the newly created ground state population are also monitored via a broad-band probe pulse (Figure 1-2). According to the Franck-Condon principle, during stimulated emission pumping the nuclear intramolecular and solvent degrees of freedom keep their excited state equilibrium positions. Again, their relaxation to the electronic ground state equilibrium values can be followed from the solute's induced ground state absorption spectrum.

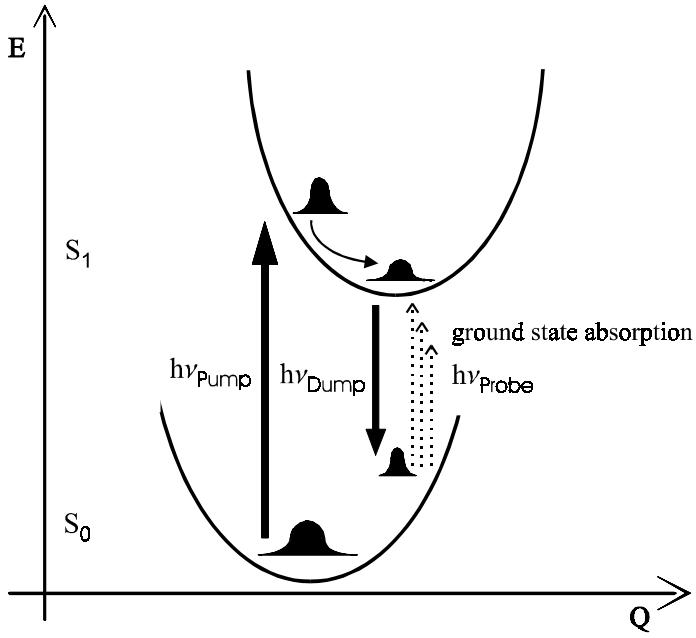

Figure 1-2: Scheme of the (pump)-dump-probe technique. Q may denote an intramolecular coordinate or the solvent configuration. The dump pulse is applied only after relaxation in S_1.

In the following, the investigated compounds and the purpose of their examination will be presented.

The donor-acceptor substituted stilbene derivative 2-(2-{(*E*)-2-[4-(dimethylamino)phenyl]-1-ethenyl}-4*H*-4-pyraniliden)malononitrile (CAS n° 51325-91-8) or DCM (Figure 1-3) was reported to be subject to an intramolecular charge reorganization after photoexcitation.

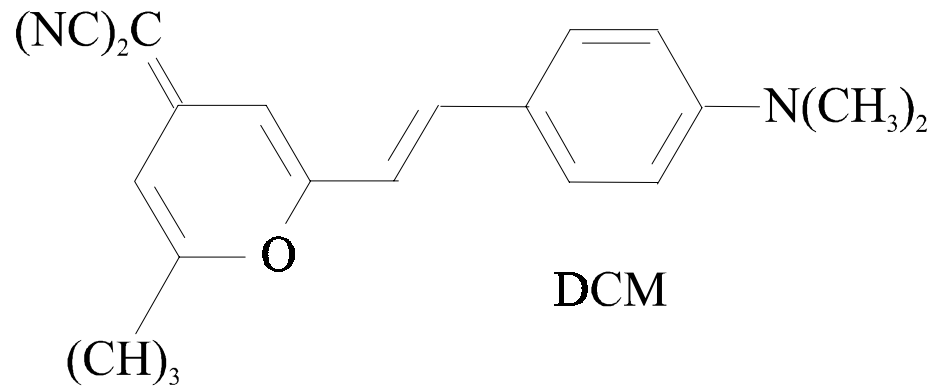

Figure 1-3: Structure of DCM.

This reaction was claimed to proceed in a sub 100 fs regime in acetonitrile, methanol, ethylene glycol and ethyl acetate [vdMeul 96], within 140 fs in methanol [Kov 96], within 300 fs in methanol and ethylene glycol [East 93] and on a solvent-dependent timescale of several picoseconds [Mart 95 and 97].

Van der Meulen et al. [vdMeul 96] found a rise of the spectrally integrated fluorescence intensity within 500 fs and proposed conversion from an initially excited state to a dark intermediate state, and subsequently to an emissive charge transfer state. A red shift and a narrowing in width of the fluorescence band were modelled and treated as originating from solvation dynamics [vdMeul 96, 98]. Easter and Baronavski considered the intensity changes in the first 300 fs to be due to intramolecular vibrational energy distribution and a charge transfer reaction, and the shift in the next 10 ps as being due to solvation dynamics [East 93]. Gustavsson et al. interpreted the emission bandshape changes as indicating vibrational energy transfer to the solvent and solvation, since they did not observe any change in the integrated intensity [Gust 95]. Kovalenko et al. [Kov 96] showed that the spectral dynamics of DCM change with excitation intensity; the occurrence of an isosbestic point in the time-dependent pump-probe spectra over the first few hundred femtoseconds was assigned to a charge transfer reaction, such as Martin et al. concluded for the picosecond timescale [Mart 95, 97]. The resulting picture of DCM relaxation after photoexcitation is obviously contradictory.

Another styryl dye, the ionic *N*-{4-[(1*E*,3*E*)-4-(3-ethylnaphto[2,1-*d*][1,3]thiazol-3-ium-2-yl)-1,3-butadienyl]phenyl}-*N*-methylmethanamine perchlorate (CAS n° 89872-07-1) or LDS 750 (Figure 1-4), was at first considered an ideal chromophore for the investigation of solvent relaxation after an instanteneous dipole moment increase upon photon absorption [Cast 87, Ros 91, Cho 92].

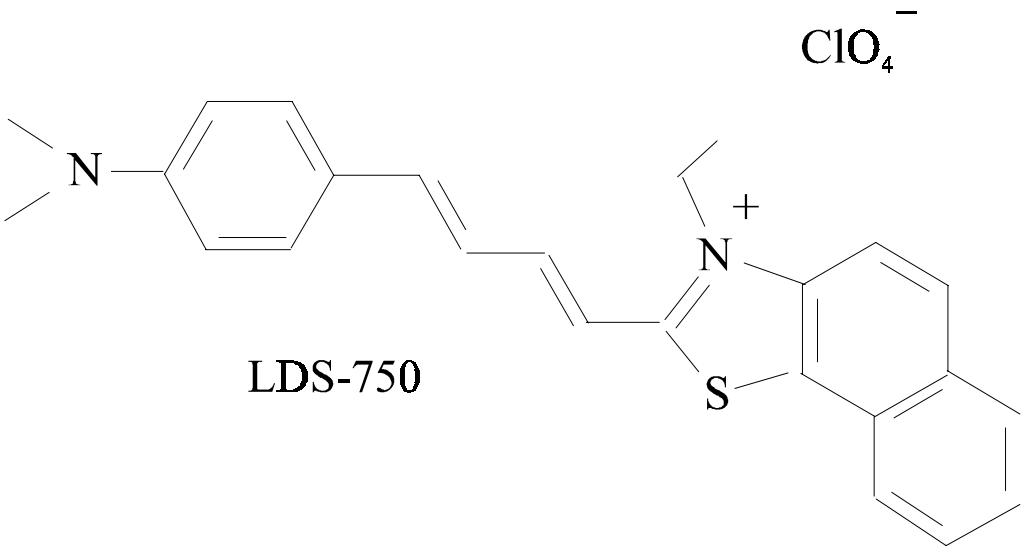

LDS-750

Figure 1-4 : Structure of LDS-750.

More recent experiments have cast doubt on this ideal behaviour and pointed to an intramolecular relaxation in the electronically excited state [Blanch 91, Gold 94, Kov 97, Bard 97, Smith 99].

Blanchard observed excitation wavelength dependent changes in the stimulated emission band of LDS 750 in a series of butanols [Blanch 91]. He concluded that several conformers existed, some among which were exclusively excited by choice of the excitation wavelength, and that subsequent equilibration by isomerization took about 50 ps. Similar, but faster effects were found by Kovalenko et al. in acetonitrile and chloroform, with respective time coefficients of 200 fs and 600 fs [Kov 97]. From the influence of the excitation intensity, feeding from higher electronically excited states was deduced. Broadening of the fluorescence band in liquid aniline, mostly within the first two picoseconds, was accounted for by a conformational relaxation [Smith 99], while the peak shift towards lower wavelengths was considered to be due to solvation dynamics alone. The temperature independence of the ultrafast loss of electronic coherence in photon echo measurements of LDS 750 in polymer films was interpreted by Bardeen et al. as being due

to either a fast intramolecular relaxation (isomerization), strong coupling to solvent fluctuations because of a very large change in charge distribution upon excitation, or coupling of a multitude of intramolecular vibrational frequencies to the optical transition [Bard 97].

The intention of this work is to clarify whether the spectral changes of DCM and LDS 750 emission after photoexcitation are due to intramolecular relaxation or to solvent relaxation, whether a charge transfer reaction takes place and how such an intramolecular process is influenced by solvent dynamics. For this purpose, pump-probe measurements were carried out on both compounds in solvents of various polarities, for different excitation wavelengths and intensities. To gain insight into the ground state relaxation dynamics and to explore a possible back-electron transfer reaction, stimulated emission pumping or dump-probe experiments were also performed for DCM in various dipolar solvents.

2 Background

Overview :

The investigations of stilbene-like donor-acceptor molecules in the literature are numerous, and the interpretation of the results is far from being unanimous. This chapter tries to provide a summary of the spectroscopic characteristics of DCM and some structurally related molecules. The relevant pathways for their relaxation after photoexcitation are outlined. On the subpicosecond timescale, electron transfer, solvent reorientation and vibrational deactivation are the mechanisms prevailing in the discussion. Several models of these processes and their applications are described.

2.1 Donor-acceptor substituted stilbenes

2.1.1 Relaxation pathways for stilbenes after photoexcitation

1,2-diarylethylenes (stilbenes) have been found to be subject to at least seven different types of competing photoreactions (see the excellent review given by Görner and Kuhn [Görn 95]).

The most investigated path is probably twisting about the central C=C double bond, or *trans-cis* photoisomerization. Owing to the larger dihedral angle of *cis*-stilbene, the energy of the *cis* ground state is higher by 10-20 kJ/mol [Görn 95] than that of *trans*-stilbene. Schematic potential energy curves as a function of the twist about the double bond are displayed in Figure 2.1-1. The planar *trans* configuration is denoted with "t", the 180° twisted *cis* configuration with "c", and "p" marks a hypothetical (perpendicular or phantom) state at a 90° twist of the ethylene bond. The barrier for *trans-cis* isomerization is much lower for the photoinduced reaction in the first singlet or triplet excited state. In the electronic ground state, the barrier for *trans-cis* as well as for *cis-trans* isomerization was found to be reduced upon 4-substitution [Görn 95]. The lowest energy "A" band of the

UV/visible absorption spectrum of stilbene has been assigned to a π, π^* -transition [Bern 73]. After excitation into this band, the *trans* isomer exhibits fluorescence in the range of 340 to 400 nm. The *cis*-stilbene emission is very weak with $\phi_F \approx 10^{-4}$ [Salt 92, 93].

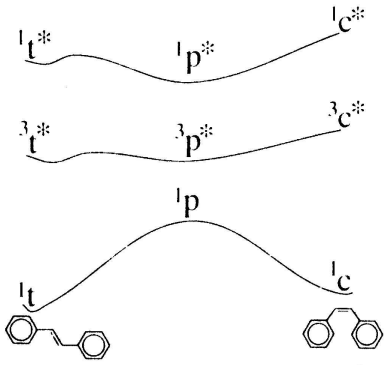

Figure 2.1-1: Trans-cis isomerization scheme of stilbene.

Intersystem crossing (ISC) is a relaxation mechanism that may also be involved in the isomerization reaction. The intersystem crossing quantum yield ϕ_{ISC} is of the order of 10^{-3} for stilbene and cyanostilbenes; Meyer et al. give an upper limit of $3 \cdot 10^{-3}$ for the ϕ_{ISC} of DCM in methanol [Mey 90]. It is strongly enhanced upon substitution by a 4-nitro or 4-bromo group, and for 4-dimethylamino-4'-nitro stilbene has been determined to be 0.4 in cyclohexane and 0.04 in more polar or polarizable solvents [Görn 87]. Correspondingly, for excited nitrostilbenes the *trans-cis* and a fraction of the *cis-trans* isomerization evolve along an intermediate in the first excited triplet state (see Figure 2.1-1), while for stilbene, fluoro-, chloro- and cyanostilbenes the singlet mechanism dominates.

In solution at room temperature, *cis*-stilbene may also deactivate via photocyclization to dihydrophenanthrene (DHP). In the absence of oxygen, DHP relaxes thermally back to *cis*-stilbene by ring-opening, whereas phenanthrene is formed in the presence of oxygen. Higher vibrational levels of excited *cis*-stilbene are involved in the cyclization process [Güst 68]. The quantum yield of photocyclization is given as 0.22 for stilbene in n-pentane [Görn 95], and 0.046 in cyclohexane [Jung 68]. It is greatly reduced for nitrostilbenes (<0.001) and estimated to >0.003 [Jung 68] for cyanostilbenes.

Photoreduction by hydrogen-donating solvents is an important relaxation pathway for

diazophenyl-ethylenes (DPEs). It probably proceeds from a spectroscopically dark excited singlet n, π^*-state which is lower in energy than the fluorescent π, π^*-state. The products of this reaction are the radical H-DPE$|$ or its protonated form H_2-DPE$|^+$ [Görn 95].

Radical anions or cations of stilbene and its substituted derivatives are produced by photoinduced intermolecular electron transfer in the presence of electron-donating or accepting substances, such as amines [Hub 84] or cyanoanthracenes [Görn 95].

On a timescale of up to a few picoseconds, photoinduced intramolecular electron or charge transfer is the primary reaction channel discussed for donor-acceptor substituted stilbenes and will be further discussed in 2.1.3. and 2.2.. It is accompanied or followed by dielectric relaxation of the surrounding solvent. In the case of vibronic excitation, intramolecular vibrational energy redistribution and vibrational energy transfer to the solvent molecules must be taken into consideration.

Internal conversion of the excited *trans*-form directly to its ground state has been assumed to explain the reduction in *trans*-*cis* quantum yield with solvent polarity for nitrostilbenes [Görn 78, Gruen 89].

2.1.2 Photophysical properties of some donor-acceptor substituted stilbenes

4,4'-Donor-acceptor substituted stilbenes are known to exhibit a large, polarity dependent Stokes shift between the main UV/visible absorption and fluorescence bands. Exemplary absorption and emission maxima are presented in Table 2.1.1 for 4-{(*E*)-2-[4-(dimethylamino)phenyl]-1-ethenyl}benzonitrile (*trans*-DCS), 4-[(*E*)-2-(2,3,6,7-tetrahydro-1*H*,5*H*-pyrido[3,2,1-ij]quinolin-9-yl)-1-ethenyl]benzonitrile (*trans*-JCS), the stilbene-derivative *trans*-DCM and *N*,*N*-dimethyl-*N*-{4-[(*E*)-2-(4-nitrophenyl)-1-ethenyl]aniline (*trans*-DANS) (Figure 2.1-2). Since only the *trans* conformers are considered here, the prefix will be omitted in the following.

The Stokes shift for nonpolar solvents is largest for DCM, whereas the solvent polarity dependence of the emission maximum is strongest for DANS. The red shift of the emission maximum in dipolar solvents is ascribed to *charge transfer interactions* between the donor and acceptor groups in the excited state, and stabilization of the polar compounds by solute-solvent interaction. The differences in polarity dependence of the Stokes shift can be related to a stronger donor character of the julolidinamine group compared to the dimethylamino

group, and a stronger acceptor character of the nitro group compared to the cyano group [Cheng 91].

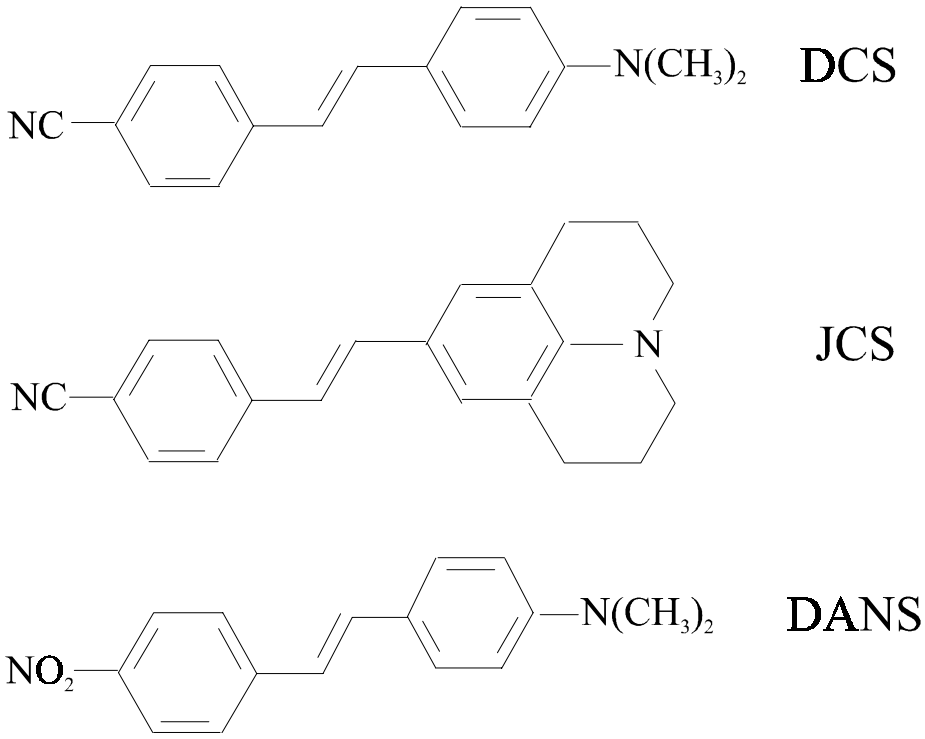

Figure 2.1-2: Structure of 4,4'-donor-acceptor substituted stilbenes.

Table 2.1.1: Maxima of the absorption and emission spectra of donor-acceptor substituted stilbenes. Structured spectra are denoted by asterisks.

	λ_{Abs} / nm		λ_{Flu} / nm	
Solute / Solvent	Alkanes	Acetonitrile	Alkanes	Acetonitrile
DCS	375*	390	430	540
JCS	399	407	461	559
DCM	455*	464	582*	637
DANS	417	435	470	>850

While the emission spectrum of DCM in nonpolar solvents is structured and broad (Figure 2.1-3), in dipolar environment it narrows, and the Stokes shift increases. This was interpreted as being due to a photoinduced intramolecular charge transfer reaction in polar solvents [Kov 96].

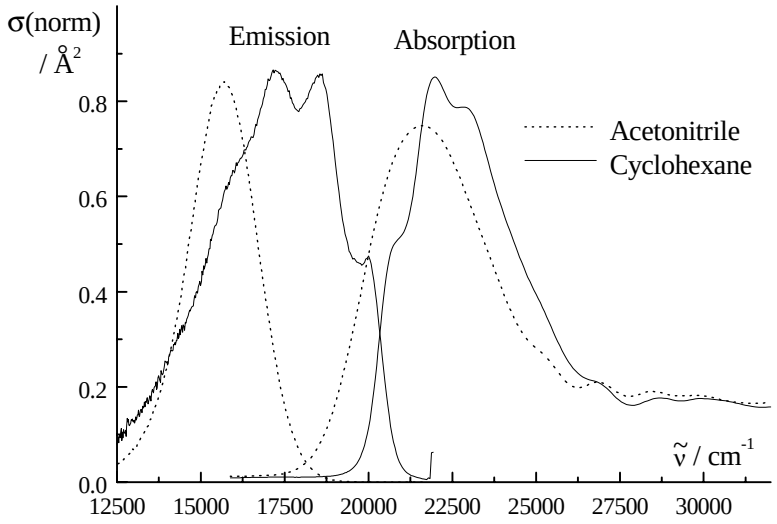

Figure 2.1-3: Stationary spectra of DCM. The fluorescence spectra have been converted to emission cross section.

The dipole moments in the ground and excited state as published for DCS, DCM and DANS are summed up in Table 2.1.2. In accordance with the order of the Stokes shift in highly polar solvents, DANS is presumed to undergo the largest change in dipole moment upon excitation, followed by DCM and DCS. Quantum chemical calculations of isolated molecules obviously tend to underestimate the excited state dipole moment in solution, possibly because of their neglect of the molecular environment. The solvent dependence of the excited state dipole moment has been demonstrated for DANS by [Bau 92] with electrooptical investigations. They obtained 25.4 ± 0.1 D in cyclohexane, 27.0 ± 0.2 D in fluorobenzene and 27.8 ± 0.3 D in dioxane for the dipole moment of DANS in its first excited singlet state.

Table 2.1.2: Dipole moments of donor-acceptor substituted stilbenes. Franck-Condon excited states are indicated by brackets. Values from electrooptical measurements are denoted by asterisks; values from semiempirical calculations are marked by double asterisks. All other dipole moments are derived from the Stokes shift between absorption and fluorescence/stimulated emission bands.

	DCS				**DCM**			**DANS**			
μ (S_0) / D	7*				6.1*	8.5**	10.2	9.47* (10.0)*	7.7*	10**	
μ (S_1) / D	21*	22.3	(20)	(13)		12.4**		31.8* (32.3)*	25.4*	20-22**	
μ (S_2) / D					26.3	14.3**					
Reference	[1]	[2]	[3]	[4]	[5]	[6]	[7]	[8]	[9]	[10]	

[1] [Lip 63], [2] [Kaws 77], [3] [Eil 96], [4] [Il'ich 96], [5] [Mey 87], [6] [Marg 92], [7] [Moy 96], [8] [Bau 77], [9] [Bau 92], [10] [Farz 99]

Quantum yields of fluorescence and of *trans-cis* photoisomerization and fluorescence lifetimes for 25°C are compared in Table 2.1.3 for the compounds listed above in different solvents. The fluorescence quantum yield increases with solvent polarity for all compounds except for DANS. DANS shows a maximum of ϕ_{Flu} in benzene; in acetonitrile its emission is strongly reduced. Internal conversion in polar solvents was held responsible for the latter effect, since the quantum yield for intersystem crossing in polar solvents is also very low [Görn 78, Gruen 89].

While for the other compounds $\phi_{trans \rightarrow cis}$ decreases with solvent polarity, the isomerization quantum yield was found to be nearly constant for DCS. The low double-bond twisting efficiency for DCM in polar solvents was explained by the energetic stabilization of the emitting (charge transfer) state relative to the 90° twisted configuration that should act as intermediate in the isomerization reaction [Mey 90, Rett 89].

Given the relation $\phi_{Flu} = k^0_{Flu} / k_{Flu} = (\tau^0_{Flu} / \tau_{Flu})^{-1}$, where k^0_{Flu} is the radiative decay rate, τ^0_{Flu} is the natural fluorescence lifetime and k_{Flu} is the total depopulation rate of the fluorescent state, τ_{Flu} should be directly proportional to ϕ_{Flu}. For JCS and DCM, the

fluorescence quantum yield changes by a larger amount than the emission lifetime, indicating a solvent-dependence of the transition dipole moment. Such a solvent-dependence may result from a solvent-dependent variation of the electronic structure of the molecule after photoexcitation. It can also be caused by the influence of the solute-induced polarization of the solvent molecules (reaction field) on the transition moment of the solute [Lip 66, 68].

(next page:)

Table 2.1.3: Quantum yields of fluorescence and trans cis-isomerization and fluorescence decay times for donor-acceptor substituted stilbenes in different solvents.

a) toluene b) MTHF c) see 4.2.1. d) relative $\phi_{trans\text{-}cis}$ with respect to that in chloroform
e) 20°C f) slower component of biexponential fit from [Mey 89]
g) from decay of stimulated emission and excited state absorption
[1] [Gruen 83], [2] [Recht 96], [3] [Les 84], [4] [Gruen 89], [5] [Mey 90], [6] [Mial 93], [7] [Abr 97], [8][Il'ich 96], [9] [Rett 89], [10] [Bau 77], [11] [Shor 58], [12] [Kov 99b].

Solvent	DCS	JCS	DCM	DANS
		ϕ (Flu)		
Cyclohexane	0.03	0.04	0.007 c)	0.33
Benzene	0.03 a)	0.12		0.53
THF	0.06 b)		0.49	0.11
Chloroform	0.05		0.35	0.018
Ethanol	0.07			
Methanol			0.43	
Acetonitrile	0.13	0.41	0.44	<0.002
DMSO		0.47	0.8	
Reference	[1]	[2]	[3]	[4]
		ϕ (*trans-cis*)		
Cyclohexane	0.45			0.28
Benzene	0.45 a)			0.02
THF	0.4 b)		0.5 d)	0.004 b)
Chloroform			1 d) 0.28	
Ethanol	0.5			<0.001
Methanol			0.07 d)	
Acetonitrile	0.4		0.05 d) 0.022	
DMSO			0.04 d)	
Reference	[1]		[5] [6]	[4]
		τ (Flu) / ns		
Cyclohexane	0.085	0.46		1.05
Benzene		0.61		3.3
THF			1.24	
Chloroform			1.38 0.74 3.3 e)	0.08
Ethanol			0.67 e)	
Methanol			1.36 1.31	
Acetonitrile	0.51	1.36	1.93 1.91	
DMSO		1.82	2.24 2.18	
Reference	[7] [8]	[2]	[5] [3] [9]	[10] [11] [12]

2.1.3 The TICT concept

The photoreaction of p-dimethyl-aminobenzonitrile (DMABN) in solution led to the concept of *twisted intramolecular charge transfer* (TICT) [Grab 79]. Within this model, the excited state photoreaction of DMABN should involve an (approximately) 90° torsion of the dimethylamino group, producing a polar, charge-separated state. The internal twist is presumed to decouple the donor and acceptor centers in the molecule electronically. The concept was transferred to other molecules with substituents of electron-donating or -accepting character linked by flexible chemical bonds [Lipp 87, Reviews by Rett 86, 92], so-called "TICT-compounds", among which belong DCM and substituted stilbenes such as DCS or JCS. As the fluorescence exhibited in the charge transfer state is red shifted with increasing solvent polarity and does not appear when the molecule is isolated, it is termed 'anomalous' fluorescence; if emission from the primarily excited precursor state can be recorded as well, one speaks of "dual emission". The latter has been reported for DCS [Eil 96], but the primarily emissive state was found already to have strong charge transfer character. Temperature and solvent dependent investigations of fluorescence lifetimes and fluorescence quantum yields let the following picture emerge for donor-acceptor substituted stilbenes. Competition of the charge transfer relaxation channel with the *trans-cis*-isomerization channel leads to an increased quantum yield and a longer emission lifetime in polar solvents for temperatures above the activation energy / k_B of the TICT reaction [Rett 89, 92]. Gruen and Görner excluded the involvement of amino group rotation in the charge transfer reaction of DCS by investigating bridged compounds [Gruen 83, 89]. Differences in the optical spectra for high concentrations (> 1 mM) of DCS and high excitation energies compared to dilute solutions and moderate excitation conditions were reported by Gilabert et al. and Lapouyade et al. [Gil 91, Lap 92]. They were explained as being due to a complex formed by two photoexcited twisted substituted stilbenes, termed "*bicimer*". The risetimes of JCS transients at 616 nm after UV excitation were found to increase with pressure up to 500 MPa, while for a compound similar to DCS, but with bridged single bounds connecting to the ethylene group, the risetimes were constant above 290 MPa [Rett 94]. This was interpreted as the effect of large-amplitude motion related to bicimer formation, which should not be present in the bridged compound. For DCS consequently a rotation of the dimethyl-anilino group around its single bond to the ethylene moiety was proposed to be involved in the bicimer as well as in the TICT mechanism [Abr 97].

The nature or existence of the charge transfer state of the TICT compounds has been the subject of controversial discussion. Alternative reaction mechanisms have been proposed for DMABN, such as coupling of the two lowest excited singlet states by the pyramidalization / planarization motion of the amino group with a coupling strength depending on solvent polarity (solvent induced pseudo Jahn-Teller coupling) [Zach 93]. Another motion, the bending of the cyano group connected with rehybridization of the carbon atom of the cyano group was also held responsible for the charge transfer reaction [Sob 96]. Gedeck and Schneider [Ged 97] calculated the free energy surfaces of DMABN as a function of the torsion of the dimethylamino group and the pyramidalization angle of the amino group. In their semiempirical treatment, the geometry of the solute was optimized in the electronic ground state and the excited state energy was obtained by configuration interaction including solvent polarization. Independent of the torsional angle, the minimum energy in the excited state was always found for planarization of the amino group. In polar solvents, a 90°-twisted conformation represented the global minimum in the lowest electronic excited state. In confirmation of the TICT thesis, the twisted conformation was lower by 6 kJ/mol in energy than the 0° torsional conformation in acetonitrile.
For DCM, Marguet et al. calculated a large increase in dipole moment (from 14.3 to 22.5 D) upon a 90° twist of the dimethylamino group in S_2 [Marg 92]. In contrast to the idea of a competition between the dimethylamino group rotation and the rotation around the central double bond, these processes were characterized as being independent of each other. No dipole moment increase was observed for other single bond rotations.

2.2 Electron transfer

Electron transfer is not restricted to molecules with flexibly bound subgroups of electron-donating or -accepting properties such as in 2.1.3., and it has been extensively treated in experiment and theory over the last decades (for reviews, see [Mar 89, Heit 93, Yosh 95]). One differentiates between "*outer-sphere*" *intramolecular* electron transfer, which designates a charge separation between a donor and acceptor site on one molecule separated by a rigid structure, *intramolecular* electron transfer *involving bond rotation* and *intermolecular* electron transfer, for example between solute and solvent molecules or weakly bound complexes.

According to the coupling strength of the reactant and product free energy surfaces, they are characterized as diabatic or adiabatic (Figure 2.2-1). The idea of the diabatic description is that the total Hamiltonian H of the system (solute and solvent) can be partitioned into a zeroth-order part H_0 of the isolated molecule and a weak perturbation V due to the solvent. The reactant or product states are eigenfunctions of H_0, with the electron localized at either the donor or the acceptor site. Movement on either free energy surface does not change the electronic state; electron transfer is induced by the perturbation V coupling reactant states φ_R and product states φ_P. Depending on the strength of that coupling given by the matrix element $V_{el} = <\varphi_P|V|\varphi_R>$, the perturbation might not be treated as weak (for $V_{el} >> k_BT$). The electronic states of the system are then eigenfunctions of the total Hamiltonian H, not of H_0, and the reaction proceeds on the adiabatic free energy surfaces from reactant to product configuration.

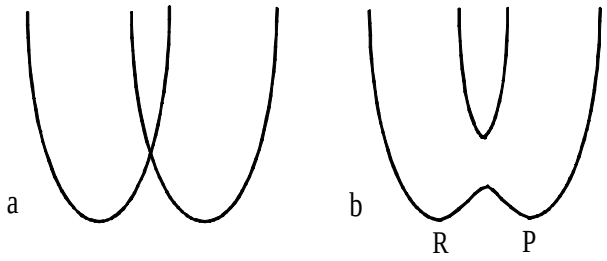

Figure 2.2-1 : Diabatic (a) and adiabatic (b) reactant and product free energy surfaces.

It is customary to distinguish *adiabatic* and *non-adiabatic electron transfer* in solution. For a small energy uncertainity of the system compared to the splitting $2V_{el}$ of the adiabatic potential surfaces, the reaction proceeds only on the lower surface and is termed adiabatic. This is expressed by the Landau-Zener *adiabaticity parameter* γ_{LZ} [Frau 85]:

$$\gamma_{LZ} = \frac{l_{LZ} \cdot 2V_{el}}{\hbar v}, \qquad (2.1)$$

where l_{LZ} is the Landau-Zener length $l_{LZ} = 2\,V_{el} / \Delta F$ and ΔF is the difference of the slopes of the reactant and product potential surfaces at the crossing point. v is the velocity with which the system moves through the Landau-Zener region around the crossing point. Thus the more steeply the potential surfaces intersect, the smaller will be the Landau-Zener length and the adiabaticity parameter.

The reaction coordinate q could be an intramolecular degree of freedom or geometrical parameter, such as in the TICT treatment, but it has been shown [Zus 80, Cal 83, Per 95] that a good choice is to define q as the vertical internal energy gap ΔU between reactant and product state, depending on the solute and solvent nuclear configuration X :

$$q(X) := \Delta U = U_P(X) - U_R(X). \qquad (2.2)$$

For outer-sphere intramolecular electron transfer, X denotes only the solvent molecules' coordinates. Thus a transformation from nuclear coordinates, some of which might lead to the same value for q, to the energy scale relevant for the reaction can be performed.

In the non-adiabatic case, the rate coefficient of electron transfer k_{NA} can be written as [Marc 85]:

$$k_{NA} = \frac{2\pi}{\hbar} \frac{V_{el}^2}{\sqrt{4\pi \lambda_S k_B T}} \exp\left(-\frac{\Delta G^*}{k_B T}\right), \qquad (2.3)$$

Here λ_S is the solvent reorganization energy, which is the free energy difference of the product and reactant states for a solvent configuration corresponding to the minimum of the product state.

Equation 2.3 presumes the validity of the transition state theory, and thereby the validity of the following assumptions:

- the reactant is kept in quasi-equilibrium with the transition state
- the system moves uniformly through the transition state region
- after crossing the transition state region, excess energy is disposed rapidly into the solvent heat bath, precluding a back reaction.

Under the assumption of linear response of the dielectric interaction between solute and solvent, the activation energy ΔG^* can be expressed as :

$$\Delta G^* = \frac{(\lambda_S + \Delta G_0)^2}{4\lambda_S}, \qquad (2.4)$$

ΔG_0 being the free energy difference between reactant and product states.

The "energy-gap" dependence of the reaction rate for electron transfer can be divided into three regions:

- $-\Delta G_0 < \lambda_S$, the "normal" regime, where the reaction rate increases with $-\Delta G_0$.
- $-\Delta G_0 = \lambda_S$, the fastest case, since no activation barrier is present.
- $-\Delta G_0 > \lambda_S$, the "inverted" regime, where the reaction rate decreases with $-\Delta G_0$.

[Marc 85]

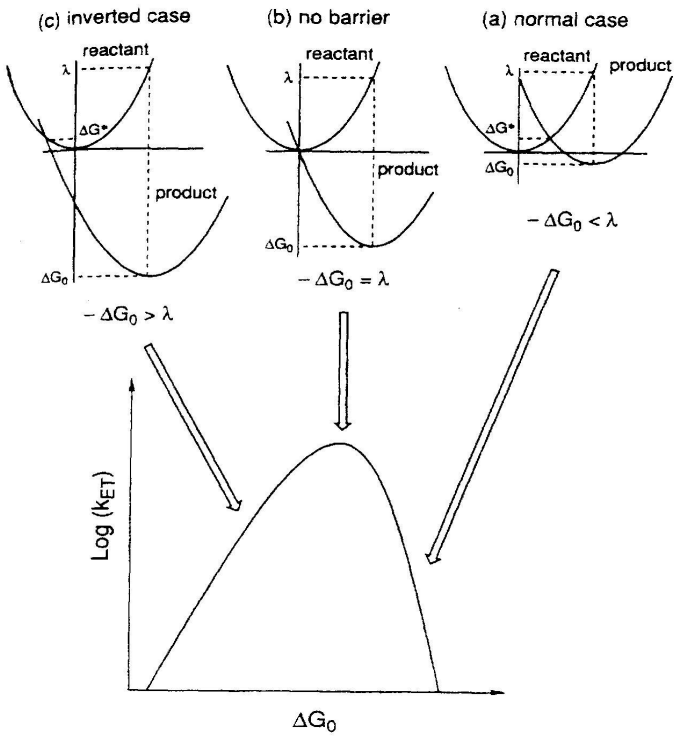

Figure 2.2-2 : Energy-gap dependence of the electron transfer rate coefficient and its relation to the relative position of the free energy surfaces of reactant and product, from [Yosh 95].

The inclusion of a high-frequency intramolecular vibrational quantum mode ($h\nu >> k_BT$) into the description enlarges the number of available reaction channels, provided good vibrational overlap exists for the reactant vibrational ground state and some vibrationally excited product states [Marc 85]. As this is predominantly the case for the inverted region, the rate coefficient for the inverted regime is slightly higher than for the normal regime, leading to the asymmetric bell-shape dependence of Figure 2.2-2.

The rate coefficient k_{NA} is the sum over all of the individual rate coefficients for different vibronic channels:

$$k_{NA} = \sum_m k_{NA}^{0\rightarrow m} \qquad (2.5)$$

$k_{NA}^{0\rightarrow m}$ is the rate coefficient for the transition from the vibrational ground state of the reactant to the m-th vibrational level of the product. It is determined by inserting the quantized free energy difference ΔG_0 for this transition, $\Delta G_0^{0\rightarrow m} = \Delta G_0 + m\hbar\omega$, into equation 2.4 and including the Franck-Condon overlap of the vibronic states in the electronic matrix element V_{el}. The intramolecular vibrational reorganization energy for the high-freqency mode is termed $\lambda_{hf,\,vib}$.

In the theory of electron transfer presented so far, it has been presumed that during electron transfer the solvent polarization is always in equilibrium. As the polarization relaxation can be as slow as picoseconds, this assumption is not always justified. Several authors tried to incorporate finite polarization response into their treatment [Zus 80, Cal 83, Rips 87]. In the limit of strong (adiabatic) coupling the solvent relaxation may even determine the electron transfer rate. Rips and Jortner [Rips 87] gave the following result for an adiabatic, solvent controlled electron transfer transition between two states coupled to a dielectric continuum:

$$k_A = \frac{1}{\tau_L}\sqrt{\frac{\lambda_S}{16\pi\, k_BT}}\exp\left(-\frac{\Delta G^*}{k_BT}\right) \qquad (2.6)$$

τ_L is the longitudinal dielectric relaxation time of the solvent (see 2.3). As usually $\lambda_S < 16\pi\, k_BT$ [Yosh 95], this imposes a limit of τ_L^{-1} on the reaction rate coefficient.

The transition to the non-adiabatic case is smooth and governed by the equation:

$$k_{ET} = k_{NA}/(1+\kappa), \qquad (2.7)$$

where κ, also termed *adiabaticity parameter*, is now given by:

$$\kappa = \frac{4\pi V_{el}^2 \tau_L}{\hbar \lambda_S}. \qquad (2.8)$$

It is obvious that the adiabaticity of the reaction depends not only on the electronic coupling element, but also on the solvent reorganization energy and the time scale of solvent relaxation. In the strongly adiabatic case ($\kappa >> 1$), the reaction dynamics reduce to diffusion over the lower adiabatic potential surface, corresponding to a Kramers-type problem [Kram 40]. This led to a stochastic treatment of electron transfer [Zus 80, Cal 83, Hynes 86], where the rate for the adiabatic case was found proportional to τ_L^{-1} as well.

It should be noted that the adiabaticity parameter κ can be expressed as a function of the Landau-Zener length l_{LZ} and the mean free path l_f, demonstrating the relation of κ to the Landau-Zener adiabaticity parameter γ_{LZ} (eq. 2.1). The mean free path is defined by $l_f = \left\langle |v(0)|^2 \right\rangle^{1/2} t_0$. Here t_0 is the average time interval between collisions, and $\left\langle |v(0)|^2 \right\rangle^{1/2}$ is the velocity of the reaction coordinate. κ is related to l_{LZ} and l_f by:

$$\kappa = 4\pi / (\eta \omega_{rot} \tau_L) \, (l_{LZ} / l_f)^2 \quad \text{[Rips 87]}, \qquad (2.9)$$

where ω_{rot} is the rotation frequency of the solvent molecules and η is a numerical factor of the order of unity.

The rate coefficient for electron transfer was limited to τ_L^{-1} by equation 2.6. Sumi, Nadler and Marcus developed a model that explained faster rate coefficients as well as nonexponential reaction dynamics [Sum 86, Nad 87]. They partitioned the reaction coordinate into a solvent coordinate X describing diffusive solvent relaxation and an intramolecular coordinate q, characterized by low-frequency vibrational motion, along which the charge reorganization takes place (Figure 2.2-3).

Both dimensionless coordinates are treated classically and the total free energy of the system is given by:

$G_R(q,X) = \frac{1}{2} a q^2 + \frac{1}{2} X^2$ for the reactant, and by

$$G_P(q,X) = \frac{1}{2} a (q - q_0)^2 + \frac{1}{2} (X - X_0)^2 + \Delta G_0 \text{ for the product.} \qquad (2.10)$$

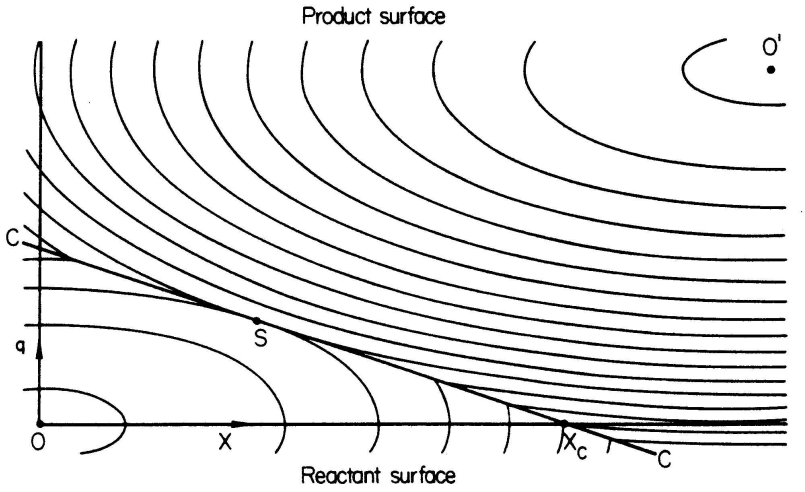

Figure 2.2-3 : Two-dimensional free energy surfaces in electron transfer reaction, from [Sum 86].

The equilibrium positions for both coordinates are zero for the reactant and q_0 and X_0 for the product. ΔG_0 is the standard free energy of the reaction. The reorganization energies are given by $\lambda_S = 1/2\ X_0^2$ and $\lambda_{vib} = 1/2\ aq_0^2$, respectively. The transition state is defined as the intersection of the reactant and product free energy surface (curve C in Figure 2.2-3). The relaxation time for vibrational motion is assumed to be substantially faster than the timescale of solvent relaxation, so that the distribution along q will be quasi-stationary. Thus a reduced distribution function P(X,t) for the reactant probability at time t and solvent configuration X may be formed by averaging over the quasi-stationary coordinate. A reaction rate coefficient k(X) for each value of the solvent coordinate can then be obtained using Marcus' theory of electron transfer [Marc 85]. The distribution function P(X,t) is taken to satisfy the diffusion-reaction equation:

$$\frac{\partial P}{\partial t} = D\frac{\partial^2 P}{\partial X^2} + \frac{D}{k_B T}\frac{\partial}{\partial X}\left(P\frac{dG_R}{dX}\right) - k(X)P\ , \qquad (2.11)$$

where D is the polarization diffusion constant :

$$D = k_B T / 2\lambda_S \tau_L . \qquad (2.12)$$

Since the operator $D\frac{\partial}{\partial X}\left(\frac{\partial}{\partial X} + \frac{1}{k_B T}\left(\frac{dG_R}{dX}\right)\right)$ is the Smoluchowski operator, the above equation is the Smoluchowski equation for diffusive motion along X, extended by a sink term $-k(X)P$ describing the reaction part. A similar equation was proposed by Bagchi, Fleming and Oxtoby [Bag 83] to account for the dynamics of activationless electron transfer

and the observed solvent viscosity dependence in the reaction of triphenyl methanes.

An important quantity, the survival probability for the system in the reactant state Q(t), can be derived from P(X,t):

$$Q(t) = \int P(X,t)\, dX . \qquad (2.13)$$

Sumi and Marcus [Sum 86] give an exact solution of equation 2.11 for the four following cases :

- The slow reaction limit

If the solvent reorientation is fast compared to the reaction, a thermal equilibrium is maintained for the distribution along X in the course of the reaction. Q(t) should show a single exponential decay with a rate coefficient slower than, and independent of the relaxation time τ_L of the reorientational fluctuations. For the non-adiabatic case, the result for k_{ET} coincides with equation 2.3, only that the solvent reorganization energy λ_S has to be replaced by the sum of the reorganization energies λ_S and λ_{vib}.

- The wide reaction window limit

If the intramolecular reorganization energy λ_{vib} is far larger than λ_S, the reaction may proceed over a range of X values much broader than the thermal equilibrium distribution of X for the reactant state. The rate coefficient can then be approximated by the average over k(X) over the X distribution in the reactant potential, yielding monoexponential dynamics for Q(t) independent of the solvent relaxation time.

- The narrow reaction window limit

If the solvent reorganization energy λ_S is far larger than λ_{vib}, the system has to cross the transition state essentially in X direction. The rate coefficient can be approximated as

$$k(X) = k_0\, \delta(X - X_C), \qquad (2.14)$$

where k_0 is a constant and X_C is the value for X at the intersection of curve C and the X axis in Figure 2.2-3. The survival probability will exhibit a multiexponential decay, the features of which will also depend on relaxation time τ_L of the reorientational fluctuations.

- The nondiffusing limit

If the reaction proceeds so rapidly that the distribution of X does not change during the course of reaction, the solvent motion is effectively "frozen". The reactant population will decrease with a different rate coefficient for each value of the initial configuration X(0),

independent of τ_L, resulting in multiexponential overall dynamics.

The Sumi-Marcus model was employed to account for non-exponential dynamics of electron transfer and for reaction rates larger than τ_L^{-1}[Su 88, Braun]. Jortner and Bixon [Jort 88] added high-frequency quantized intramolecular vibrations to their treatment of electron transfer including solvent relaxation. Since the reaction rate was viewed as the sum of the reaction rates to different vibrational product levels (see equation 2.5), fast solvent dynamics were implicitly assumed. Thus, the applicability of the Bixon-Jortner model is limited to cases where solvent relaxation is dynamically unimportant.

Walker et al. [Walk 92] extended both theories to a hybrid model allowing for two classically treated low-frequency modes X and q, characterizing the solvent reorientation and the charge reorganization, and a high-frequency quantum mode. Furthermore, they took into account the initial solvent distribution being displaced from thermal equilibrium by laser pulse excitation.

In their model the rate coefficient for the transition from the reactant vibrational ground state of the high-frequency mode to the m-th vibrationally excited level of that mode in the product state is a function of the solvent configuration X; through its activation energy it depends on the low-frequency intramolecular reorganization energy $\lambda_{lf,vib}$, the solvent reorganization energy λ_S and the difference in vibrational quanta $m\hbar\omega$:

$$k(X) = \sum_m k_{NA}^{0\to m}(X) \,, \tag{2.15}$$

$$k_{NA}^{0\to m}(X) = \frac{2\pi V_{el}^2}{\hbar\sqrt{4\pi\lambda_{lf,vib}k_BT}}\left|\langle 0|m\rangle\right|^2 \exp\left(-\frac{\Delta G_{0\to m}^*}{k_BT}\right) \text{ and} \tag{2.16}$$

$$\Delta G_{0\to m}^* = \frac{\left(\Delta G^0 + \lambda_S + \lambda_{lf,vib} + m\hbar\omega - 2X\lambda_S\right)^2}{4\lambda_{lf,vib}} \tag{2.17}$$

where the Franck-Condon overlap of the vibrational quantum states is accounted for by the term $\left|\langle 0|m\rangle\right|^2$. Such as for the previous models, fast vibrational relaxation compared to the electron transfer reaction is presumed. The solvent relaxation is again described by monoexponential dynamics characterized by the longitudinal dielectric relaxation constant τ_L. Walker et al. derived values for the reorganization energies $\lambda_{lf,vib}$ and λ_S from fits to

stationary absorption spectra of betaine-30 and tert-butylbetaine in different solvents. They could explain the observed temperature dependence of electron transfer dynamics in glycerol triacetate (GTA) and correctly predicted the dimension of the electron transfer rate also for slow-relaxing solvents, where it becomes independent of the timescale for solvent reorientation. An induction period for the decay of the survival probability in the simulations of betaine-30 in a fast relaxing aprotic dipolar solvent was interpreted as being due to the competition between solvation and reaction dynamics, fast solvent relaxation leading to an evolution of the system towards lower barrier heights $\Delta G^{*}_{0\rightarrow m}(X(t))$ than those for the initial values of X(0) [Walk 92]. In n-butanol, the deviation of the rates for betaine-30 electron transfer rates from those for solvent relaxation at low temperatures were ascribed to non-diffusional solvation mechanisms, especially hydrogen-bond rearrangement [Reid 94].

Fuchs and Schreiber [Fuchs 96] also described the temperature dependence of betaine-30 electron transfer dynamics. Limiting themselves to a single reaction coordinate, they treated the system and a coupled bath formed by other intramolecular modes and the solvent quantum mechanically. They achieved good agreement with the experimental data and the simulations of Walker et al. for temperatures down to 228 K [Walk 92].

Van der Meulen et al. simulated the solvation dynamics of DCM after photoexcitation inducing instanteneous charge separation and recombination using a Smoluchowski equation approach [vdMeul 98]. They included anharmonic dependencies of the ground and excited state free energy curves on the reaction coordinate and succeeded in qualitatively explaining the frequency shift and the reduction in width of the fluorescence spectra of DCM in ethylene glycol on a timescale of up to 30 ps.

To allow for non-Debye relaxation behaviour of the liquid, including memory and inertial effects, Hynes proposed a generalized Langevin equation for the electron transfer reaction coordinate q [Hynes 86]:

$$\ddot{q}(t) = -\omega_L^2 q(t) - \int_0^t d\tau\, \xi_L(t-\tau)\, \dot{q}(\tau) \qquad (2.18)$$

where $\omega_L^2 q(t)$ is the the derivative of the quadratic potential $V(q) = \frac{1}{2}\omega_L^2 q^2(t)$, ω_L being the frequency of oscillation in the diabatic reactant and product potential wells.

The longitudinal time-dependent friction coefficient $\xi_L(t)$ is related directly to the dielectric response function of the liquid, without presuming any model for its dielectric behaviour. With a random force term f(t) added to the right hand side accounting for orientational fluctuations of the solvent molecules, Kang et al. [Kang 90] used this equation to model the time-dependent emission spectra of bianthryl in dipolar solvents. An initial probability distribution is assumed and its evolution obtained by calculating trajectories starting with these initial values.

Another possibility to account for non-exponential solvent dynamics is to introduce a time-dependent solvent polarization diffusion coefficient D(t) in the diffusion-reaction equation 2.11 [Hynes 86] and to solve this so-called generalized Smoluchowski equation directly for the time-dependent probability distribution. This method was applied by Tominaga et al. [Tom 91] to describe the electron transfer dynamics of ADMA. Rasaiah and Zhu [Zhu 92, Ras 93, Ras 94] showed that the survival probability is the solution of an integral equation derived from reaction-diffusion equations. There D(t) is related by:

$$D(t) = -k_B T \frac{d(\ln C_{\Delta E}(t))}{dt} \qquad (2.19)$$

directly to $C_{\Delta E}(t)$, the time correlation function of the solvent polarization fluctuations (see 2.3).

In the frame of the TICT-model, the twist angle θ is an obvious choice for a reaction coordinate. The coupling of a second, solvent coordinate to the twisting motion is provided by the dipole moment μ(θ) of the molecule which is assumed to depend parametrically on θ and enters the expression for the time-dependent solvent electrical field E(t). A Langevin equation for the evolution of θ was presented by Schenter and Duke, including time-dependent friction [Schent 91]. The propagation of an initial distribution f(θ,E,t) for DMABN was computed, where the solvent was treated as a dielectric continuum. The dynamics of the trajectories let a picture of three distinct timescales emerge: first, an initial equilibration of θ, second, low barrier crossing and third, dielectric relaxation of the solvent. Polimeno et al. [Pol 94] solved a two-dimensional Smoluchowski equation with constant diffusion coefficients for the solvent and the twist angle coordinate, given by a Debye and Stokes-Einstein relation, respectively.

Kim and Hynes [Kim 97] constructed and diagonalized the diabatic Hamiltonian for a

solute-solvent system to attain adiabatic excited states and their free energies as a function of the twist and the solvent coordinate. The electronic coupling and the solute dipole moment were parametrized as a function of the twist angle, and the parameters for the diabatic potentials were taken from ab-initio calculations. Extending earlier work of Fonseca et al. [Fons 94], they analyzed the free energy surfaces of DMABN via the minimum free energy solution-phase reaction path, deducing that the reaction in acetonitrile proceeded chiefly along the twist coordinate. In methanol, which is characterized by an even faster inertial component in its solvation dynamics than acetonitrile [Bing 95], the solvent motion was found to be involved to a greater extent before and during the crossing of the transition state. They also formulated a generalized Langevin equation for the twist coordinate, including dissipative and inertial solvent friction, and achieved excellent agreement between rate coefficients calculated after Grote-Hynes theory [Grot 80] to experimental data on DMABN.

Two vibrational modes were included in the electron transfer treatment of oxazine 1 in dimethylaniline (DMA) by Wolfseder et al. [Wolf 98]. As Fuchs and Schreiber [Fuchs 96] and Kühn et al. [Kühn 96], they used a reduced density matrix approach. Three electronic states (ground state, primarily excited state and dark charge transfer state) and the two most dominant vibrational modes from the Raman spectrum of oxazine 1 constitute the "system", while the remaining inter- and intramolecular degrees of freedom are combined into a heat bath. The vibrational Hamiltonians h_i are described in the harmonic approximation by annihilation and creation operators, and in the excited states also by the electron-vibrational coupling κ, which is related to the intramolecular reorganization energy and the nuclear equilibrium displacement of the mode between electronic ground and excited state. The vibrational frequencies are assumed to be equal for the three electronic states. The system Hamiltonian contains the electronic and vibrational energies for the ground, reactant and product state and the electronic coupling:

$$H_S = \sum_{G,R,P} |\varphi_i\rangle h_i \langle\varphi_i| + \left\{ |\varphi_P\rangle g \langle\varphi_R| + \text{h.c.} \right\} \qquad (2.20)$$

g is a constant determining the electronic coupling $V_{el} = |\varphi_P\rangle\, g\, \langle\varphi_R|$.

The reduced density matrix ρ is defined as the trace over the bath degrees of freedom of the total statistical operator W(t) applied to the "system" states:

$$\rho_{i,j}(t) = \mathrm{Tr}\left\{|i\rangle W(t)\langle j|\right\}. \qquad (2.21)$$

ρ satisfies the Liouville equation :

$$\frac{\partial}{\partial t}\rho(t) = -i\left[H_S + H_{int}(t), \rho(t)\right] + L(\rho). \qquad (2.22)$$

L(ρ) is a relaxation operator or dissipative term; it contains the vibrational relaxation rates representative of the disspation of heat into the bath. The Hamiltonian $H_{int}(t)$ signifies the interaction energy of the molecular system and the laser pulse fields E(t). It is approximated using the dipole operator μ :

$$H_{int}(t) = -|\varphi_R\rangle\, \underline{\mu}_{GR} \cdot \underline{E}(t)\, \langle\varphi_G|. \qquad (2.23)$$

The Liouville equation was solved numerically for a limited number of vibrational occupation numbers and the polarization $\underline{P}(t)$ obtained after

$$\underline{P}(t) = \mathrm{Tr}\left\{\underline{\mu}\, \rho(t)\right\}. \qquad (2.24)$$

From $\underline{P}(t)$ the time-resolved transmission signal was calculated and compared directly to the experimental signals. Oscillations occuring in the simulated as well as in the measured spectrally integrated intensity were interpreted as hint that coherent wave-packet motion could be coupled to the electron transfer reaction. The population probability $W_R(t)$ (different from the survival probability only in that while Q(0) = 1, $W_R(0) = 0$) was also calculated as the trace over the vibrational states of the density matrix element ρ_{RR} :

$$W_R(t) = \mathrm{Tr}\left\{\rho_{RR}(t)\right\}. \qquad (2.25)$$

After an initial rise, it was found to exhibit a biphasic decay on timescales of about 50 and a few hundred femtoseconds. The 50 fs component was viewed as inherent (system-depending), while the slow component was thought to reflect vibrational cooling [Wolf 98]. Pronounced oscillations with a period of approximately 55 fs persisting until around 1000 fs in visible transients of the same system were considered a case of continued wave packet motion in the reaction product [Eng 99]. A biexponential decay with time coefficients of 30 and 80 fs was manifested by spectrally averaged transmission changes in the red and blue spectral regions associated with the absorption of the primarily excited oxazine1^+/DMA complex and the product oxazine$^\bullet$/DMA^+. The shorter component was discussed with regard to the period of the coherently excited vibration(s): if the interaction region between

the reactant and product states is at the outer turning point of the vibrational motion in the reactant state, the system should stay for half a vibrational period in the reactant state before a reaction could take place.

The importance of higher vibrational states was stressed for electron transfer of coumarin 337 to DMA by Wang et al. [Wang 97]. They measured IR and visible transients and estimated the solvent and intramolecular reorganization energy for C337 after photoexcitation from stationary absorption and fluorescence spectra to ≈1525 cm^{-1} and ≈300 cm^{-1}, respectively. Since electrochemical measurements led them to evaluate the free reaction enthalpy for the reaction of the isolated compounds to the far larger value of –6600 cm^{-1}, electron transfer via nonequilibrium vibrations of the product state was taken into consideration.

2.3 Solvation dynamics

The movement of solvent molecules in a liquid induces fluctuations $\delta\Delta E(t)$ in the energy gap ΔE between the solute electronic ground and first excited state, causing spectral broadening of the intrinsic stationary absorption and emission bands. The *fluctuations* are characterized by their normalized *equilibrium correlation function* $C_{\Delta E}(t)$:

$$C_{\Delta E}(t) = \frac{\langle \delta\Delta E(0)\ \delta\Delta E(t) \rangle}{\langle \delta E^2 \rangle}. \qquad (2.26)$$

Here $\langle\ \rangle$ stands for averaging over a canonical ensemble. The adaptation of solvent molecules to a change in the solute's electric field going along with electronic excitation is termed solvation dynamics. The electronic polarization of the liquid is assumed to respond instanteneously to the perturbation, whereas nuclear reorientation follows more slowly and leads to an energy shift in time for the electronic transition energy $\Delta E(t)$. A normalized *solvent or spectral response function*, also called "non-equilibrium solvation correlation function", is defined as:

$$S_{\Delta E}(t) = \frac{\langle \Delta E(t) \rangle - \langle \Delta E(\infty) \rangle}{\langle \Delta E(0) \rangle - \langle \Delta E(\infty) \rangle} = \frac{\nu(t) - \nu(\infty)}{\nu(0) - \nu(\infty)}, \qquad (2.27)$$

where ν is the mean transition frequency. $\nu(t)$ can experimentally be obtained by monitoring the mean emission frequency of a chromophore after electronic excitation, the evolution of which is called time-dependent Stokes shift.

If the perturbation from the electronic transition is not large, *linear response theory* provides a relation between the equilibrium fluctuations and the dissipative relaxation dynamics, so that $S_{\Delta E}(t) \cong C_{\Delta E(t)}$. Molecular dynamics simulations of the neat liquid can be performed under equilibrium conditions and the results can be compared to measurements of the time-dependent Stokes shift. In this way, the liquid response was found to proceed on various timescales. An ultrafast part of sub-100 fs, approximated by a Gaussian function in time, was assigned to *inertial motion* of the "free streaming" of solvent molecules uncoupled from each other [Stratt 94, Ros 94, Mar 94, Rain 94]. This effect was first reported for solvation dynamics of LDS-750 [Ros 91, Cho 92], although this was

criticized later [Kov 97]. Oscillations are observed in the simulations on a slightly longer (up to several hundreds of femtoseconds) timescale and were attributed to collective, underdamped motions or *librations* of the solvent molecules. Only recently the latter features have also been confirmed experimentally by pump-probe measurements of amino-nitrofluorene in acetonitrile [Ruth 98]. After about 0.5 ps the motions of the liquid were considered to be *diffusive* or overdamped in nature, with an approximately exponential behaviour in time. The time coefficients of the diffusive relaxation depend strongly on the solvent and range from around 0.6 ps for acetonitrile up to hundreds of picoseconds for viscous alkanols [Horng 95].

Treatments of the stationary Stokes shift with *reaction field models* were initiated by Lippert [Lipp 57] and McRae [McRae 57] and others based on an idea of Onsager [Ons 36]. The reaction field model pictures the liquid as a *dielectric continuum* of dielectric constant ε (continuum model). The solute is represented by a point dipole at a center of a spherical cavity of radius a filled with dielectric material having a dielectric constant ε_c. The latter is related to the solute's molecular polarizability α through the Clausius-Mosotti equation:

$$\alpha / a^3 = (\varepsilon_c - 1)/(\varepsilon_c + 2) .$$

The interaction energy of solute and solvent can be written in the form:

$$E = -\frac{1}{3}(\varepsilon_c + 2)\, \underline{\mu}\, \underline{R} , \qquad (2.28)$$

where $\underline{\mu}$ is the solute dipole moment and $\underline{R}$ is the reaction field on the solute arising from the polarization of the surrounding dielectric by the solute dipole. The reaction field includes the orientational (nuclear) and instanteneous (electronic) polarization of the liquid. McRae also considered the polarization of the solute induced by the reaction field and dispersive forces between solute and solvent molecules. In this work, results from the treatment of Amos and Burrows [Amos 73] are used:

$$\nu_{Flu} \cong \nu_{0,Flu} + \frac{2\,\mu_e(\mu_g - \mu_e)}{hca^3}\left[\frac{\varepsilon_0 - 1}{\varepsilon_0 + 2} - \frac{\varepsilon_\infty - 1}{\varepsilon_\infty + 2}\right] + \frac{\mu_e^2 - \mu_g^2}{hca^3}\left(\frac{\varepsilon_\infty - 1}{\varepsilon_\infty + 2}\right) \qquad (2.29)$$

and

$$\nu_{Abs} \cong \nu_{0,Abs} + \frac{2\,\mu_g(\mu_g - \mu_e)}{hca^3}\left[\frac{\varepsilon_0 - 1}{\varepsilon_0 + 2} - \frac{\varepsilon_\infty - 1}{\varepsilon_\infty + 2}\right] + \frac{\mu_e^2 - \mu_g^2}{hca^3}\left(\frac{\varepsilon_\infty - 1}{\varepsilon_\infty + 2}\right). \qquad (2.30)$$

Here ε_0 and ε_∞ are the static and high-frequency limit dielectric constant of the solvent, with $\varepsilon_\infty = n^2$, and μ_g and μ_e are the solute's ground and excited state dipole moment, respectively.

The second term on the right hand side of equations 2.29 and 2.30 characterizes dipole-dipole interactions, the third describes interactions between the solute dipole and the electronic polarizability of the solvent. The term in angular brackets is the Debye reaction field factor F.

For the Stokes shift $\Delta\nu = \nu_{Abs} - \nu_{Flu}$ the following equation holds:

$$\Delta\nu \cong \Delta\nu_0 + \frac{2(\mu_g - \mu_e)^2}{hca^3}\left[\frac{\varepsilon_0 - 1}{\varepsilon_0 + 2} - \frac{\varepsilon_\infty - 1}{\varepsilon_\infty + 2}\right]. \qquad (2.31)$$

The static reaction field model was extended into the frequency domain by assuming Debye relaxation for $\varepsilon(\omega)$ [Bag 84, vdZwan 85]:

$$\varepsilon(\omega) = \varepsilon_\infty + \frac{\varepsilon_0 - \varepsilon_\infty}{1 - i\omega\tau_D}. \qquad (2.32)$$

τ_D denotes the Debye relaxation time. After Fourier transformation, the reaction field and the solute dipole moment are now time-dependent, with a step function assumed for $\mu(t)$. The fluorescence shift $\nu(t) - \nu_\infty$ was found to be proportional to $\exp(-t/\tau_F)$ [Bag 84], where τ_F is related to τ_D by $\tau_F^{-1} = \tau_L^{-1} + 2D$. D is the rotational diffusion coefficient of the solute and τ_L is the longitudinal relaxation time of the solvent:

$$\tau_L = \frac{\varepsilon_c + 2\,\varepsilon_\infty}{\varepsilon_c + 2\,\varepsilon_0}\,\tau_D. \qquad (2.33)$$

For a small rotational diffusion coefficient this is approximated as:

$$\tau_F \approx \tau_L \approx \varepsilon_\infty \tau_D / \varepsilon_0, \qquad (2.34)$$

so that

$$S_E(t) \approx \exp(-t/\tau_L). \qquad (2.35)$$

The model may be extended to cover multiple Debye relaxation times, with $\varepsilon(\omega)$ given as

$$\varepsilon(\omega) = \varepsilon_\infty + (\varepsilon_0 - \varepsilon_\infty)\sum_{k=1}^{n}\frac{g_k}{1 - i\omega\tau_k} \text{ and } \sum_{k=1}^{n} g_k = 1. \qquad (2.36)$$

It can also be used to extract the Stokes shift dynamics directly from the experimental

dielectric frequency response of the liquid, as in [Ruth 98].

The essential notion of the *instanteneous normal mode* (INM) picture of liquid dynamics is that at short enough times, even the molecules in a liquid will start to look as if they are vibrating. This harmonic motion can, for a given solvent configuration, be represented along independent normal modes q_i. To find out each mode's effectiveness in altering the transition energy ΔE, the derivatives of ΔE with respect to the INM coordinates are computed. They are used to reweight the normal mode spectrum, yielding a "*solvation spectrum*" which for short times can be exactly related to C(t). Applying projection operator techniques, this spectrum can be decomposed into subspectra as e.g. resulting from rotational or translational contributions to the molecular motion. Thereby it was confirmed that the dominant solvation mechanism for dipole and quadrupole interaction leading to changes in ΔE is librational, whereas translational motion is held responsible for dispersive interaction [Lad 95, 96a].

The concept of a *spectral density of solvation modes* was also used by Cho et al. [Cho 92], Bagchi and Roy [Bag 94] and Yang et al. [Yang 95] to compare results from heterodyne detected optical Kerr effect (OKE) measurements and the time-resolved Stokes shift. Ladanyi and Klein [Lad 96b] confirmed that the response of the liquid to the perturbation induced by changes in the solute electronic structure or by the polarized field of the pump pulse (OKE) proceeds via similar mechanisms.

Experiments on solvation dynamics in *nonpolar solvents* Gardecki et al. [Gard 95] have shown large time-dependent frequency shifts also for cases where dipolar solvation mechanisms can be excluded because of the small solvent polarity. Gardecki et al. ascribed them to solvation via interaction with large quadrupole and higher electrostatic moments of these solvents. For the solvation dynamics of nonpolar solutes studied by transient hole-burning in nonpolar solvents [Four 93], a subpicosecond, viscosity independent and a slower, viscosity dependent dynamic component were found. Berg [Berg 94] suggested that a change in the solute size on excitation could produce a significant solvent response. A model of the solute as a spherical cavity and the solvent as viscoelastic continuum with time-dependent compression and shear moduli yielded two distinct components for the solvation dynamics: the fast creation of vibrations (phonons) of the instanteneous structure of the liquid, and a slower reorganization of that structure. The model was also successfully

applied to the temperature-dependence of the solvation dynamics of the nonpolar s-tetrazine in the highly dipolar propylene carbonate [Ma 95].

2.4 Vibrational relaxation

As in the case of electronic spectra, the vibrational lines obtained directly by Raman or IR spectroscopy in solution are broadened by energy relaxation processes and frequency modulation due to changes in solvent configuration (pure dephasing). The latter is divided into a part of inhomogeneous broadening, where the solvent modulation is slow on the timescale of the transition and can be pictured as frozen, resulting in a distribution of solvent configurations, and homogeneous broadening by fast solvent movement. The exact form by which the solvent modulation influences the lineshape depends on the model for the solvent fluctuation correlation function (for a review of different models, see [Flem 96]). If the solvent fluctuations are delta-correlated, no memory effect exists (Markovian dynamics), and inhomogeneous broadening induces a Gaussian lineshape. For only homogeneous broadening present, the lineshape is Lorentzian, with its width $\Delta\omega$ given by

$$\frac{\Delta\omega}{2\pi} = \frac{1}{2T_1} + \frac{1}{T_2^*} \quad . \tag{2.37}$$

Here $1/T_1$ is the rate coefficient for vibrational energy relaxation and $1/T_2^*$ is the rate coefficient for the pure dephasing. ($1/T_2 = 1/(2T_1) + 1/T_2^*$ is the rate coefficient characteristic for the decay of coherently excited vibrations, also termed dephasing).

The loss of vibrational energy of large molecules with a high density of vibrational states has been pictured to involve two temporally distinct steps. Energy initially localized in one or more Franck-Condon active modes is rapidly redistributed among the entire vibrational space of the molecule because of anharmonic coupling between modes (*intramolecular vibrational redistribution*, IVR). The vibrationally hot molecule subsequently equilibrates thermally with the solvent by vibrational energy transfer between low-frequency solute and solvent modes (*vibrational cooling*). Evidence for the sequentiality of this process has been obtained by time-resolved transient absorption or emission experiments of organic dyes [Els 91, Hüb 91, Zhong 96, Ang 89, Mok 89]. The relevant timescale for IVR was reported to be

sub-60 fs for rhodamine 6G [Ang 89], nile blue, DODCI, cresyl violet and oxazine 725 [Tayl 84], LDS 698, 751, 765 and 821 [Zhong 96] and coumarin 102 [Kov 98] in dipolar protic and aprotic solvents. It was found to be dependent on the excitation wavelength for oxazine 1, increasing from 30-50 fs for visible to 180 fs for UV excitation [Laerm 89] and to amount to several hundreds of femtoseconds for coumarin 6 [Hüb 91].
Vibrational cooling was reported to be at least by an order of magnitude slower than IVR [Zhong 96, Hüb 91, Mok 89, Ang 89]. For azulene in different solvents [Suk 90] and over the complete gas-liquid transition for supercritical fluids [Schwarz 96] it could be described by extensions of the isolated binary collision model.

Several recent experiments suggest that the separability of the timescales for IVR and vibrational energy transfer to the solvent may not be universal. From the delayed rise of the dye IR 125 stimulated emission in ethylene glycol [Hasch 95], an estimate of one picosecond was deduced for internal conversion from higher-lying electronic states S_n to the lowest singlet state S_1, including IVR and energy transfer to the solvent. To explain the opposite temperature dependence of vibrational lifetimes of chromium and wolfram carbonyls in chloroform, Tokmakoff et al. [Tok 94] invoked coupling of the excited vibrational modes to intramolecular and solvent high frequency modes and to low-frequency solvent phonon modes, with temperature-dependent phonon occupation numbers and phonon density of states.
Sension et al. [Sens 93] showed that IVR in the S_1 state of *cis*-stilbene in solution is not complete on the scale of the isomerization, but continues up to ≈6 ps. Jean and coworkers have presented time-resolved resonance Raman investigations of *trans*-stilbene [Qian 93, Qian 95, Schultz 97]. Using the bandwidth of the ethylenic mode at ≈1565 cm^{-1}, the vibrational cooling time was determined to 10 ps in alkanes and alcohols [Qian 93]. Biexponential decay of the corresponding anti-Stokes resonance Raman line was observed and the shorter 2 ps-component interpreted as being due to IVR [Schultz 97]. Neither the slow part of the ethylenic band intensity decay, nor that of other modes in the anti-Stokes RR spectrum could be modelled assuming a Boltzmann distribution of the vibrational temperature calculated from the excess energy. They concluded that energy flow to the solvent started before IVR was complete. Nakabayashi et al. [Nak 98] confirmed a nonstatistical distribution of intramolecular vibrational energy for *trans*-stilbene in 1-

butanol picoseconds after photoexcitation.

Vibrational relaxation in liquids has been modelled under the assumption that in analogy to the gas phase an effective collision process between the solute and solvent molecules plays a central role. The *isolated binary collision* (IBC) model predicts collision frequencies and relates the vibrational relaxation to the properties of collision events, such as the energy transferred per collision [Harr 90]. As for solvation dynamics, the concept of instanteneous normal modes has been applied to vibrational relaxation. It was demonstrated that, although they account only for a small part of the INM spectrum, binary modes which vibrate the solute against its nearest neighbour contribute preferentially to solvation dynamics and to vibrational relaxation [Lars 97]. Studying a model dipolar solute in liquid water by molecular dynamics simulations, the vibrational energy relaxation was found to be proportional to the magnitude of charge at each end of the solute by Whitnell et al. [Whit 92]. They also proposed that a large number of solvent molecules participate in the energy flow process, questioning binary descriptions. Cho [Cho 96] explored the influence of Coulombic interaction on vibrational relaxation and for an anharmonic vibrational coupling potential elucidated a direct relation between the rates for pure dephasing and vibrational energy transfer, and frequency-dependent dielectric friction.

In this work the comparatively simple model of *Montroll and Shuler* [Mon 57] will be used to simulate vibrational relaxation. They studied the relaxation of different initial non-equilibrium distributions of harmonic oscillators of frequency ω contained in a heat bath with constant temperature, formed by harmonic oscillators of the same frequency. The oscillators can exchange energy by radiation and by collision only with the bath, interacting with the vibrational and translational degrees of freedom of the bath oscillators which themselves remain Boltzmann-distributed.

Transitions will take place only between adjacent vibrational levels. The probability for the transition of $n \rightarrow n+1$ as $i \rightarrow i-1$ per collision of oscillators initially in states $|n\rangle$ and $|i\rangle$ is assumed to be a linear function of the vibrational excitation of both oscillators:

$$P_{n,n+1;i,i-1} = (n+1)\, i\, P_{10} \quad , \tag{2.38}$$

where P_{10} is the transition probability per collision for transitions between the first vibrational excited state and the ground state.

The time-dependent probability fraction of $x_n(t)$ of oscillators in state $|n\rangle$ is then given by a

master equation:

$$\frac{dx_n}{dt} = \gamma_{vr}\left\{n\exp(-\theta)\,x_{n-1} - \left[n+(n+1)\exp(-\theta)\right]x_n + (n+1)x_{n+1}\right\} \qquad (2.39)$$

with $\theta = \frac{h\nu}{k_B T}$ and $\sum_n x_n = 1$.

γ_{vr} is the total vibrational relaxation rate of the oscillator for collisional and radiative transitions between levels |1> and |0>.

Equation 2.39 was solved for an initial distribution of x_n:

$$x_n(0) = \begin{cases} 1 & \text{if } n = m \\ 0 & \text{otherwise} \end{cases} \qquad (2.40)$$

to obtain:

$$x_n(t) = \frac{(1-\exp(\theta))\exp(m\theta)}{\exp(-\tau)-\exp(\theta)}\left(\frac{\exp(-\tau)-1}{\exp(-\tau)-\exp(\theta)}\right)^{m+n}$$
$$\cdot\left[1-u^2\right]^{1+m+n} F(1+n,\ 1+m,\ 1;\ u^2) \quad . \qquad (2.41)$$

Here $\tau = \gamma_{vr} t\,(1-\exp(-\theta))$, and F is the hypergeometric function.

3 Experimental

Overview :

The experimental set-up was designed to provide short (sub-100 fs) pulses of microjoule energies in the UV and in the red spectral region for photoexcitation and stimulated emission pumping of DCM and photoexcitation of LDS 750. It also produced a femtosecond broadband continuum (≈ 350-900 nm) to monitor the transient absorption and emission changes of the photoexcited dyes. Control of the temporal delay between excitation and probing pulses was achieved by a computer-controlled optical delay stage in the path of the pump (and, for the case of DCM, also of the dump) pulse. A/D conversion and storage of the measured data were effected by means of a PC A/D converter card and a home-programmed user interface. The pump-probe experiments on DCM were performed with a set-up based on that described in [Bing 95], producing tunable excitation pulses between 450 and 530 nm and a probe continuum of approx. 45 fs pulselength. The diameter of the pump beam on the sample was ≈150 µm, and the focus diameter of the probe continuum ≈80 µm.

The next three subsections will give a description of the short pulse generation, amplification and pump-probe set-up, whereas the following three subsections will be concerned with synchronization, signal detection and noise reduction. A description of the basic data correction procedures concludes the treatment of the femtosecond set-up. The last three subsections deal with the characteristics of the employed chemicals and the experimental conditions for the photostationary absorption, fluorescence, molecular beam and Raman measurements. All measurements were conducted at ≈ 20 °C, if not indicated otherwise.

3.1 Short Pulses

3.1.1 Generation

The colliding pulse mode-locked (CPM) laser is a ring dye laser pumped by a continously (cw) emitting argon ion laser, which here was a Lexel 3500-7 (Polytec) operating between 0.9 and 1.2 W at 514 nm only. The CPM generated optical pulses of 60 fs pulsewidth at a fundamental of 630 nm with a repetition rate of 76 MHz (Figure 3.1-1). The home-built laser resonator consisted of the six-mirror, four-prism configuration of Valdmanis and Fork [Vald 86]. Fused silica prisms with an apex angle of 68.9° were used. The gain mirrors had a curvature of R=100 mm, the absorber mirrors had R=50 mm. A jet with a thickness of 100-150 µm of a solution of 3.4 mM rhodamine 6G in ethylene glycol was the gain medium, and a approx. 17 µm thick jet of a 0.89 mM solution of DODCI in the same solvent served as saturable absorber. The output power in one of the beams behind a 3% output coupler was around 8 mW, which corresponds to a pulse energy of about 0.1 nJ.

The principle of the CPM pulse generation is passive mode locking caused by the presence of a saturable absorber. As in all femtosecond laser oscillators, stable performance can be achieved because of the interplay of self phase modulation and group velocity dispersion [Mart 84]. Self phase modulation is due to the optical Kerr effect in the ethylene glycol jets and to gain and absorber saturation (see also 2.4). It contributes a positive frequency chirp to the pulses, generating new frequency components and therefore broadening the laser bandwidth [Sieg]. The four prism set introduces in total a negative group velocity dispersion (a negative chirp) [Bor 84, Fork 84], depending on the distance between the second and third / third and fourth prism. It should compensate the linear positive chirp from the glycol jets and the prism material itself. The amount of the latter can be adjusted by translating a prism in a direction normal to its base (see also 2.4).

The geometric stability range of a resonator can be calculated with the help of ABCD matrices [Sieg]. A similar calculation to that in [Bult] was used to obtain the stability range of the set-up. Starting from empirical distances between the gain and absorber mirrors, so that the fluorescence was imaged at a distance of 2 m from the left gain mirror and 4-4.5 m from the right one, the gain and absorber mirror distances were symmetrically varied in steps of 10 and 5 µm, respectively, to find a stable mode-locking regime. Care should be

taken to maintain the jets in the Brewster angle and to adapt the jet and pump geometries, if the folding mirrors are not moved symmetrically. The angles of incidence were 1.2° for the gain and 2.9° for the absorber mirrors.

Mode-locking was achieved in the most stable fashion near the laser threshold of 0.9 - 1.2 W. Removing the absorber jet lowered the threshold to 240 mW. High absorber concentrations, raising the laser threshold above 1.3 W, led to instabilities due to competitive modes and were therefore avoided. For better solubility, 50 ml of methanol was added to the ethylene glycol when preparing the DODCI solution. The measurement quality was greatly improved by replacing the dyes already after 50 h of operation, although at that time no sign of degradation, e.g. amplitude instability, had shown yet. When replacing the DODCI solution, the corresponding pump was cleaned once with acetone.

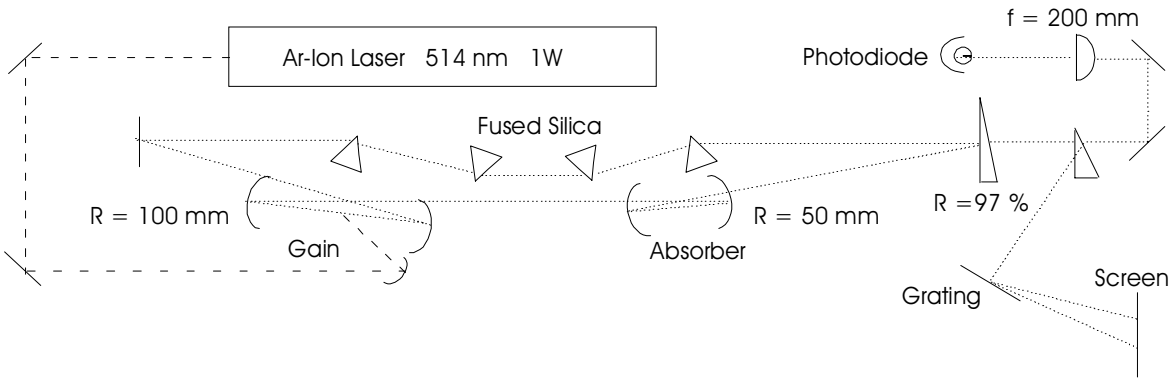

Figure 3.1-1 : CPM-Laser set-up.

3.1.2 Amplification

Nonlinear processes, such as stable continuum generation and frequency doubling require a pulse energy in the mikrojoule regime. Three dye amplification stages provided pulse energies of 0.2 µJ after passing the first stage and a saturable absorber, 26 µJ after the second stage and up to 240 µJ after the third stage. The amplified pulses were broadened in time due to positive group velocity dispersion of the materials in the optical paths and had to be recompressed to 65 fs pulselengths using a prism compressor.

The pump laser for the amplification stages was a Q-switched, seeded Nd:YAG laser (Continuum), delivering approx. 70 mJ of the extra-cavity frequency-doubled fundamental at 532 nm at 30 Hz repetition rate. The pulselength in seeded operation was 4-5 ns, with a timing phase jitter of 1 ns rms between the electronic timing pulse for the Pockels cell

effecting the Q-switch and the actual optical output pulse. This jitter, as well as the Gaussian spatial beam profile displaying alternating dark and bright elliptic features in the far field, led to energy fluctuations of the amplified pulses of up to 10%. Only 11 mJ of the 70 mJ energy available were necessary for the optical pumping of three fused silica cells with rhodamine 101 perchlorate as the gain medium, using 2 mJ, 1.8 mJ and about 7 mJ for the first, second and third cell, respectively. Solvents and concentrations were as follows: first cell, 0.76 mM solution of rhodamine 101 in methanol, second cell, 0.52 mM in propylene carbonate, third cell (bethune cell), 0.15 mM in methanol. Behind the first cell, the amplified spontaneous emission was blocked by a saturable absorber, a jet of 2.5-3 mM malachite green in ethylene glycol. The amplified beam was spatially filtered by a 150 µm pinhole between the second and third cell.

For further details regarding the optical geometry of the amplification stages, please see Figure 3.1-2. The prism compressor consisted of two SF10 prisms placed at an apex distance of 72 cm (see 2.4). After compression and spatially limiting the beam to the central Airy disk, the pulse energy ranged between 140 and 160 µJ containing approximately 1% of amplified spontaneous emission (ASE).

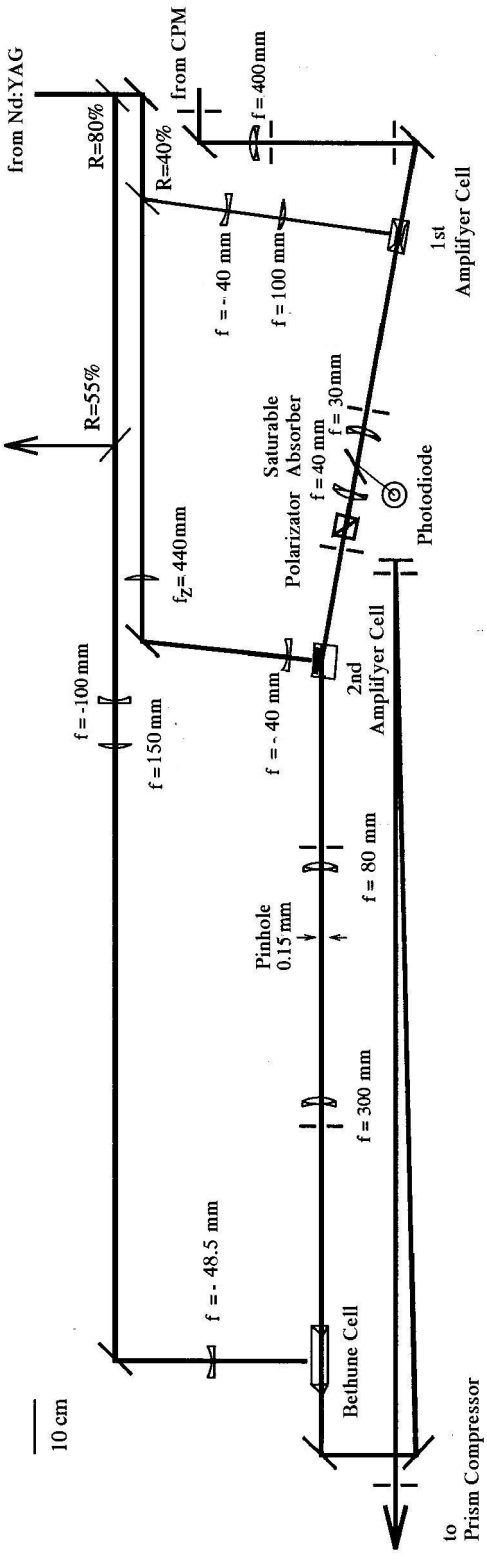

Figure 3.1-2 : Laser pulse dye amplification set-up, after [Loch].

3.1.3 Diagnostics

To ensure an optimal performance, several parameters of the generated and amplified pulses were under constant control. The *spectrum* of the pulses behind the output coupler of the CPM oscillator was monitored simply by the second order reflection from a grating (d=2400 g/mm). It should be smooth, extending from approx. 615 nm to 645 nm, and stable especially with regard to its red edge. The *pulsewidth* was controlled by means of second harmonic generation from two parts of the beam superimposed at a finite angle in a nonlinear KDP crystal (non-interferometric autocorrelation). One of these parts was shifted in time with respect to the other with the help of a mirror mounted on a piezoelectric crystal for the pulses from the CPM oscillator or by a stepper motor driven translation stage for the amplified pulses, while the generated UV light was detected with a photomultiplier or with a photodiode, respectively. An autocorrelation trace of the amplified pulses is given in Figure 3.1-3.

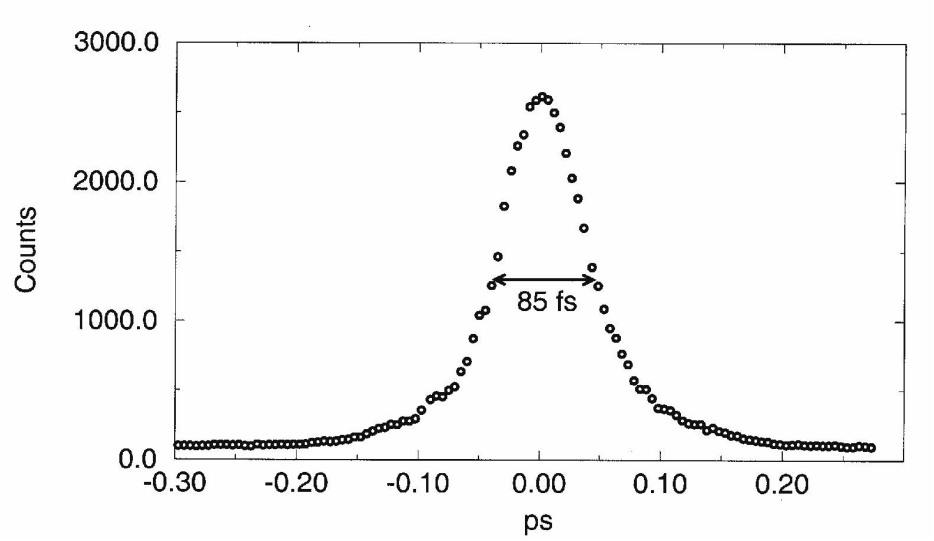

Figure 3.1-3: Autocorrelation trace of the amplified CPM pulses.

With the assumption of a $sech^2$ pulse shape, the pulselength is calculated as 0.65 of the intensity autocorrelation full width at half maximum (fwhm) [Sala 80] of 85 fs, which corresponds to a pulselength of 55 fs. To measure the pulsewidth of pulses shorter than 40 fs, a phase-sensitive (interferometric) autocorrelation technique would be chosen [Szab 88].

To check on *pulse-to-pulse energy fluctuations* or a *drop in pulse energy*, a RJP-735 pyrometer (Laser Precision Corporation / Polytech) was used. Proper *synchronization* between the to-be amplified pulses from the CPM and the Nd:YAG emission as pump source for the amplifier stages was monitored with a fast (risetime 280 ps) photodiode and a Tektronix 7104 oscilloscope of one GHz bandwidth.

The *spatial profile* of the beam was checked to ensure a smooth TEM (0,0) mode output and prevent hot spots.

Another diagnostic means which has become a standard in the last few years of optical short pulse spectroscopy is the frequency-resolved optical gating (FROG). Here the *intensity and phase* of the pulse are measured simultaneously. The beam is split and the parts are mixed in a nonlinear medium, for example a Kerr medium, creating a Kerr polarization rotation of one part of the beam, which is then frequency resolved and serves as the input to an algorithm retrieving the electric field of the pulse [DeLong 94]. The amount and type of relative phase-shift (linear or quadratic chirp, see 2.4) can be directly perceived from the frequency-resolved output, which facilitates its compensation.

3.1.4 Handling

In general, the optical path length for a beam passing through a medium of length l and refraction index n is given as n l. The refraction index may be intensity-dependent (electrooptical Kerr effect), subjecting short pulses propagating through materials to intensity-dependent nonlinear processes such as *self-focusing* and *self-phase modulation*. The pulses are also broadened in time due to different propagation times for their spectral components, imposing a delay of the higher energetic parts relative to the lower energetic ones (*group velocity dispersion*).

Self-focusing is an induced lens effect. Assuming a single-mode beam with a Gaussian transverse profile propagating in a medium with refractive index n given by

$$n = n_0 + \Delta n\left(\left|E^2\right|\right), \qquad (3.1)$$

where $\Delta n\left(\left|E^2\right|\right)$ or $\Delta n\ (I)$ is an optical-field induced refractive index change. If Δn is positive, the central part of the beam having a higher intensity experiences a larger refractive index than the edge and therefore travel at a slower velocity than the edge. As the

beam travels, the originally plane wavefront gets progressively more distorted, similar to the effect of a positive lens. Self-focusing can cause material damage and limits the focusability of the beam.

Self-phase modulation stems from the same intensity-dependent refractive index change $\Delta n(|E^2|)$. Consider a time-dependent envelope E(t) of an optical pulse and an instantaneous response $\Delta n(|E(t)^2|)$ given by $n_2 |E(t)^2| = n_2 I(t)$ of the refractive index. In a length l of the nonlinear medium, the pulse is subject to an intensity-dependent phase shift

$\Delta\varphi(t) = (\omega / c)\, n_2 I(t)\, l$ and a corresponding frequency modulation $\Delta\omega(t) = -\frac{\partial(\Delta\varphi)}{\partial t}$, which appears as a broadened spectrum [Sieg].

Self-phase modulation is one of the contributing mechanisms for continuum generation, which may be desired for tunability reasons, but is an annoying effect if it takes place in the probe cell or in a nonlinear crystal intended for second harmonic generation (see 2.5). Therefore, care was taken to avoid self-focusing or self-phase modulation by expanding the amplified beam to one cm diameter with a telescope (f = -50 and f = 200 mm) just behind the third amplification stage. When any focus was required, usually the largest acceptable focused spot size was used. For a Gaussian beam of wavelength λ, the focused spot size d_0 behind a lens with focal length f is approximated as $d_0 \approx 2f\,\lambda / D$ [Sieg]. D is the diameter of the beam when passing the lens. The depth (length) of focus is $\approx \pi/2\, (d_0 / \lambda)^{\square}\, \lambda$.

Group velocity dispersion is a consequence of the frequency dependence of the refraction index. For most transparent dielectric materials in the visible region of the electromagnetic spectrum the following approximation holds :

$n_0(\omega) = A + B\,\omega^{\square}$. (3.2)

The high frequency components of the pulse are more delayed than the low frequency ones, thus the pulse broadens in time. To compensate this so-called "positive dispersion" (wavelength-dependence) of the group velocities, a prism or grating set-up introducing a net group velocity dispersion with the opposite sign can be used [Bor 84, Fork 84, Treacy 69]. These frequency-dependent delay lines are called *pulse compressors*, as each can compensate a quadratic phase shift reducing the pulselength of the broadened pulse.

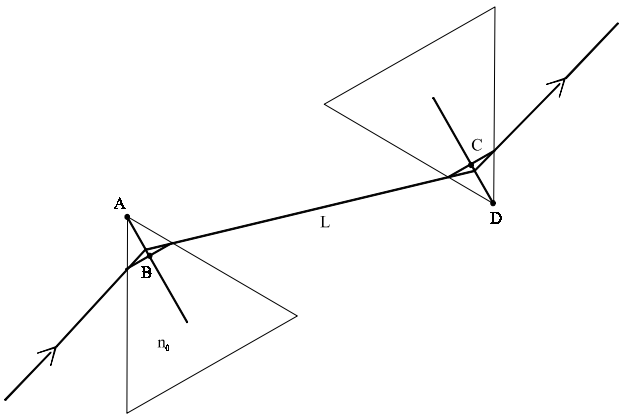

Figure 3.1-4: Prism pair used for pulse compression.

According to a Fourier theorem, the time-bandwidth product of any pulsed signal is constrained by the uncertainty principle $\Delta f_{rms}\,\Delta t_{rms} \rho\ 1/2$, where Δf_{rms} and Δt_{rms} are the root-mean-square widths of the signal in frequency and in time. As a consequence, the achievable pulsewidth (fwhm) τ for a Gaussian pulse with a frequency width of Δf is limited to a minimum of $\tau \approx 0.44 / \Delta f$ [Sieg].

In a *prism compressor*, the beam passes twice through two prisms separated by a length L. The *group-velocity dispersion* φ'' is defined as the third term of a Taylor expansion of the pulse phase in frequency:

$$\varphi(\omega) = \varphi(\omega_0) + (\omega - \omega_0)\,\varphi' + \tfrac{1}{2}(\omega - \omega_0)^2\,\varphi'' \qquad (3.3)$$

The corresponding instantaneous temporal phase to the third term in equation 3.3 is proportional to the square of time, t^2, and the corresponding instanteneous frequency has a linear dependence on t. That is why a quadratic phase shift means a linear frequency shift (linear chirp), a cubic phase shift means a quadratic chirp etc.

For the prism set-up of Figure 3.1-4, with e defined as AB + CD , φ'' is given as

$$\varphi'' = \frac{4\lambda_0^3}{\pi c^2}\left\{-L n_0'^2 + e\left[\frac{n_0 n_0''}{1 + n_0^2} + n_0'^2\left(1 - \frac{1}{n_0^2\,(1 + n_0^2)}\right)\right]\right\}, \qquad (3.4)$$

where n_0 is the refraction index of the prism material and n_0' is its first derivative in wavelength ($n_0' = (dn / d\lambda)_{\square\square}$) at the wavelength λ_0; n_0'' is the second derivative. The negative contribution to the group velocity dispersion scales with the distance L between the prisms, whereas the path e within the prisms adds positive group velocity dispersion. Values

for n_0, n_0', n_0'' and φ'' at λ = 620 nm for different materials are presented in Table 3.1.4.

Table 3.1.4 : Values for the refractive index and its wavelength derivatives for different media at 620 nm [Salin 87].

Medium	n_0	n_0' / μm^{-1}	n_0'' / μm^{-2}
SF10	1.7244	-0.1079	0.5725
FeD 05-25	1.8011	-0.13326	0.67787
SiO_2	1.4572	-0.02984	0.12144
BK7	1.5159	-0.03756	0.16641
H_2O	1.33	-0.02729	0.1303

SF10 prisms were chosen for compression of the amplified pulses due to their high value for n_0', enabling a more or less compact design of the compressor. When the prisms were polished with ceroxide once a year to avoid reflection losses, the overall energy transmittance of the compressor was $\approx$90 %, a large value compared to the maximum of approx. 50% transmittance of an even more compact grating compressor.

Propagation through materials does unfortunately not only involve a quadratic phase shift, but also cubic and higher order terms, which means that equation 3.3 is only valid as a first approximation. The cubic phase shift can be compensated by using a combination of prism and grating compressor, as these devices introduce a cubic phase shift with an opposite respective sign [Cruz 88]. Also, mirrors with chirped multilayer coatings have been shown to compensate quadratic and cubic phase shifts [Szip 94]. A monotonic variation of the multilayer period throughout the deposition process leads to a wavelength-dependent penetration depth of the optical field in the coating and to the desired group velocity dispersion.

As a consequence of the Fourier theorem mentioned above, a restriction in spectral width will impose an increase in pulselength. Therefore, only broadband dielectric high reflection mirrors centered at 616 nm or aluminium mirrors were used to propagate the beam.

3.1.5 Tunability

Nonlinear optical processes offer the possibility of changing the pulse's central wavelength, providing flexibility to experimental demands. Sum- and difference frequency generation, parametric oscillation and - amplification have been described. To obtain UV photons, here second harmonic generation (SHG) was used, which can be viewed as the degenerate case of sum frequency generation. A broadband probe pulse was created by continuum generation in water.

KDP (Kalium dihydrogen phosphate) was chosen as a crystal with a high susceptibility for second harmonic generation of 630 nm. To overcome the obstacle of different velocities of the fundamental (630 nm) and the second harmonic (315 nm), phase matching is required. As KDP is a uniaxial dichroic crystal, the refraction indices for 630 nm and 315 nm can be the same for a certain direction of propagation [Berg].

A 0.15 mm thick KDP slab was used, cut so that a beam entering the slab perpendicular to its surface, thus suffering minimal reflection losses, would propagate at 56.7° to the optical axis and induce a nonlinear polarization oriented at 45° in the x-y plane perpendicular to the optical axis. The second harmonic emerged polarized perpendicular to the fundamental (type I phase matching). From approx. 40 µJ at 630 nm focused with a lens of f=1330 mm into the crystal, 8 µJ at 315 nm were obtained and separated from the fundamental by reflection off four UV-high reflective dielectric mirrors transparent in the visible (Figure 3.1-5).

Continuum short pulse generation in liquids and solids was first observed in 1970 [Alf 70]. Self-phase modulation and self-focusing occur when a femtosecond pulse is focused e.g. into water, fused silica or sapphire. The self-focusing leads to filament formation with beam diameter narrowing [Shen 84]. In the filaments efficient nonlinear optical processes such as stimulated Raman scattering, stimulated parametric four-photon interaction and cascading frequency conversion take place [Wang 89, Penz 93, Witt 96]. The parametric four-photon interaction is degenerate in the pump laser frequency ($\omega_P + \omega_P$ –> $\omega_S + \omega_I$, ω_S is the signal, ω_I the idler frequency). The filaments impose a longitudinal phase-matching condition on this process. Transversally a phase-mismatch is allowed, which gives rise to an enlargened divergence of the white light emission compared to the fundamental [Witt 96].

If the spectral extent of the laser pulses covers a Raman frequency, stimulated Raman

scattering changes over to the more efficient impulsive stimulated Raman scattering [Witt 96]. Impulsive stimulated Raman scattering of low-frequency Raman modes and Raman amplification of generated parametric four-photon light are held responsible for the Stokes-dominated asymmetry in the generated white-light or supercontinua.

In our case, after careful attenuation of the fundamental and dye filtering the continuum had a bandwidth of approx. 15000 cm^{-1}, extending from 375 nm to 850 nm. It was generated by focusing 36 µJ of the 630 nm fundamental with a lens of f = 200 mm into a water cell of 1.5 mm length, with 0.2 mm fused silica windows. The continuum was energetically most stable when the colour spots from the different filaments nearly faded into each other and the fundamental emerged as a double-horseshoe-like spot. From the higher noise level of the baseline (optical density in the absence of the pump pulse) on the low-frequency side of the fundamental, a strong Raman contribution to the lower energy side of the continuum is concluded.

A non-divergent, low energy white light continuum can be generated by keeping the energy of the fundamental pulses just above the threshold for continuum generation. If a part of this continuum is selected by interference filters of appropriate bandwidth and optically compressed (see 2.4), it can exhibit a pulselength drastically shorter than that of the fundamental pulses [Sim 91].

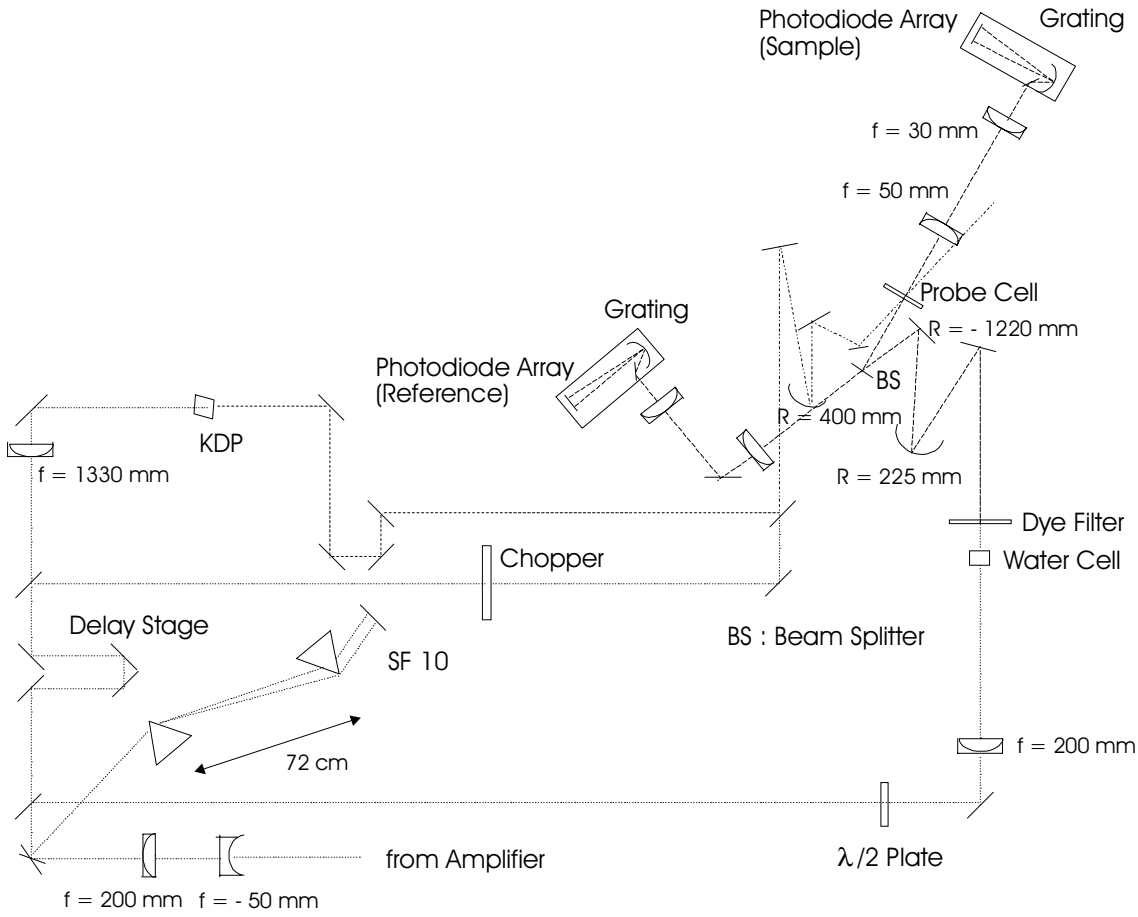

Figure 3.1-5: Pulse compression, second harmonic generation and measurement set-up.

3.2 Broadband Pump-Probe Measurement Set-up

The measurement set-up, as well as the frequency doubling and continuum generation arrangements are presented in Figure 3.1-5.

To modify the spectral shape of the supercontinuum, which is otherwise dominated by the generating fundamental frequency, it traversed a thin (0.45 mm total thickness, 0.17 mm fused silica windows) cuvette containing a filter solution made from 14 different dyes in ethanol.

The continuum beam was then focused into the probe cell with a combination of curved mirrors (R= 224 and R=-1220), by which combination astigmatism can be avoided. To prevent any ASE present from interfering with the experiment, the central spot of the continuum was blocked on the concave mirror. The ASE should show far less divergence

than the supercontinuum and can thus be eliminated for the most part.

The astigmatism of a given optical arrangement can be calculated with ABCD matrices. Here the angle of incidence upon the concave mirror was empirically found to be critical for astigmatism compensation and minimized to $\theta = 5.5°$. The continuum beam was split by a 50 % broadband beamsplitter (from Laser Optics) into a probe and a reference part. The degree of reflection from the beam splitter was observed to be dependent on the angle of incidence (Figure 3.2-1), increasing strongly for larger angles in the range above 650 nm. Due to pulse-to-pulse spatial changes of the continuum, this caused additional transmission changes leading to an increase of the noise level, which was dealt with by reducing the incidence angle of the continuum onto the beam splitter to $\theta = 12.5°$.

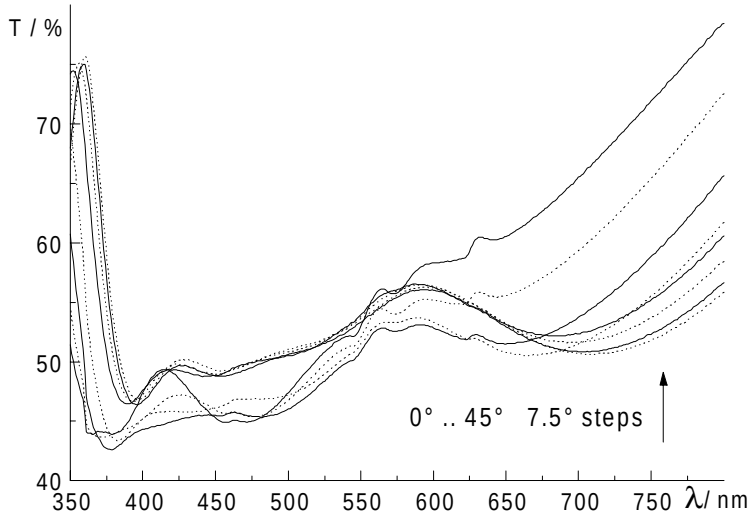

Figure 3.2-1: Transmission of the beamsplitter for different angles of incidence. Solid and dotted curves alternate for successive angles.

Only the reflected part of the continuum was focused into a flow cell, which had fused silica windows and a 0.3 mm thickness of the probe solution. The continuum beam crossed the fundamental and, for the stimulated emission pumping experiments, also the UV beam in the probe cell at an angle of $\theta = 12°$. The polarization of the 630 nm beam used for continuum generation was rotated to an angle of approx. 54° with respect to the UV beam polarization. As shown in [Bult], continuum generation does not change the polarization, so that there was an angle of 54° between the pump and probe polarizations, the so-called "magic angle" of exact 54.7 ° preventing polarization reorientation effects on the signal

[Less 76]. The 630 and 315 nm beams were focused collinearly into the probe cell with an aluminium mirror (R = 400 mm). The sizes of the foci were determined with a microscope to 200 µm for the continuum and approx. 250 µm for the 630 nm beam and for the 315 nm beam. The foci of the two latter were located approx. 5 mm behind the probe cell. The 630 nm beam was modulated at 15 Hz by an externally triggerable light chopper (EG&G 651 with controller 650).

As the probe part of the continuum had been reflected by the beam splitter and thereby transversally inverted, the reference part was treated likewise and reflected by an additional mirror. Both parts were collimated with identical achromatic lenses (f=50 mm) and focused (with f=30 mm) on the slit of two home-built Rowland type polychromators [Bing, Laur]. The gratings were from Zeiss, with a line spacing of 248 g/mm, blazed for 225 nm and a radius of 116.31 mm. In the focal plane of each a photodiode array was placed (S3904-512Q from Hamamatsu, 512 pixel, sensitive in the range 200-1000 nm). The intensities of both part of the continuum, I_{Probe} and I_{Ref} were recorded as a function of wavelength in a range of 420 nm between 350 and 930 nm. The transmission I_{Probe} / I_{Ref} was calculated and averaged over 30-200 laser shots. As every second pump pulse was blocked by the optical chopper, every second transmission value was summed up to give the baseline, that is the transmission without the pump pulse, which was then subtracted from the averaged transmission. Temporal delay between the pump and probe pulses was provided by a delay stage M-013 from Physical Instruments driven by a 5-phase stepper motor C-545 with 0.25 µm position accuracy and step width. It was controlled with a home-interfaced module SMA 05-Z from Ovis. The delay stage was positioned in the beam path of the fundamental behind the beamsplitter that reflected the part necessary to generate the probe continuum, so that the pump and dump pulses were synchronously delayed or rather, made to arrive earlier than the probe pulse. Delay of the fundamental used for continuum generation could cause systematic drifts in the output energy of the continuum, a rise of which might have led to saturation of the diode arrays.

3.3 Test, calibration and resolution

To check and find the *temporal overlap* of the pump- and probe pulses (time-zero), a dye, for example oxazine 750 in ethanol, was placed in a cuvette at the pump and probe beam intersection. Its long-lived stimulated emission can be induced by either 315 nm or 630 nm excitation and is easily found.

Since the stepper motor accuracy is specified as 0.25 µm corresponding to 1.7 fs temporal delay, the *temporal resolution* of the system was limited by the far larger pulselengths of the probe and the 630 nm pump or dump pulse. It was characterized by the rise of induced transmission of malachite green in ethanol (Figure 3.3-1), which produces a signal over the whole visible spectrum. Its rise was assumed to be a convolution of a step function and the cross-correlation of pump and probe pulses; the width of the latter is then given by the time between 12% and 85% of the signal rise. For an angle of 25° between pump and probe beams, as present in the DCM experiments, the time resolution was approximately 120 fs. After decreasing the angle to about 14°, the time resolution improved to approx. 100 fs for the LDS 750 experiments.

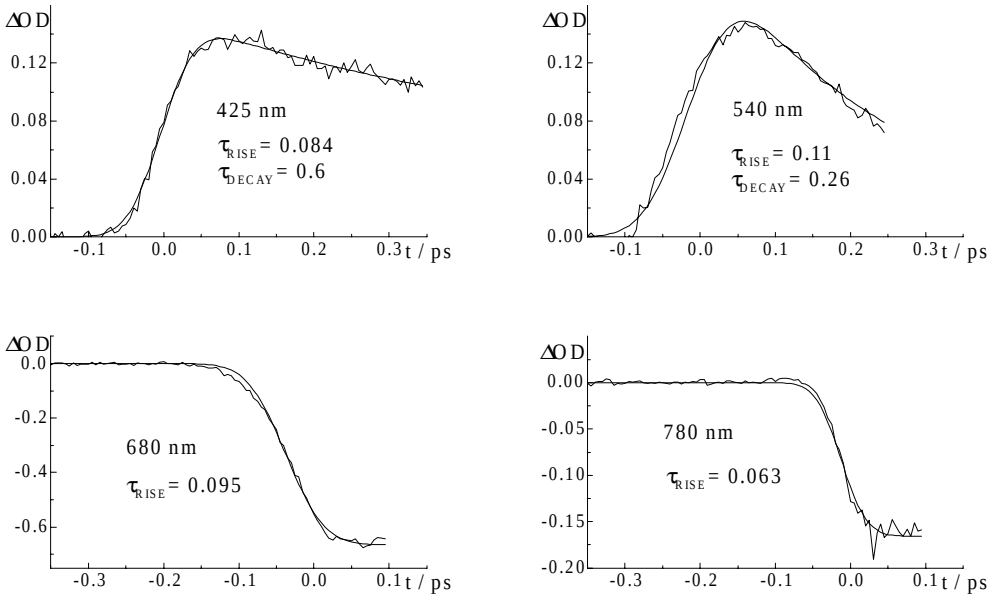

Figure 3.3-1: Malachite green kinetics demonstrating the system temporal resolution. Rise and decay times as obtained from fits to (sums of) exponentials are given in ps.

A mercury lamp was used for *spectral calibration* (Figure 3.3-2). The calibration spectrum also characterizes the wavelength resolution of the spectrometers to about 3 nm. In order to avoid any obstacle in the continuum beam path which could make the probe path different from that of the reference, the slits of the polychromators were opened during measurements. The focus of the continuum in the respective slit positions was about 100 µm in diameter, decreasing the spectral resolution to about 10 nm.

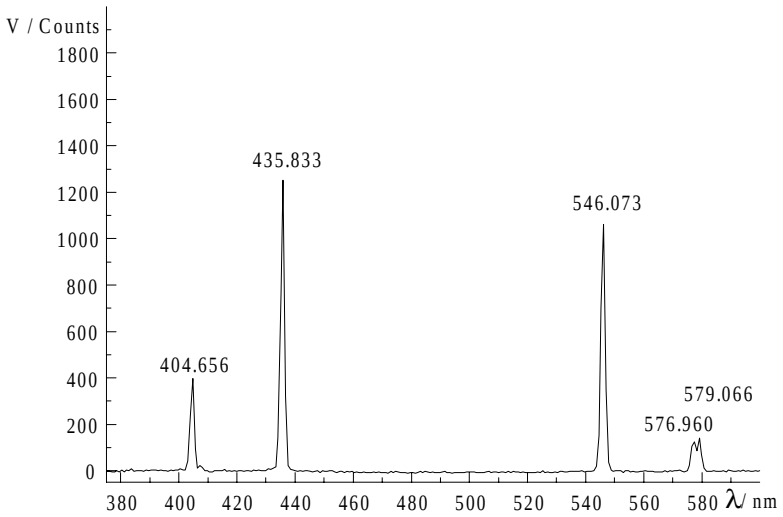

Figure 3.3-2: Spectrum of a mercury lamp recorded with the home-built polychromators.

To ensure that no transient from the solvent complicated the interpretation, the pump energy during measurements of DCM or LDS 750 was reduced to a level where no signal was obtained from the *pure solvent* (0.5-3 µJ). Stationary absorption spectra were recorded before and after the measurement to check for signs of photodegradation of the probe solution.

As the continuum experiences group velocity dispersion when traversing the cell windows and the solution, the time-zero overlap of pump and probe pulses takes place at different times for different wavelengths. From the electronic response of the pure solvent [Kov 99a], the amount of this *'time-zero dispersion'* can be derived. Therefore, measurements in the pure solvents with high excitation pulse energy (5-8 µJ) were also performed.

The main sources of noise were found to be pulse-to-pulse spatial fluctuations of the probe continuum, giving rise to differences in the transmission ratios of the broadband beam splitter, and misalignment of the probe continuum optical path. The probe or the reference continuum must not be cut off at its edge or be guided through the lenses in a way different

from the other. As the supercontinuum is not spatially homogeneous, the spectral intensity profile will change if part of the continuum is cut off, so that the probe and reference light will then exhibit different spectral characteristics. The *total noise* was 1-5 mOD, independent of signal height up to signals of about 100 mOD, when the system was well aligned and had been warming up for at least 3 h.

3.4 Synchronization and electronics

The Nd:YAG laser used to pump the amplification stages as well as the detection set-up had to be synchronized to the laser pulses delivered with 76 MHz by the CPM dye laser. The maximum repetition rate for the amplified pulses was limited by the Nd:YAG laser to 30 Hz. The corresponding trigger scheme is illustrated in Figure 3.4-1. A photodiode (250 ps risetime, BP 28) monitored the CPM signal, which was then divided to 150 Hz and 30 Hz by a home-built frequency-divider (see annex, Figure A-1). The light chopper was triggered with 150 Hz, and the 30 Hz signal was fed into a multi-channel delay generator (Stanford Research, DG 535). It delivered TTL pulses of various lengths and delays used as trigger for the Nd:YAG flashlamp, Nd:YAG Q-switch pockels cell, the polychromators and the A/D converter card. The delay between the Nd:YAG flashlamp and the Q-switch trigger was optimized for maximum pulse energy of the Nd:YAG pulses to 355 µs. The 30 Hz input signal from the pulse divider was variably delayed so that a femtosecond CPM pulse arrived at the same time at the amplifier stage as the maximum of the 5 ns long Nd:YAG pulse. Control of this was effected by monitoring the amplified spontaneous emission and the CPM pulse reflected from the saturable absorber as mentioned in 3.1.3.

The polychromators were controlled by the unit C4070 from Hamamatsu and home-built control circuits described in detail in [Bing]. These produced a 600 kHz clock impulse and two start impulses, separated by 5 µs, of 100 kHz synchronized to the external trigger for read-out of the photodiode arrays. The photodiode arrays were read out at 200 kHz, the maximum frequency for A/D conversion of the converter card (Meilhaus PC30-PGH). Alternating between the probe and the reference array, intensity values were read into two channels and converted into 12 bit digital values. A trigger signal for the 2 x 512 A/D conversions necessary every laser shot was also delivered by the polychromators' control circuits. Synchronisation of the measurement cycles was provided by gating the timer

element 8254 of the A/D converter card with one of the outputs of the delay generator. The timer counted downwards from a software set value (60000) with its own 2 MHz clock impulse, starting to count when the gate went high. After 15000 counts, the measurement cycle started. This value was optimized empirically so that the jitter of about 2 ms of the polychromator signal versus its external trigger would not lead to breaks in the sequence of photodiode outputs.

The commands for the start of the measurement cycle, A/D conversion, data averaging and storage and delay stage control were incorporated in a measurement user interface programmed in TurboPascal 7.0. It was an extension of that used in [Bing] and [Laur] and the converter card was adressed with the help of driver software provided by Meilhaus. This card had also 4 D/A channels and 24 digital in/outputs available for measurement and control purposes; two of the latter were used for delay stage control. For a typical measurement of 5 ps length with 10 fs steps and 150 averages around 45 minutes were needed.

A/D conversion took place in burst mode and was DMA controlled. The option of double-ended A/D conversion, where the shielding cable's voltage level is subtracted from the signal as a reference for each channel, showed to be noisier (by a factor of three) than the simpler single-ended conversion. Shielded BNC cables were employed and ground loops were avoided.

The dynamic range of 4096 counts of the converter card was set to correspond to 10 V. It could not be fully exploited since the photodiodes were already saturated at 8.9 and 7.9 V for the probe and the reference array. The dark current amounted to 170 and 110 counts, respectively, and was subtracted from the measurement. It fluctuated by about 6 counts, which was averaged out.

Two of the 24 digital outputs from the converter card were used to control the stepper motor of the pump pulse delay stage. The level of the first digital output set the direction of the move, and the number of low/high transitions of the second output corresponded to the number of steps to be taken. Owing to 'cross-talk' of the digital output channels, 'low' of any channel was at 0.5 V when one of them was constantly high. The output of the second channel was therefore fed to an additional monoflop, which provided an adequate output signal with the low level at $\approx$ 0 V. To prevent a mechanical hysteresis of the delay stage, moves backwards were realized by a slightly longer move backward than necessary and

another compensating move forward. Especially for long-distance moves a delay loop in the program proved important to ensure that the stepper motor had actually terminated the last move when it started the next.

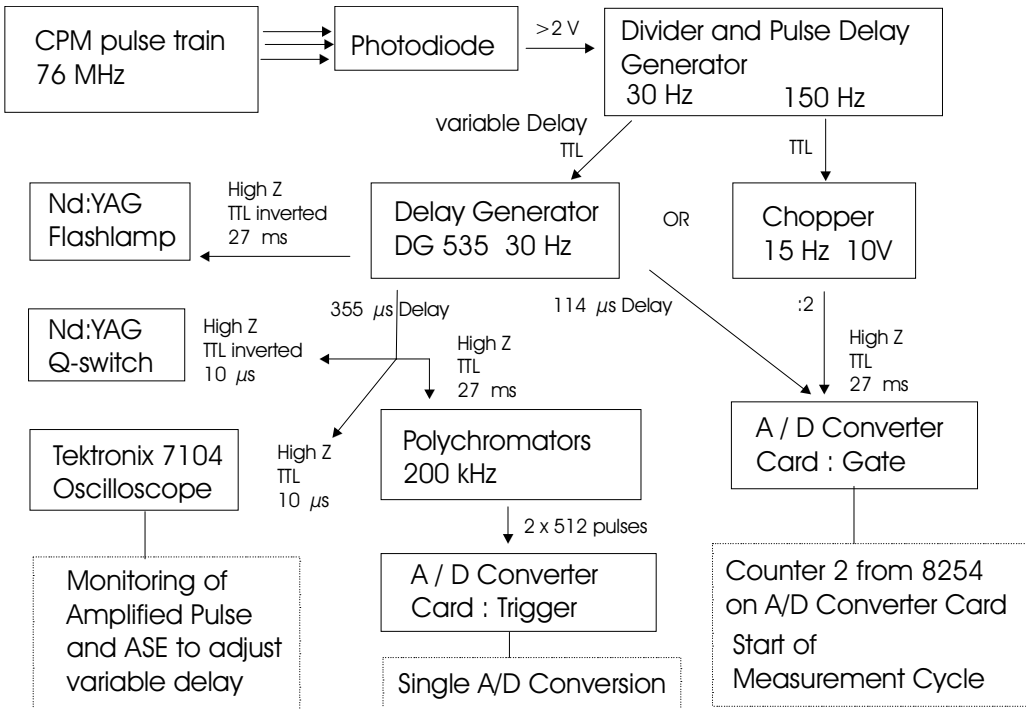

Figure 3.4-1: Synchronization scheme.

3.5 Data correction

All data presented are corrected for background signal and for dispersion of the temporal zero-position. Stray light from the pump pulse contributes, if present, also for negative time delays and can be easily subtracted from the set of spectra. To obtain the wavelength-dependent delay times of maximum overlap between the excitation or dump pulse and the probe continuum, the changes in optical density were recorded for a pure solvent. The coherent electronic contribution and the signal from impulsive stimulated Raman scattering exhibited for high pump energy by the solvent are centered around the peak of the cross-correlation of the optical pulses [Kov 99a]. Thus the temporal zero-position can be measured as a function of wavelength, with an accuracy of about 20 % of the temporal resolution. The experimental kinetic traces were shifted each by the negative of their zero-

position value and recombined to the time-dependent spectra.
When this improved the signal quality, the spectra were smoothed with binominal averaging.

3.6 Chemicals

LDS-750 and DCM were obtained from Exciton and Lambda Physics and used as received. Apart from malachite green (Kodak), all dyes used for short pulse generation or amplification or filtering were from Lambda Physics. All solvents were of spectroscopic grade (Merck Uvasol), apart from propylene carbonate, which was of HPLC grade. DCM and LDS 750 concentrations were about 0.2 mM in all solvents except cyclohexane, where the DCM concentration was below 0.1 mM.

3.7 Photostationary spectra

Stationary absorption spectra were recorded with a Shimadzu UV-3101PC spectrometer. Fluorescence spectra were measured using a SPEX Fluorolog1680 0.22 m double monochromator spectrometer. Photon counts were corrected by comparison with a secondary emission standard to determine the intrinsic fluorescence quantum distribution.

3.8 Molecular beam spectroscopy

The experimental set-up was that described in [Mühl 99a]. DCM was sublimated at 240 °C, and subsequently cooled by adiabatic jet expansion with Neon as buffer gas (1.2 bar). The fluorescence was detected with a monochromator and photomultiplier, blocking the excitation light with a glass filter (GG475 from Schott). The excitation wavelength was then scanned from 423 to 484 nm.

3.9 Raman spectroscopy

All Raman measurements were performed at the Bundesanstalt für Materialforschung (BAM), Berlin-Adlershof.

The resonance Raman (RR) spectrum of DCM in methanol was detected in a flow cell and back-scattering geometry by means of a nitrogen-cooled CCD camera, which was part of a double-stage DILOR-XY-Raman spectrometer with a spectral resolution of 4 cm^{-1}. Excitation was at 457.9 nm of an Ar^{+}-laser with a focus size of 70 µm and excitation power between 1 and 1.5 mW. The concentration of DCM in methanol was 0.5 mM. The RR spectrum of DCM in crystallic form was recorded with the same spectrometer using an Olympus-BH2 microscope and a 50x object lens. The excitation power was reduced to 0.01 W, with a focus size of 2 µm and a maximum irradiation time of 10 s.

Non-resonant Raman spectra were recorded with a nitrogen-cooled DTGS detector of type 418-S of a BRUKER-IFS 66 v Fouriertransform Raman spectrometer with a spectral resolution of 1 cm^{-1}. Excitation was at 1064 nm of a diode-pumped Nd:YAG laser in 180° backscattering geometry, with a laser power of 10 mW for the crystal spectrum and 1000 mW for the spectra of DCM solutions. The beam diameter was 100 µm in solution and 1 mm on the probe surfaces. The solutions were saturated with DCM at room temperature.

4 Results

Overview :

Time-resolved pump-probe experiments and stimulated emission pumping (dump-probe) experiments have been carried out on DCM and LDS 750 in solution. To obtain additional information on DCM properties in the liquid phase, stationary UV/VIS absorption and fluorescence spectra and Raman scattering spectra were measured. The (0,0) transition energy in the gas phase for excitation into the first electronically excited singlet state could be derived from the fluorescence excitation detection of jet-cooled DCM.
In the next two subsections, results of the time-resolved and stationary measurements on DCM will be presented. The following subsections are concerned with semiempirical calculations of isolated DCM and simulations of vibrational and solvent relaxation of DCM solutions.
The results on LDS 750 will be presented at the end of this section.

4.1 Time-resolved spectroscopy

Pump-probe experiments were carried through on DCM in cyclohexane, toluene, tetrachloromethane, chloroform, methanol and acetonitrile for different pump pulse central wavelengths and pump energies. Dump-probe experiments were realized on DCM in methanol, acetonitrile and propylene carbonate with a pump pulse central wavelength of 315 nm and a dump pulse centered at 630 nm. The delay between pump and dump pulse was 100 ps, which should ensure solvent equilibration.

4.1.1 Spectral decomposition

Typical *pump-probe spectra* of DCM in acetonitrile are shown in Figure 4.1-2a) for an excitation wavelength of 530 nm and a excitation pulse energy of 0.4 µJ. The pump-induced changes in the optical density (differential optical density) are plotted against the

wavelength for a time series of transient spectra.

Positive contributions to the differential optical density are observed in the spectral region from 400 to 480 nm, whereas in the region from 480 to 750 nm the signal is negative. The total spectrum consists of an overlap of different spectral contributions from the excitation-induced loss of population (hole) in the electronic ground state and the created population (particle) in the first or higher electronically excited states and their transitions to higher or lower electronic states. By its similarity to the stationary fluorescence spectrum, the large negative band centered at 624 nm for delay times larger than 1 ps is assigned to stimulated emission of the particle in the S_1 state. After spectral relaxation, another negative contribution is visible centered around 500 nm. This is assigned to the bleach of the ground state absorption. The remaining positive part of the signal is assigned to absorption of the particle (excited state absorption). It is evident that for a excitation pulse energy of 0.4 µJ the signal intensity in the latter spectral region remains approximately constant over a delay time range of 100 fs - 2 ps. The same observations and assignments can be made for pump-probe spectra of DCM in acetonitrile and in chloroform.

For excitation conditions with the pump pulse centered near the maximum of the ground state absorption band, as e.g. it is the case with 470 nm excitation of DCM in strongly dipolar solvents (see 2.1.2), the excitation-induced ground state absorption bleach should remain constant in its maximum frequency and experience only spectral broadening in time. Here, it was assumed that the corresponding hole distribution relaxes faster than the instrumental response function, so that the bleach band can be viewed as constant on the timescale of measurement. The constancy of the excited state absorption and ground state absorption bleach bands enable a spectral decomposition as follows. As the fluorescence lifetime of DCM is of the order of nanoseconds in most solvents, after complete spectral relaxation the form of the stimulated emission band should be given by the stationary emission cross section. From the stationary fluorescence spectrum the cross section for emission is calculated [Ernst] and scaled upon the red edge of a pump-probe spectrum for a delay time between several picoseconds for acetonitrile to several tens of picoseconds for methanol. The stimulated emission spectrum estimated this way is subtracted from the measured transient, so that the remaining difference spectrum consists of excited state absorption and bleach of ground state absorption (Figure 4.1-2b). These contributions are convoluted in time with the instrumental response function and subtracted from the time-

resolved spectra of the measurement to yield the *time-resolved stimulated emission spectra* (Figure 4.1-2c). The interest in isolating the emission spectra lies in the possibility to compare directly with the theory of solvation dynamics and related fluorescence upconversion experiments.

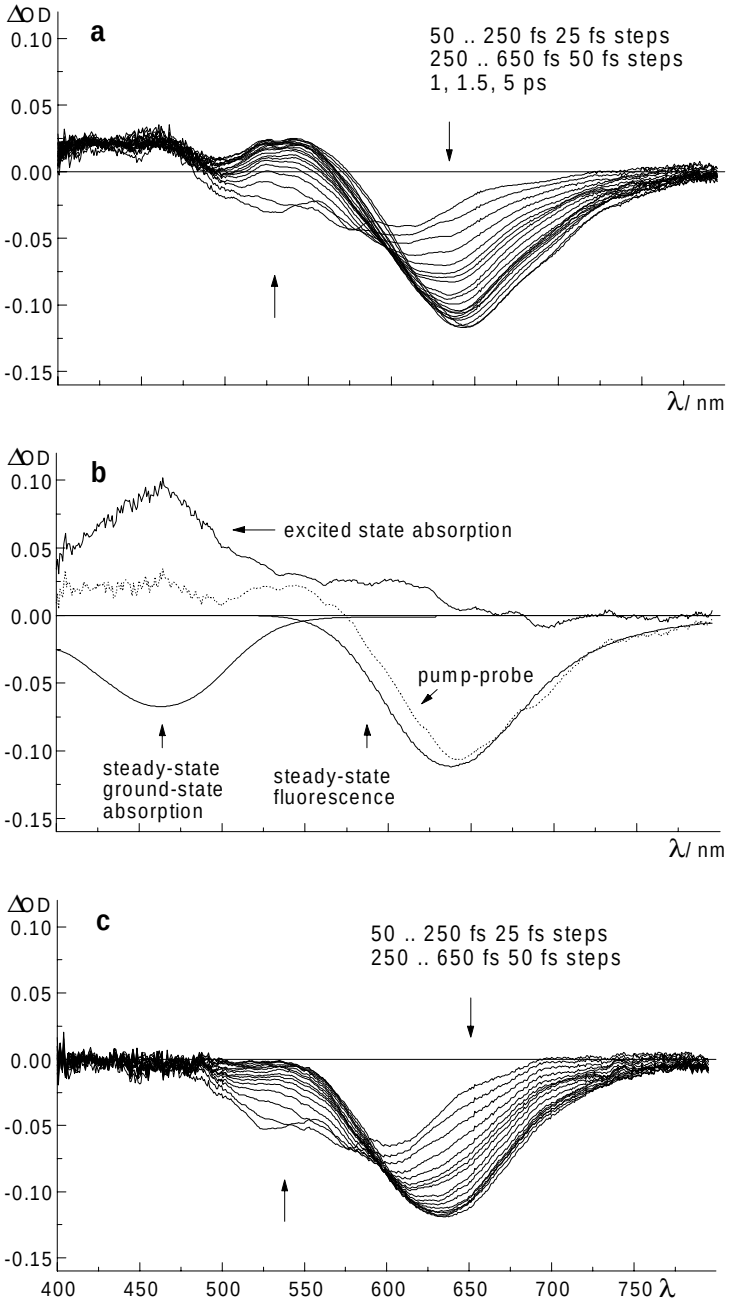

Figure 4.1-2: a) Pump-probe spectra of spectra of DCM in acetonitrile after excitation at 530 nm with 0.4 µJ excitation pulse energy. b) Spectral decomposition of the pump-probe spectra in a). The fluorescence spectrum has been converted to stimulated emission (gain). c) Isolated stimulated emission spectra obtained from the spectral decomposition.

In analogy to the decomposition of the pump-probe-spectra, the dump-probe spectra can be analyzed to achieve isolation of the transient ground state absorption spectra.

Typical *dump-probe spectra* of DCM in methanol are shown in Figure 4.1-3 a). Their form is the negative of the pump-probe spectra: stimulated emission pumping creates a hole in the excited state population and 'bleaches' excited state absorption and stimulated emission, the contributions of which now have respective negative and positive signs. The particle in the ground state contributes additional absorption (positive sign). To ensure that no excitation into higher electronic states by absorption of the dump pulse occurred, pump-probe and dump-probe spectra were compared for delay times after spectral relaxation has been completed (Figure 4.1-4), and coincidence was found.

The spectral decomposition for the dump-probe spectra was performed in a way similar to the spectral decomposition for the pump-probe spectra (Figure 4.1-3 b). The dump pulse was centered near the peak frequency of the emission spectrum of DCM in strongly dipolar solvents (see 2.1.2), so that the maximum frequency of the stimulated emission bleach should remain constant in time. It was assumed that the bleach contributions relaxed fast and were constant on the timescale of the experiment. The stationary emission cross section was scaled onto the red edge of the dump-probe spectrum after relaxation and subtracted. Further separation of the remaining sum of excited state absorption and ground state absorption was only possible under the assumption of similar transition dipole moments for ground state absorption and emission from S_1. The integrals over the corresponding bands should then be the same [Stri 62]. If the form of the relaxed ground state absorption band is given by the stationary absorption spectrum, its height can be obtained by scaling the part of its area which shows approximate mirror symmetry to the fluorescence spectrum onto the band area of the scaled emission cross section. By subtraction of the thus determined ground state absorption and stimulated emission contributions from the relaxed dump-probe spectrum, the excited state absorption spectrum was obtained (Figure 4.1-3 b). Together with the stimulated emission band it constituted the hole's contribution to the experiment. This bleach spectrum was convoluted in time with the instrumental response function and subtracted from the set of measurements to achieve isolation of the *time-resolved ground state absorption spectra*. It should be noted that a temporary isosbestic point at 537 nm is already observed in the dump-probe spectra.

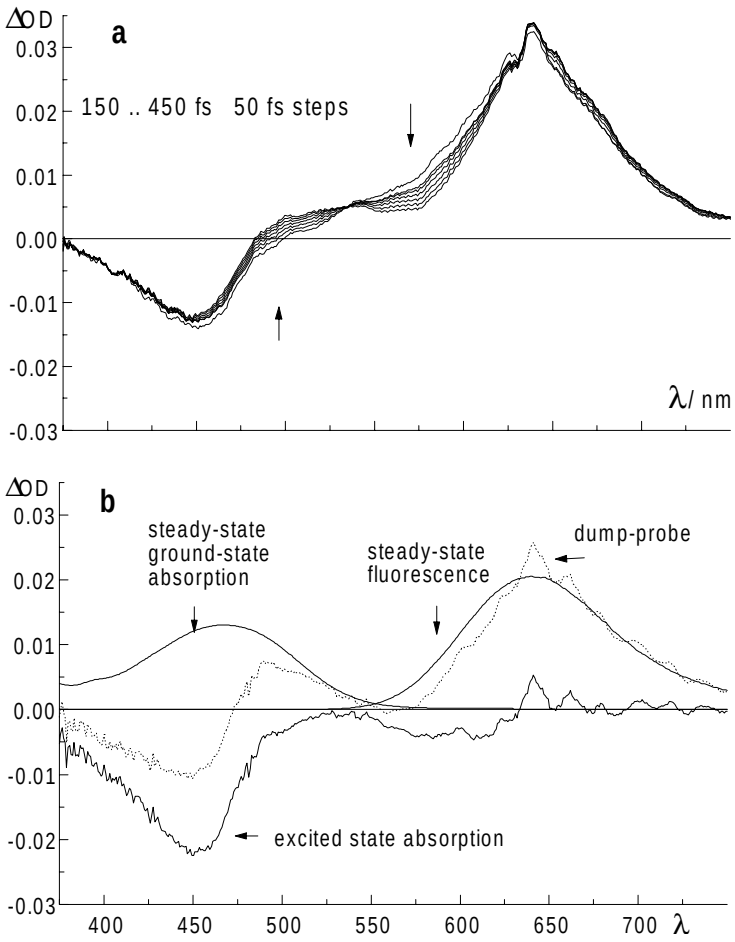

Figure 4.1-3 : a) Dump-probe spectra of spectra of DCM in methanol after stimulated emission pumping at 630 nm. b) Spectral decomposition of the dump-probe spectra in a). The fluorescence spectrum has been converted to stimulated emission (gain).

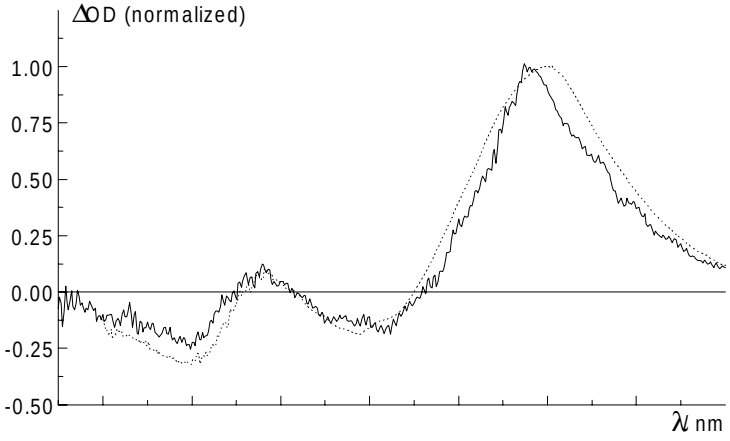

Figure 4.1-4 : Comparison of pump-probe (dashed) and dump-probe spectra (solid) of DCM in methanol at a delay time of 20 ps.

4.1.2 Spectral dynamics

4.1.2.1 Dump-probe experiments

Isolated ground state absorption ("particle") spectra of DCM in *methanol* are presented in Figure 4.1-5. Negative contributions to the differential optical density and the spike at 649 nm stem from an imperfect subtraction of the "hole" spectrum and from stray light by the dump pulse, respectively. For delay times within the response function width of the experimental set-up, the absorption spectrum starts to rise at time zero centered above 600 nm and shifts during its rise to approximately 565 nm (Figure 4.1-5 a). The subsequent spectral relaxation proceeds via the growth of a shoulder on the blue side of the absorption maximum and a decay on its low-energy side up to 400 fs, exhibiting a temporary isosbestic point at 537 nm (Figure 4.1-5 b). Until about 10 ps, the absorption band moves to the blue (Figure 4.1-5 c).

Isolated absorption spectra of DCM in *acetonitrile* are shown in Figure 4.1-6. The initial spectra around time zero are also centered at about 633 nm and shift during their rise-time to approx. 577 nm (Figure 4.1-6 a). After 100 fs they still show some structure, which is lost during the next 150 fs. On this timescale, the rise of a blue shifted shoulder and a decay of the low-energy side of the absorption band take place, similar to the spectral evolution in methanol. For acetonitrile the high-energy shoulder is centered around 500 nm, and an isosbestic point is observed at 519 nm. For later delay times up to around 1.5 ps, the isolated absorption spectrum shifts further to the blue and grows slightly (Figure 4.1-6 c).

For DCM in *propylene carbonate* the relaxation for 120-300 fs (Figure 4.1-7 b) parallels that in methanol and acetonitrile, with a decay on the low-energy side of the absorption spectrum, and a rise on the higher energy side. The isosbestic point is found at approx. 558 nm. In the course of the following 15 ps (Figure 4.1-7 c), the absorption band maximum shifts from approx. 545 nm to the position of the stationary absorption spectrum and decreases in amplitude.

It is interesting that a second, weaker absorption band with maxima at 375 nm and 393 nm in acetonitrile and 377 nm and 398 nm in propylene carbonate remains constant after the initial rise.

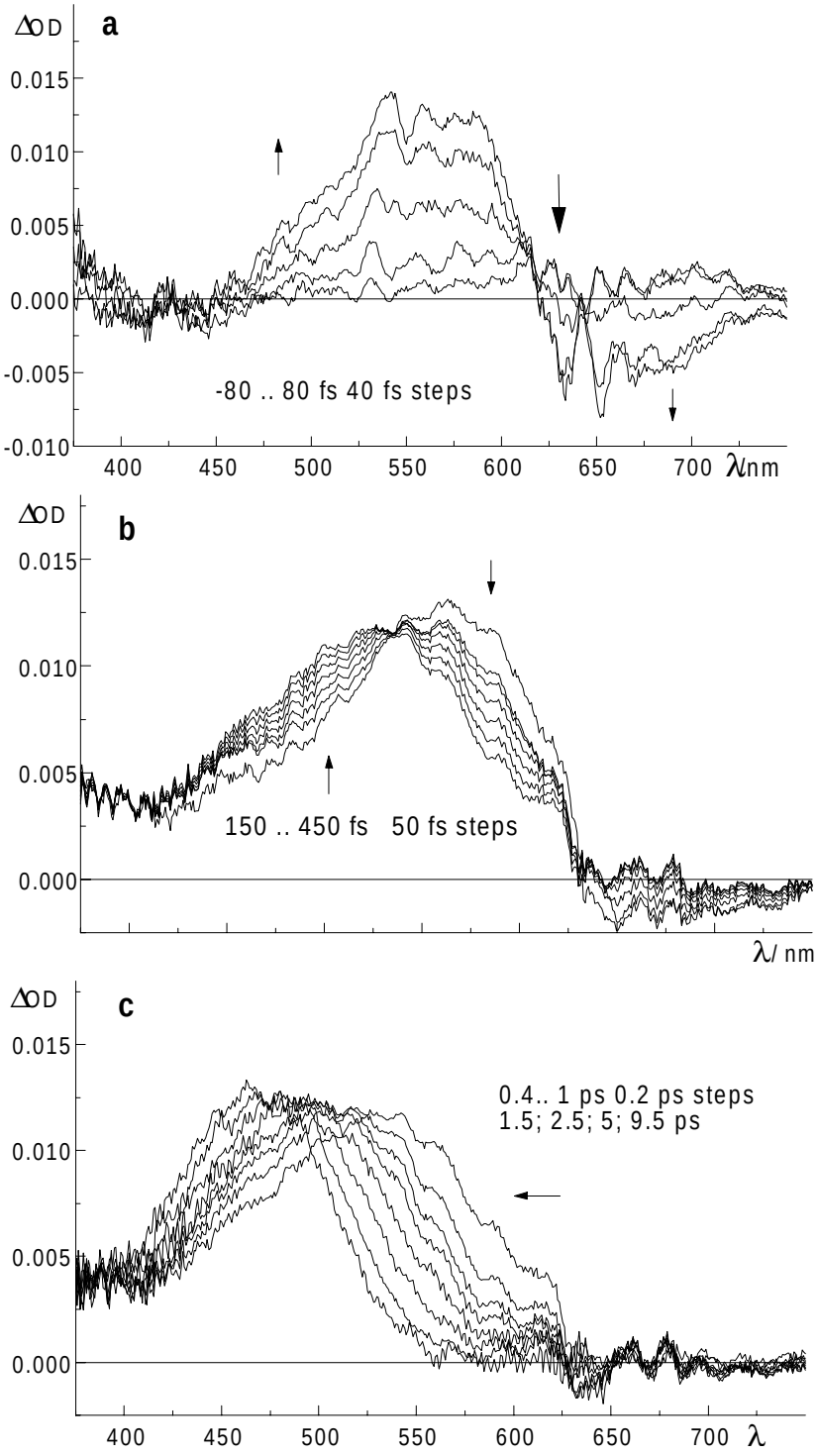

Figure 4.1-5 : Isolated absorption spectra of DCM in methanol for different delays after stimulated emission pumping at 630 nm (dump wavelength indicated by large arrow in a).

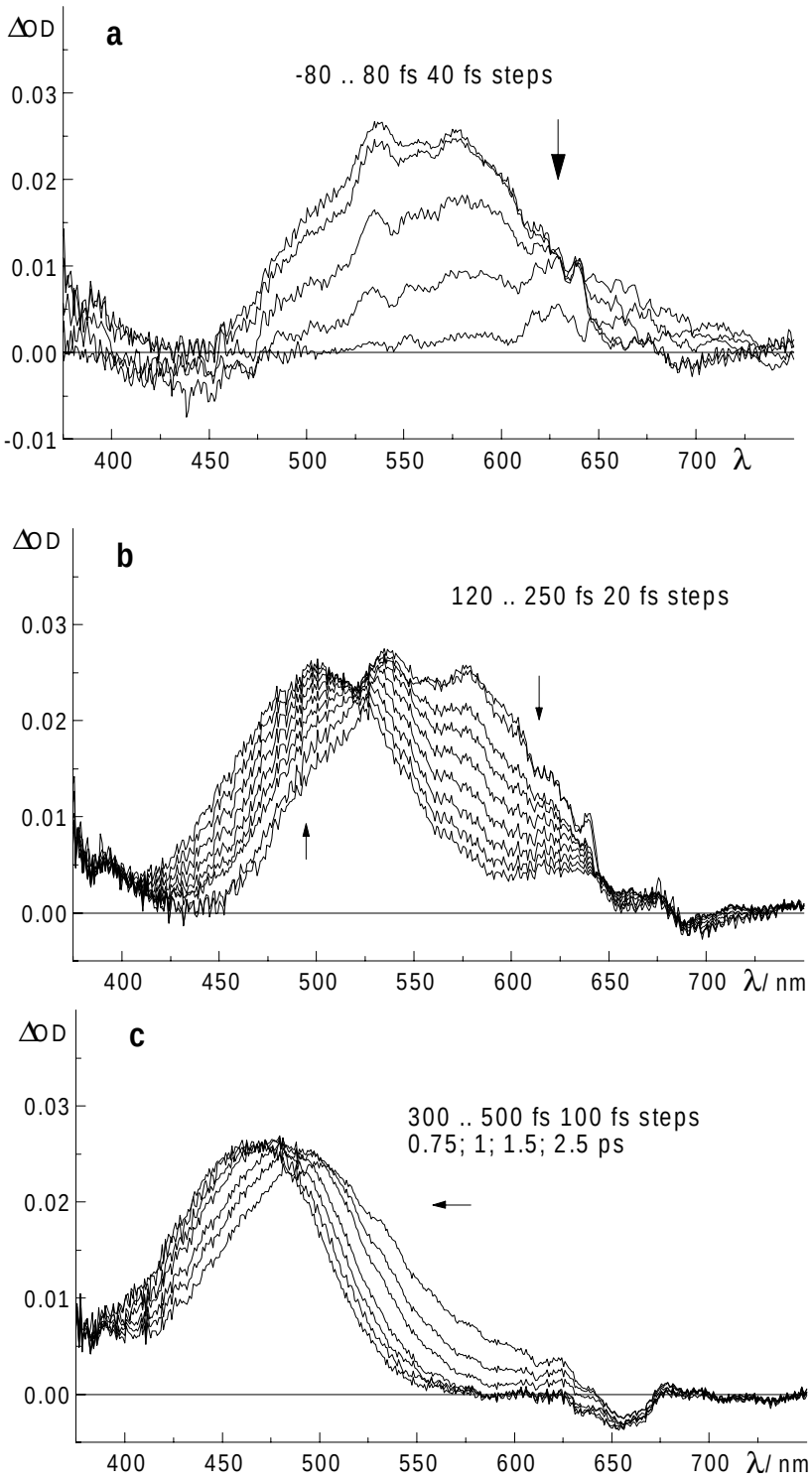

Figure 4.1-6: Isolated absorption spectra of DCM in acetonitrile for different delays after stimulated emission pumping at 630 nm (indicated by large arrow in a).

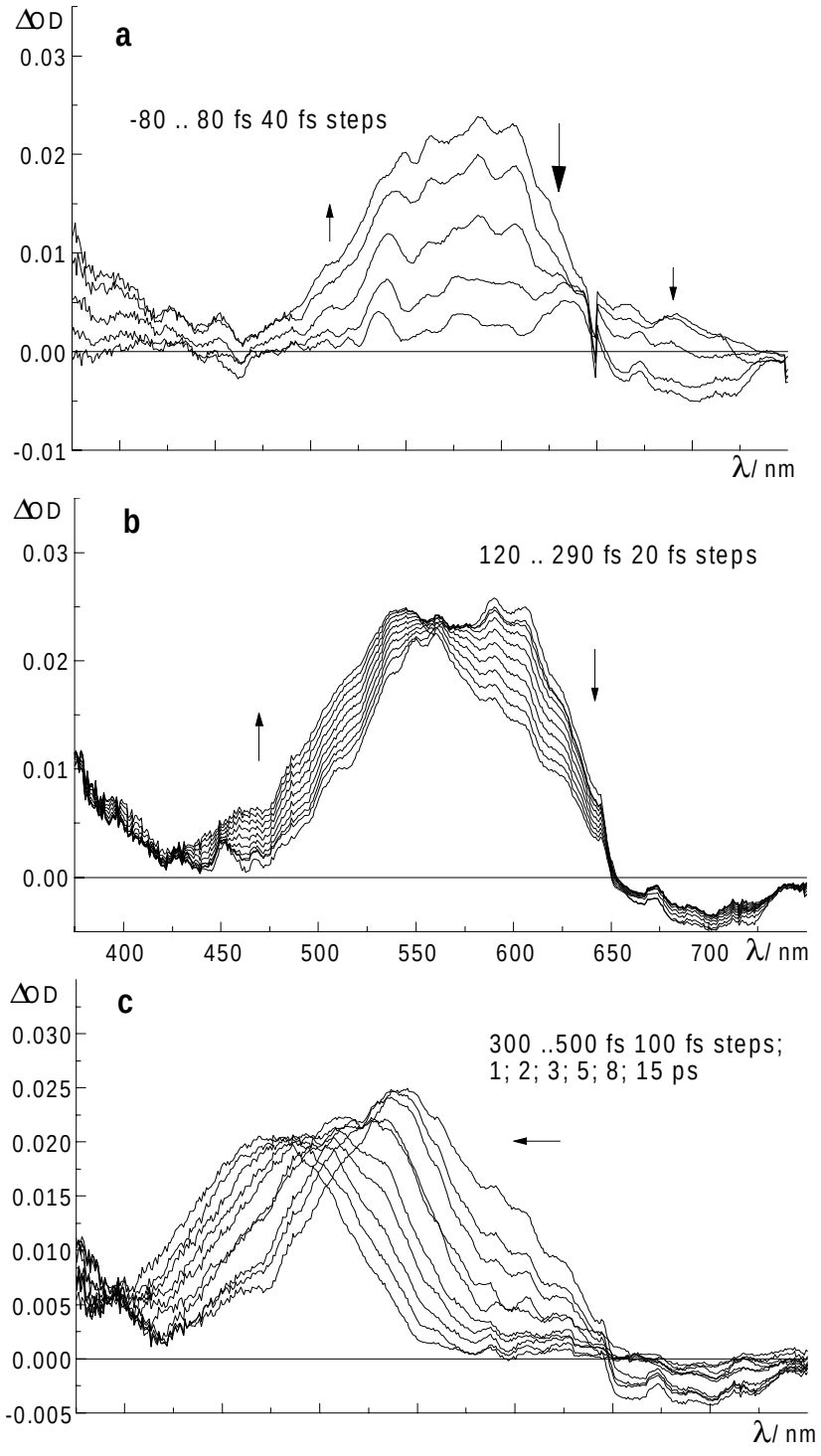

Figure 4.1-7 : Isolated absorption spectra of DCM in propylene carbonate for different delays after stimulated emission pumping at 630 nm (indicated by large arrow in a).

4.1.2.2 Pump-probe experiments

Isolated stimulated emission spectra of DCM in *methanol* are shown in Figure 4.1-8 and Figure 4.1-9 a) for an excitation wavelength of 530 nm and an excitation energy of 0.4 µJ. The initial spectra are highly structured (Figure 4.1-8). Over the first 600 fs (Figure 4.1-9 a), a blue shifted shoulder of the main fluorescence band centered approximately at 530 nm disappears, while the main band around 600 nm grows. For longer delay times up to 8 ps, the emission band exhibits a further slight growth and a spectral red shift (not shown). For comparison, Figure 4.1-9 b) shows the spectral evolution of the emission over the same timescale as in a) but for an excitation pulse energy of 0.8 µJ. Instead of a shoulder, another emission band centered at approx. 505 nm declines in amplitude while the band centered at 630 nm grows. This growth continues with a smaller amplitude accompanied by a red shift until about 10 ps (Figure 4.1-10). Spikes as well as positive spectral contributions remaining constant in the course of time are the consequence of the inexact subtraction procedure to isolate the emission bands and should be ignored.

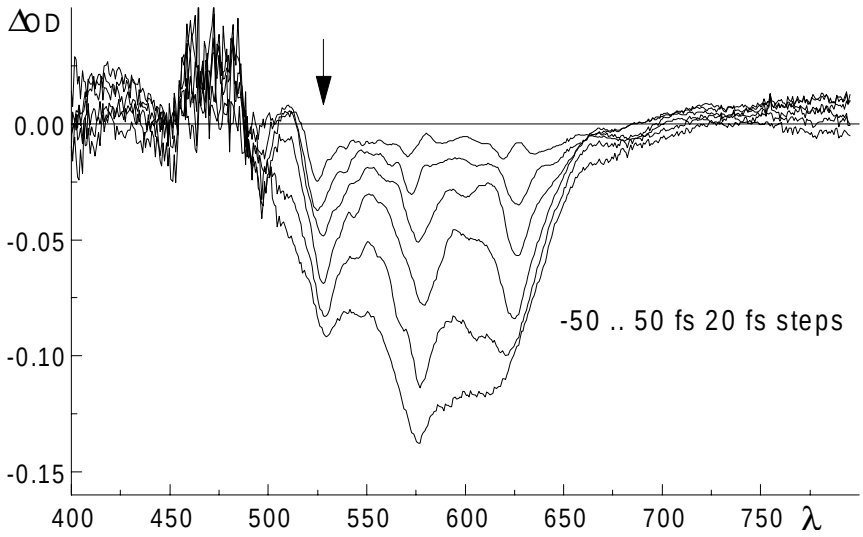

Figure 4.1-8: Early isolated stimulated emission spectra of DCM in methanol after excitation at 530 nm with 0.4 µJ excitation pulse energy. The excitation wavelength is indicated by an arrow.

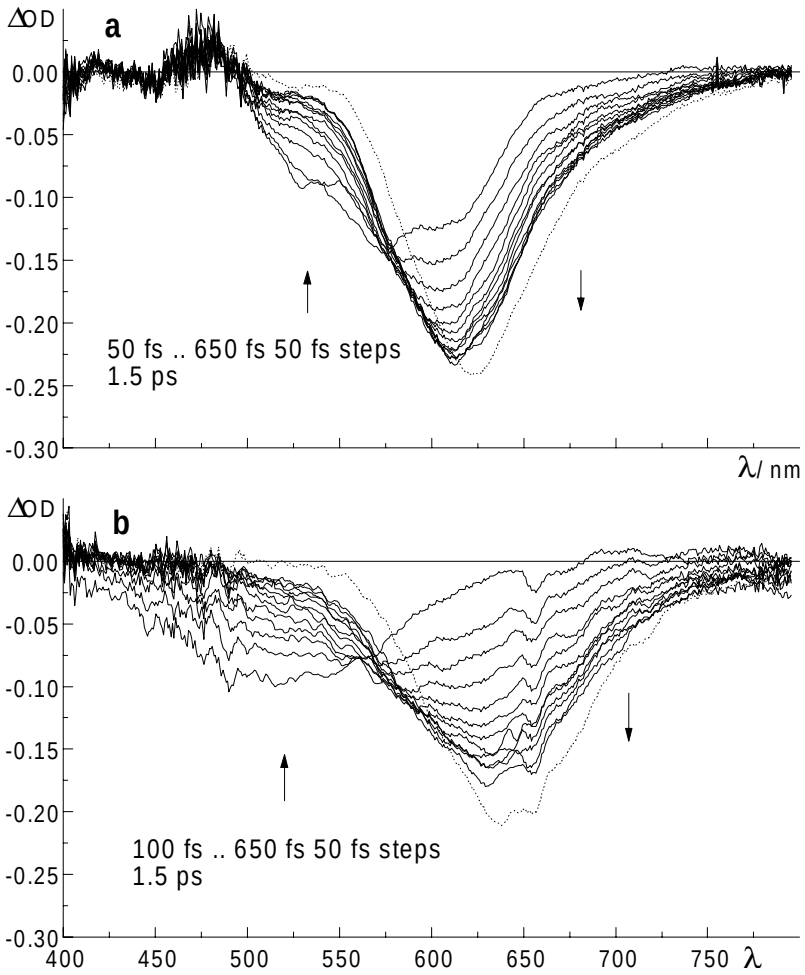

Figure 4.1-9: Isolated stimulated emission spectra of DCM in methanol for different delays after excitation at 530 nm a) with 0.4 µJ excitation pulse energy, b) with 0.8 µJ exc. pulse energy.

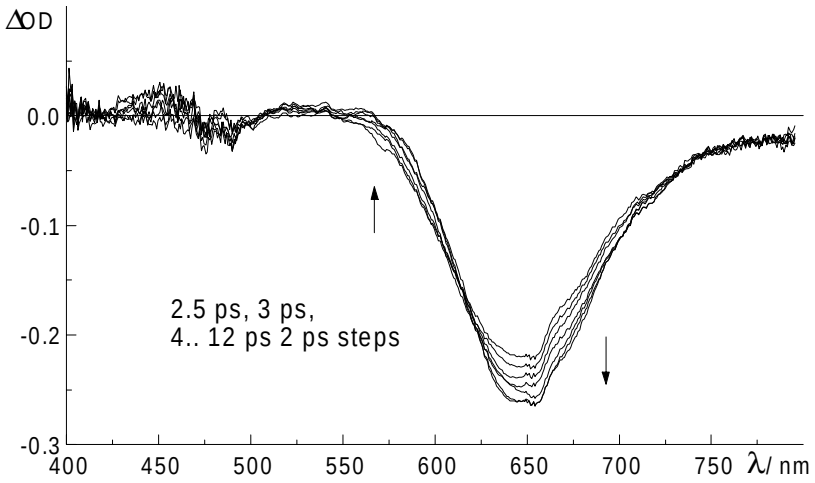

Figure 4.1-10: Isolated stimulated emission spectra of DCM in methanol for different delays on a picosecond timescale after excitation at 530 nm with 0.8 µJ excitation pulse energy.

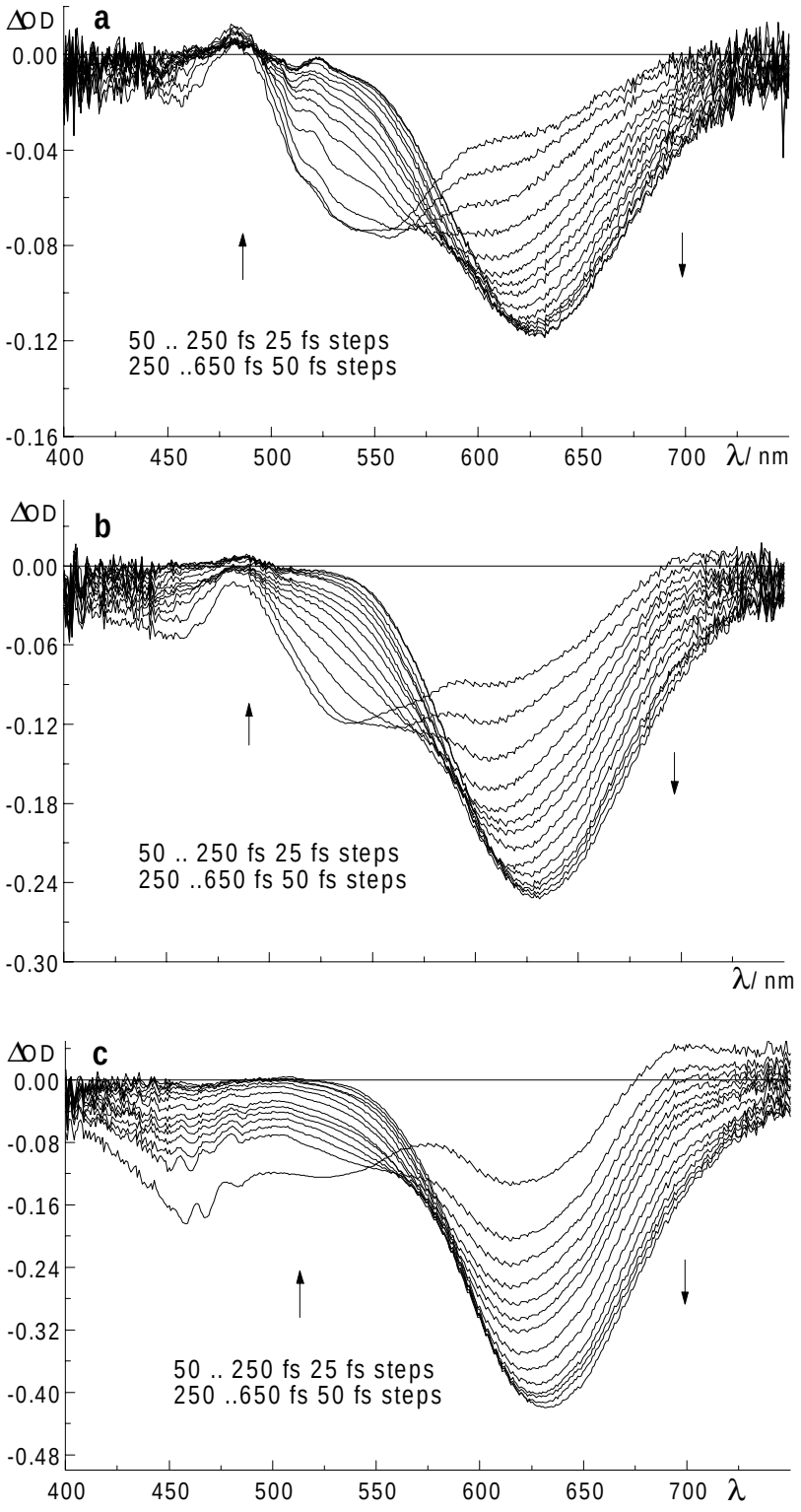

Figure 4.1-11: Isolated stimulated emission spectra of DCM in acetonitrile for different delays after excitation at 470 nm with a) 0.2 µJ excitation pulse energy, b) 0.4 µJ exc. pulse energy, c) 0.9 µJ exc. pulse energy.

Isolated emission spectra of DCM in *acetonitrile* during the first 650 fs are presented in Figure 4.1-11 for excitation at 470 nm and pump energies of 0.2, 0.4 and 0.9 µJ. While the maximum amplitude of the stimulated emission scales linearly with excitation energy (excluding saturation), the fraction of the emission band subject to a delayed rise increases in the course of figures a) to c). For the lowest excitation pulse energy (Figure 4.1-11 a), there is spectral evolution mainly from 495 nm onwards. An emission shoulder centered at approx. 540 nm decays, whereas the main band centered at 620 nm grows. For the intermediate excitation pulse energy, another band at 460 nm decays simultaneously with that centered at 540 nm. For the highest excitation pulse energy (Figure 4.1-11 c) only one band centered at 464 nm decays parallel to the rise of the band centered at 620 nm. The red shift of the rising fluorescence band is most pronounced for the lowest excitation pulse energy and declines with increasing excitation energy. Within the next picosecond, the 620 nm emission band continues to shift towards lower frequencies and grow slightly for all pump energies (shown in Figure 4.1-12 for excitation conditions as in Figure 4.1-11 b) and c).

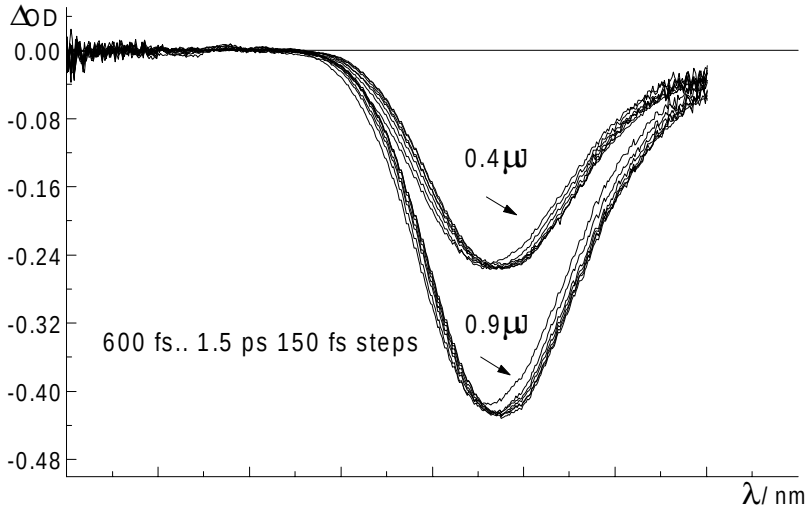

Figure 4.1-12: Isolated stimulated emission spectra of DCM in acetonitrile for different delays on a picosecond timescale after excitation at 470 nm with excitation energies of 0.4 and 0.9 µJ.

For the less polar solvents investigated (chloroform, toluene, tetrachloromethane and cyclohexane) the separation of the emission bands was not straightforward. Due to a large relative amplitude of the excited state absorption, the scaling of the stationary emission spectrum onto the red edge of the relaxed pump-probe spectrum often gave unsatisfactory

results. Therefore, for these solvents the pump-probe spectra will be discussed instead of the isolated emission spectra.

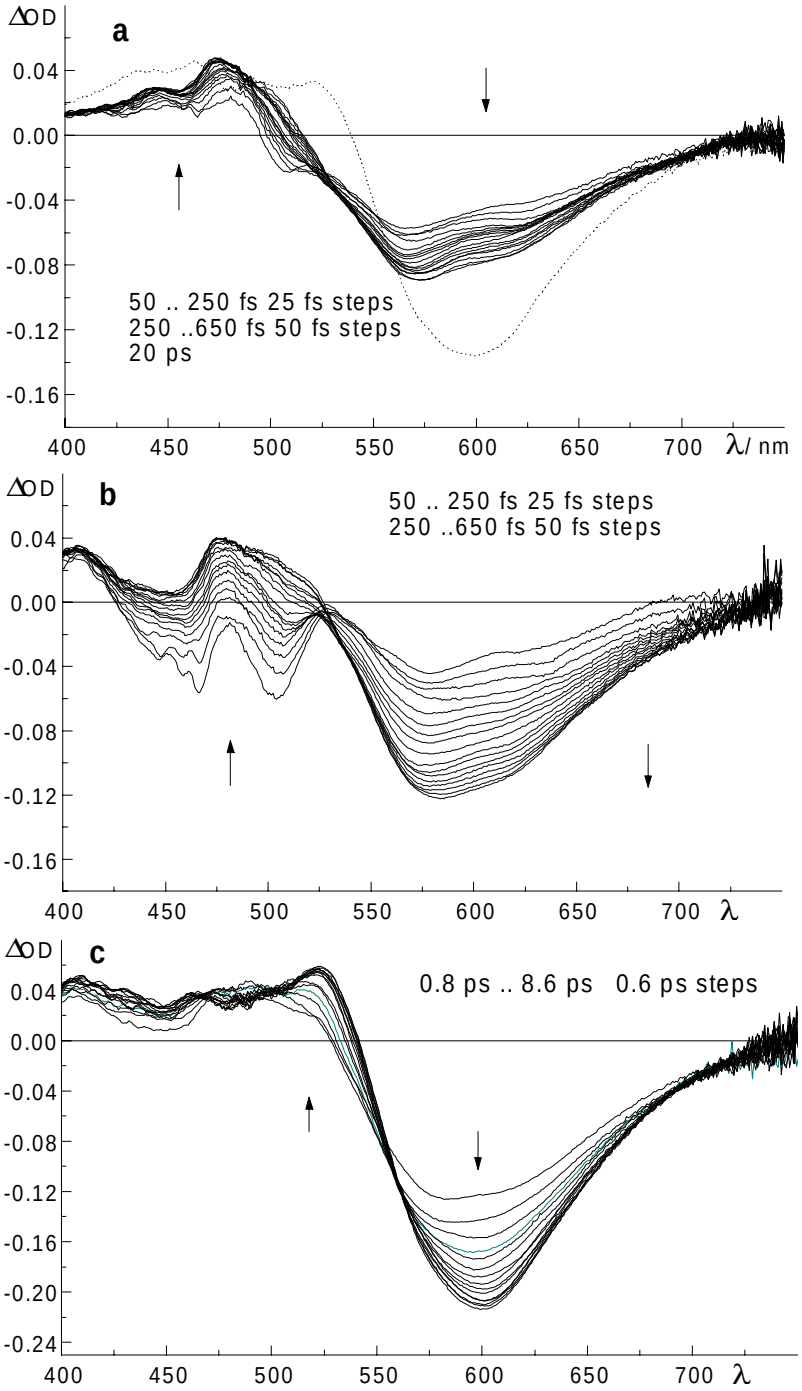

Figure 4.1-13: Pump-probe spectra of DCM in chloroform for different delays after excitation at 470 nm : a) with 0.4 µJ excitation pulse energy; the dotted curve indicates the spectrum after 20 ps, b) with 0.8 µJ exc. pulse energy, c) with 0.8 µJ exc. pulse energy on a picosecond timescale.

Pump-probe spectra of DCM in *chloroform* for excitation at 470 nm and two different pump pulse energies (0.4 and 0.8 µJ) are presented in Figure 4.1-13. The evolution in the first 250 fs is clearly dominated by changes in the stimulated emission or the bleach band. For higher excitation energy two bands centered at 465 and 505 nm disappear, while a broader emission band centered at 580 nm grows in (Figure 4.1-13 b). In the lower excitation energy measurement, these bands are recognizable as a shoulder at 507 nm and a small spike at 464 nm, which also vanish, while the broad, dominant emission band at 575 nm increases in amplitude (Figure 4.1-13 a). If these changes were due to a decrease of the ground state bleach, there is no physical reason why the stimulated emission band should grow simultaneously, so that as for the more polar solvents they are ascribed to emission dynamics. For longer delay times up to 20 ps (Figure 4.1-13 a) and c), the emission band keeps growing and shifts from 580 nm to 604 nm. In Figure 4.1-14, pump-probe spectra of DCM in chloroform after 530 nm excitation with 0.7 µJ excitation energy are presented for the same timescale as in Figure 4.1-13 a) and b). The spectral evolution is similar to that in Figure 4.1-13 b), but the decaying blue shifted emission bands are now centered at 495 and 527 nm, while the rising band is still centered around 585 nm.

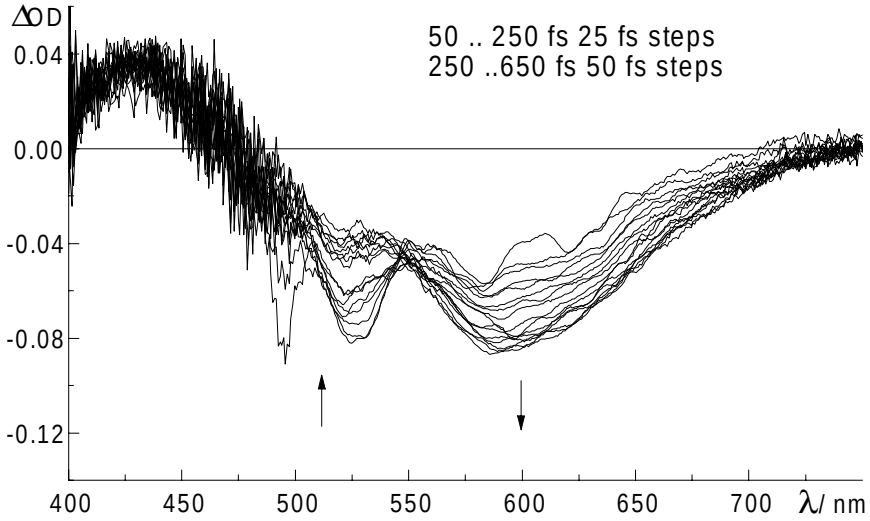

Figure 4.1-14 : Pump-probe spectra of DCM in chloroform for different delays after excitation at 530 nm with 0.7 µJ excitation pulse energy.

Figure 4.1-15 a) and b) give two examples for the time-dependendent changes of the differential optical density of DCM in *toluene* and for their dependence on excitation

energy. The two sets of spectra were measured with excitation energies of 0.7 and 1.4 µJ, respectively, and with an excitation wavelength of 450 nm. The initial structure (with emission maxima as indicated in the figures) broadens or disappears mostly within the first 250 fs. The emission (the same argumentation for the assignment of spectral changes as for chloroform applies) decreases below approx. 530 nm and increases above this wavelength. The relative amplitude of the emission showing a delayed rise is larger for higher excitation energy, as it was found for the other solvents. On a longer timescale of up to 20 ps, the spectral evolution continues in a similar way, but more slowly than for the first hundreds of femtoseconds (Figure 4.1-16). The isosbestic region is transferred from approx. 517 nm to around 527 nm.

Pump-probe spectra of DCM in *tetrachloromethane* for three different excitation energies and for the first 250 fs are shown in Figure 4.1-17. The ratio between the two maxima of the excited state absorption bands at 482 and 516 nm changes with increasing excitation pulse energy in favour of the latter. Also the excited state absorption in the region above 545 nm is dominant when compared to the stimulated emission for higher pump energies, yielding positive differential optical densities. These tendencies can also be found for DCM in toluene, and spectral evolution on the short timescale is the same as described for this solvent.

The time-dependent changes of differential optical density in the pump-probe spectra of DCM in *cyclohexane* parallel those in tetrachloromethane and toluene (Figure 4.1-18), with the difference that a very fast decay component of the high-energy side of the spectrum is not accompanied by a rise in the region above 535 nm.

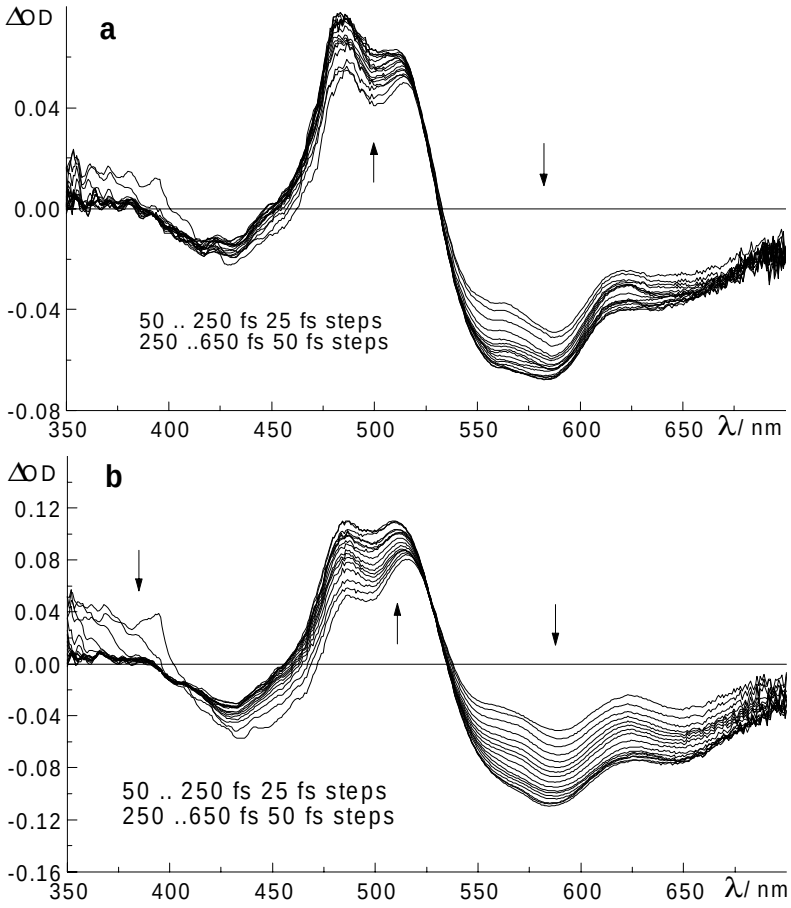

Figure 4.1-15: Pump-probe spectra of DCM in toluene for different delays after excitation at 450 nm with a) 0.7 µJ excitation pulse energy, b) 1.4 µJ exc. pulse energy.

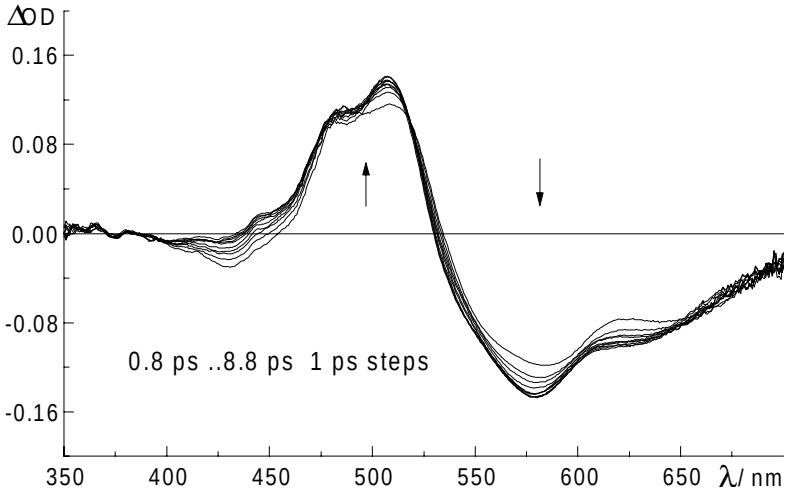

Figure 4.1-16: Pump-probe spectra of DCM in toluene for different delays on a picosecond timescale after excitation at 450 nm with 1.4 µJ excitation pulse energy.

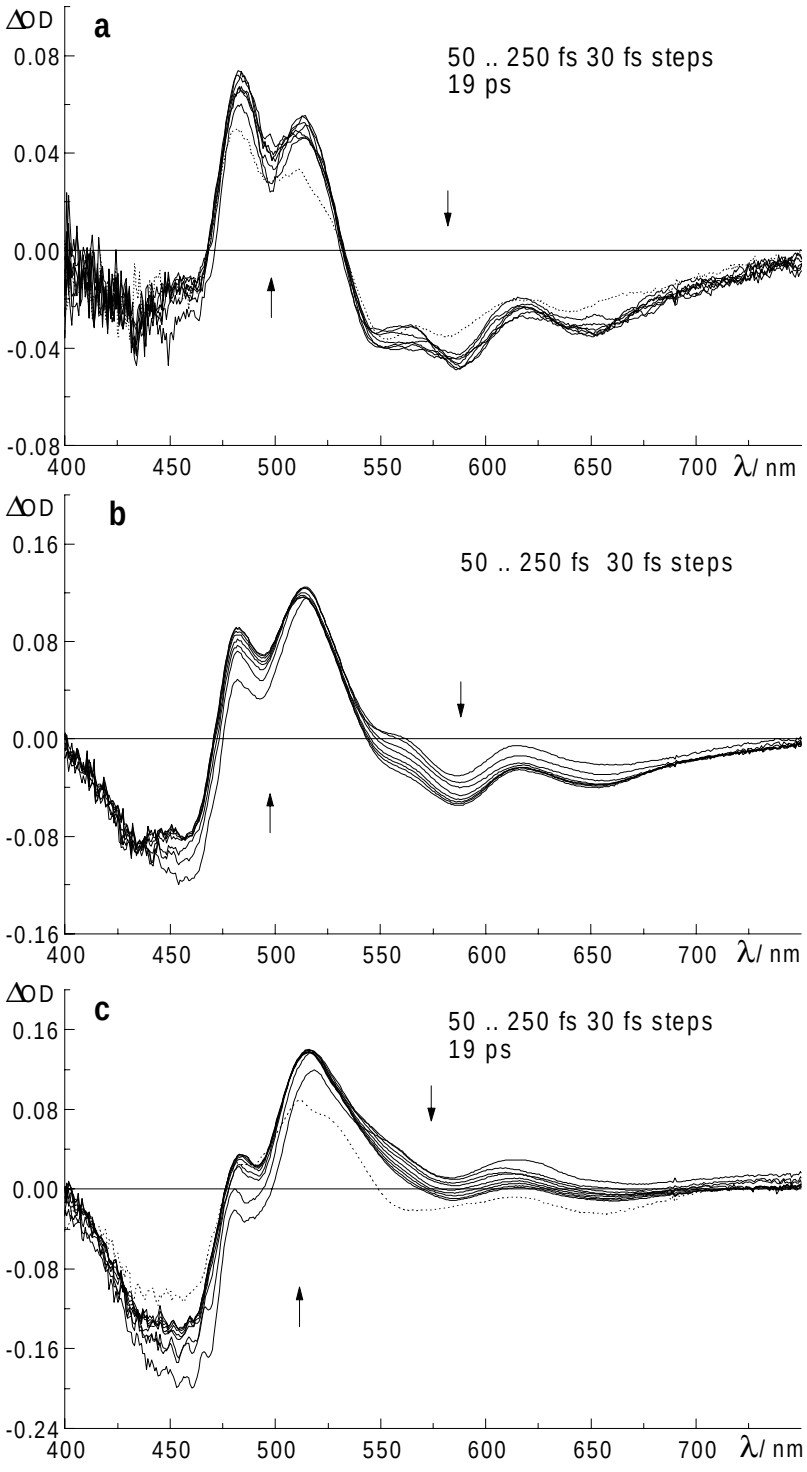

Figure 4.1-17: Pump-probe spectra of DCM in tetrachloromethane for different delays after excitation at 450 nm with a) 0.3 µJ excitation pulse energy, b) 0.6 µJ exc. pulse energy, c) 0.9 µJ exc. pulse energy.

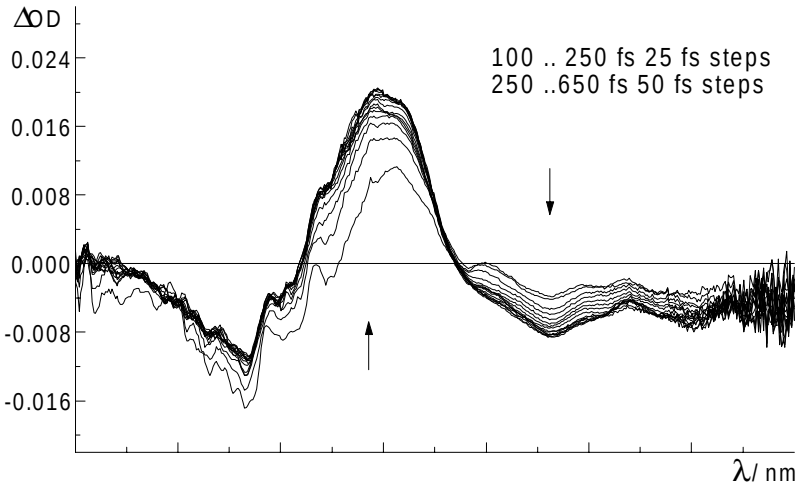

Figure 4.1-18 : Pump-probe spectra of DCM in cyclohexane for different delays after excitation at 450 nm with 0.8 µJ excitation pulse energy.

4.1.3 Dynamic Stokes shift

The broad emission and absorption bands of chromophores in solution can empirically be described by *lognormal line shape* functions g (ν) [Sian 69]:

$$g(\nu) = \begin{cases} g_0 \exp\left(-\ln(2) \left(\frac{\ln\left[1 + 2b(\nu - \nu_0) / \Delta\right]}{b} \right)^2 \right) & \text{for } 2b(\nu - \nu_0) / \Delta > -1 \\ 0 & \text{for } 2b(\nu - \nu_0) / \Delta \leq -1 \end{cases}$$

(4.1)

where g_0 is the amplitude, ν_0 is the maximum frequency, b is the asymmetry and Δ is the width of the spectral distribution. The lognormal lineshape is essentially that of an asymmetric Gaussian. This function can be made use of to model absorption and emission bands, as long as their shape is not complicated by structure [Mar 87]. It was applied to the isolated time-resolved emission and absorption spectra with nonlinear least-squares fitting, using a Simplex search method. Any (sub)structure of the absorption and emission bands was ignored. The time evolution of the maxima and width of the spectral bands can then be extracted from the function parameters, either directly from ν_0 and Δ or by calculating the

first and second moment of the distribution from b, ν_0 and Δ [Bult].

It has been stated [Horng 95] that the peak frequency ν_0 is better reproducible than the average frequency, so that here ν_0 is chosen to describe the energetic evolution of the spectra. The spectral width was found to be far more sensible to noise, systematic errors and deviations from different days of experiment than the peak frequency and is therefore not discussed further. The *spectral response function* $S_{\square E}(t)$ was calculated from ν_0 (t) according to equation 2.27, where the values for ν_0 for infinite time were taken from the stationary absorption or emission spectra. The peak values of the spectra at zero time were estimated from the measured spectra for the pump-probe experiments. A time-zero analysis such as in [Horng 95] failed, because the measured peak frequencies of the stimulated emission for early delay times are higher than those obtained by applying their time-zero analysis (17100 versus 16240 cm^{-1} for acetonitrile). For the dump-probe measurements, no time-zero analysis was possible because of the reduced width of the emission spectra in strongly dipolar solvents compared to those in methyl butane, and the peak values of the spectra at zero time were estimated from the dump pulse wavelength.

Figure 4.1-19 shows the spectral response function of DCM in *acetonitrile* (circles), obtained from spectral evolution of the solute in the excited state and in the ground state. Also displayed (straight line) is a fit to the spectral response function from fluorescence upconversion investigations of the relaxation of coumarin 153 in its first singlet excited state by Horng et al. [Horng 95]. There is good agreement between the data from different methods and molecules for delay times from 0.4 ps onwards. For earlier delay times the curves differ, the values for DCM exhibiting a kind of plateau up to 100 fs and declining steeply afterwards. The limited time resolution of approximately 120 fs in the dump-probe and of appr. 60 fs in the pump-probe experiments forbids the interpretation of the very early dynamics.

For the response function after stimulated emission pumping of DCM in *propylene carbonate* as presented in Figure 4.1-20, good agreement with the spectral response from coumarin 153 is noted from approx. 0.6 ps onwards.

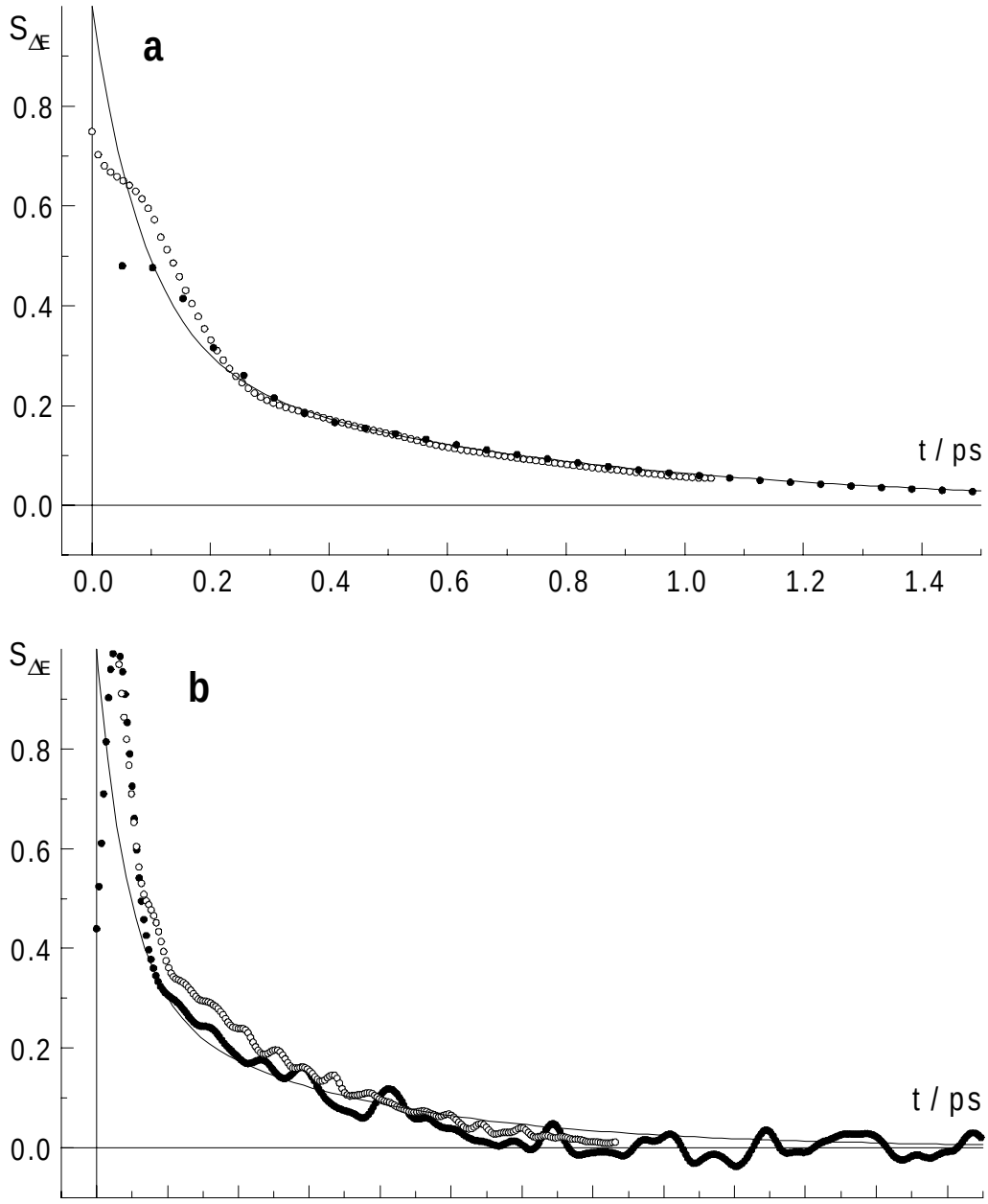

Figure 4.1-19 : Spectral (or solvent) response function $S_{\Delta E(t)}$ of DCM in acetonitrile calculated from the peak frequency ν_0 of a) isolated transient ground state absorption spectra (solid and hollow symbols refer to different dump-probe measurements) b) isolated stimulated emission spectra (solid and hollow symbols refer to different pump-probe measurements). Also shown (solid lines) is a fit to the spectral response function of coumarin 153 from fluorescence spectra in acetonitrile [Horng 95].

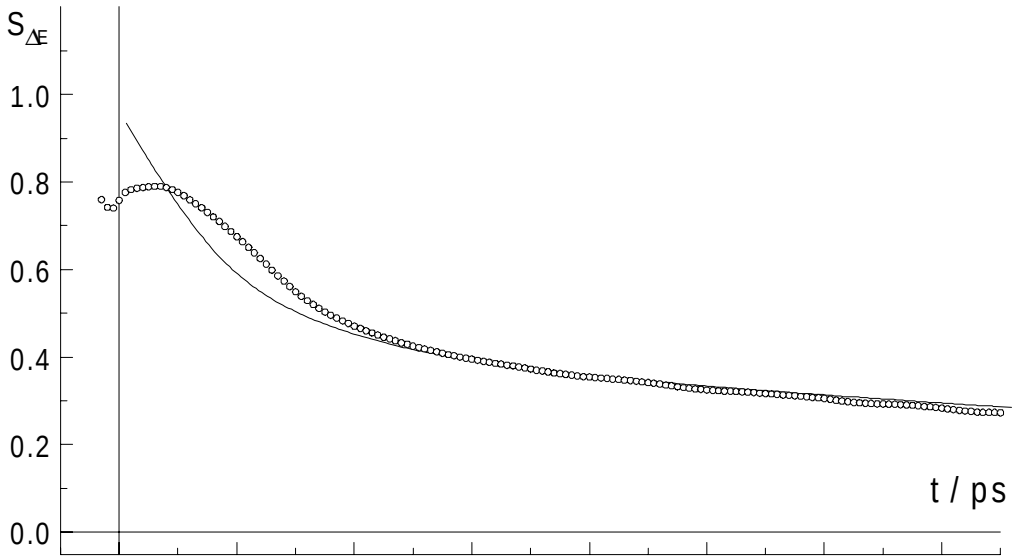

Figure 4.1-20 : Spectral response function $S_{\Delta E(t)}$ of DCM in propylene carbonate from the peak frequency ν_0 of isolated transient ground state absorption spectra. Also shown (solid line) is a fit to the spectral response function of coumarin 153 from fluorescence spectra in propylene carbonate [Horng 95].

The rigid coumarin 153 has been considered an ideal probe molecule for solvent dynamics, although very recently evidence was also given for intramolecular relaxation processes [Mühl 99a]. The deviation manifested in all strongly dipolar solvents for early times could be traced to the fact that [Horng 95] chose an average to calculate $S_{\Delta E}(t)$ from the first moment and the peak frequency of the fluorescence quantum distribution (not converted to cross section), whereas here the peak frequency of the stimulated emission or absorption band was used. It could also be due to intramolecular relaxation of either molecule. The latter hypothesis is supported for DCM by the fact that the early spectral dynamics in the excited state are characterized by the presence of several emission bands, and in the ground state by the rise and decay of shoulders of the structured absorption band. As a consequence, to model the early spectra correctly a sum of several lineshape functions would have to be employed. The good agreement of the spectral response functions of DCM and coumarin 153 for times above 0.4-0.6 ps is interpreted in the sense that solvent dynamics dominate the spectral evolution of both molecules on this timescale.

In Figure 4.1-21, the evolution of a normalized integrated *intensity correlation function* $S_{\square}(t)$ calculated from the total intensity (see 4.1.4) of the measured dump-probe spectra analogously to the spectral response function, is compared *to* $S_{\square E(t)}$ and demonstrates their similar relaxation. This indicates a variation of the transition moment or of the population of the emitting state (see 4.1.4., 5.1) with solvent relaxation, without influence on the emission bandshape.

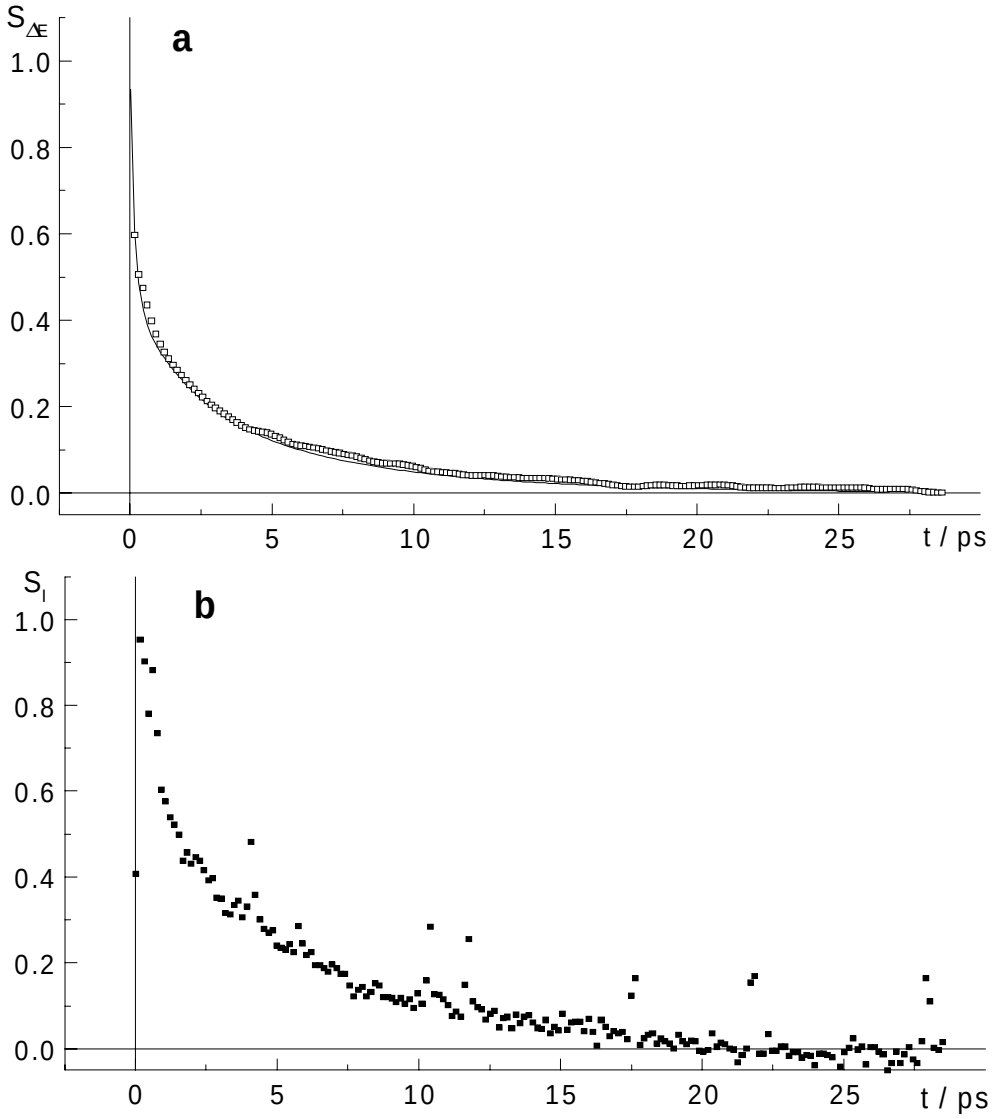

Figure 4.1-21: a) As in Figure 4.1-20, but for a picosecond timescale. b) Intensity correlation function $S_{\square(t)}$ of dump-probe spectra of DCM in propylene carbonate.

4.1.4 Total intensity

The intensity of a spectral band in a pump-probe or dump-probe experiment is given by its integrated amplitude (divided by frequency to correct for the explicit frequency dependence of the absorption and stimulated emission cross section):

$$A = \int \frac{\Delta \text{ OD } (\tilde{\nu})}{\tilde{\nu}} d\tilde{\nu} = \int \frac{\Delta \text{ OD } (\lambda)}{\lambda} d\lambda \qquad (4.2)$$

It is proportional to the population of the electronic state from which the transition occurs, and to the electronic transition moment [Lip 68, Tom 91], see also 5.1, and is therefore an indicator for state-to-state dynamics. The integral over the complete measured time-dependent spectra was calculated for delay times up to 2 ps, to see whether and how the observed spectral dynamics are reflected in the total intensity evolution.

Some time-dependent areas of the *pump-probe spectra* for different solvents are diplayed in Figure 4.1-22 b). The integration range was 350-750 nm for the nonpolar solvents (cyclohexane, tetrachloromethane and toluene), and 400-800 nm for all the others. The area decreases by 10-50% in the course of the first 500 fs due to the delayed rise of part of the stimulated emission band for all solvents. The intensity changes are largest in methanol and least pronounced in chloroform.

The curves were fitted to a sum of an instanteneously and a more slowly exponentially rising component with a negative total amplitude, convoluted with the instrumental response function (a Gaussian with a width of 60 fs). The time coefficients for the slow rise are listed in Table 4.1.1 and Table 4.1.2 under "bandintegral / pump-probe", with the amplitude ratio between the two rising components indicated in brackets. Also shown are the excitation energies for the measurements. While the values from different experiments vary over a range of approx. 0.18 ps, the average time coefficient is nearly solvent-independent around 0.2 ps.

For all solvents, the relative amplitude of the slowly rising component increased with excitation pulse energy in consecutive experiments, exemplarily demonstrated in Figure 4.1-23 for methanol.

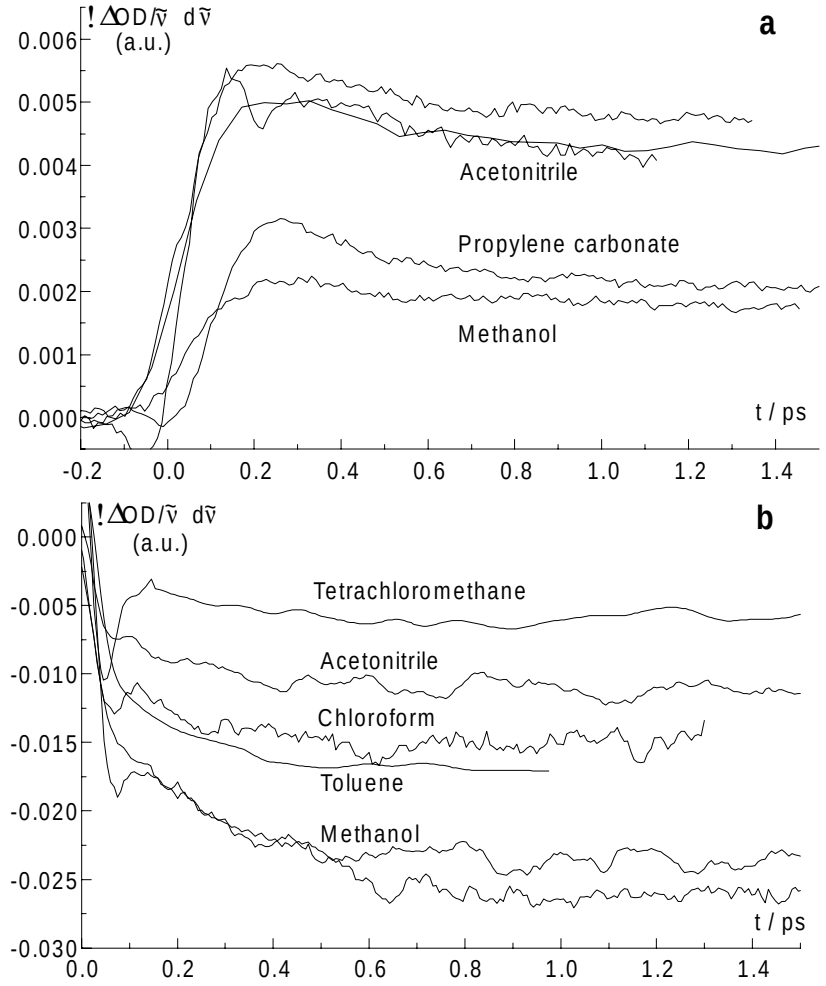

Figure 4.1-22: Total intensity of a) dump-probe b) pump-probe spectra of DCM in different solvents and for several measurements.

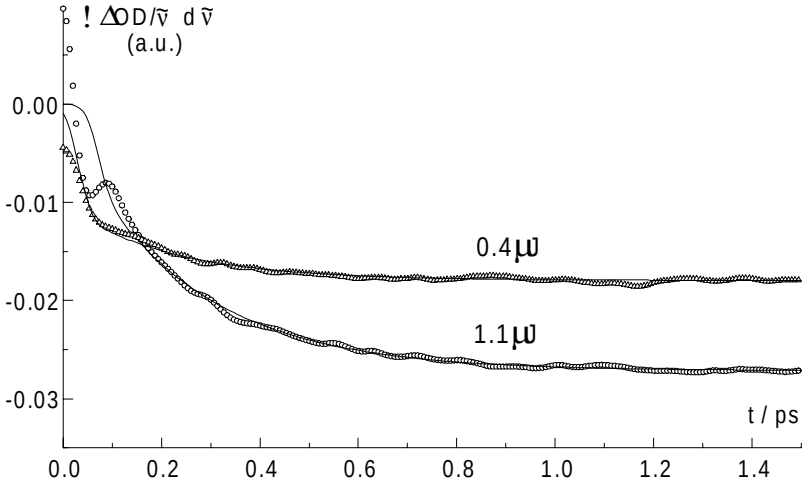

Figure 4.1-23 : Total intensity of pump-probe spectra of DCM in methanol (symbols) and fits (solid lines) for different pulse energies (excitation at 470 nm).

Apart from acetonitrile, where it increases with excitation pulse energy (Figure 4.1-24), no correlation of the time coefficients with any experimental parameter could be found. From linear regression a relative amplitude of 0.26 of a fast decay with τ = 0.09 ps in acetonitrile is extrapolated in the limit of zero excitation energy, with correlation coefficients of 0.87 for the amplitude fraction and 0.92 for τ.

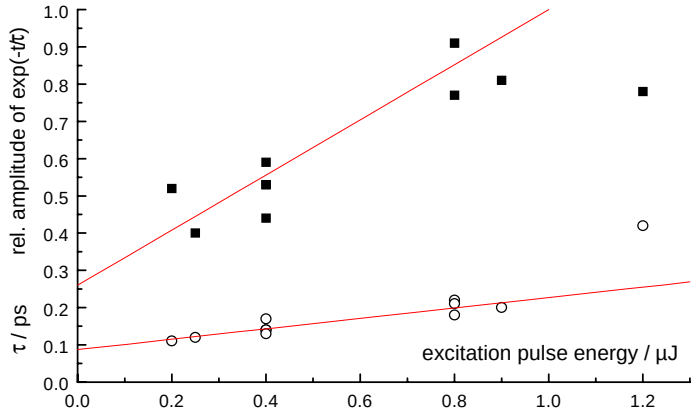

Figure 4.1-24: Amplitude fraction of exponential decay of the total intensity of pump-probe spectra of DCM in acetonitrile (solid squares) and its time coefficient τ in ps (hollow circles) on the same axis as a function of excitation pulse energy.

The time-dependent area of the *dump-probe spectra* integrated over the range of 390-780 nm is displayed in Figure 4.1-22 a) for the solvents acetonitrile, methanol and propylene carbonate. After an initial rise, which for the solvents methanol and propylene carbonate is slower than the response function of the dump-probe set-up (approx. 0.12 ps), the curves exhibit a plateau and a slow decay up to around 0.6 ps for acetonitrile and methanol and up to 0.8 ps for propylene carbonate. The combination of a rise and decay with similar characteristic times rendered it difficult to adapt any functional description, as in this case the time coefficients e.g. for a combination of an exponential rise and exponential decay are highly correlated. Results from nonlinear least-squares fitting of a sum of an instanteneous initial rise and one or several exponential decays are listed in Table 4.1.1 and Table 4.1.2 under "bandintegral / dump-probe". A fast (0.2 - 0.3 ps) and a slower decay component were observed, the time coefficient of which strongly depends on the solvent, in acetonitrile being fastest (0.8 ps) and in propylene carbonate slowest (6.6 ps). The slow decay has been illustrated for propylene carbonate in Figure 4.1-21 b).

Table 4.1.1: Time coefficients (in ps) from precursor-successor fits to the transient spectra ("spectra") and fits to their integrated area ("bandintegral") in highly dipolar solvents. Relative amplitude fractions are shown in brackets.

	Methanol	hν/μJ	Prop. Carbonate	hν/μJ	Acetonitrile	hν/μJ
Spectra	0.26	0.4			0.20	0.2
Pump-probe	0.28	0.7			0.22	0.4
	0.28	0.8			0.20	0.4
	0.20	1.1			0.23	0.9
	0.32	1.2				
Average	0.27±0.03				0.21±0.02	
Spectra	0.33		0.33		0.29	
Dump-probe					0.17	
Bandintegral	0.21 (0.56)	0.15			0.11 (0.52)	0.2
Pump-probe	0.25 (0.47)	0.4			0.12 (0.40)	0.25
	0.20 (0.45)	0.4			0.14 (0.44)	0.4
	0.21 (0.38)	0.4			0.14 (0.59)	0.4
	0.25 (0.29)	0.7			0.17 (0.53)	0.4
	0.20 (0.73)	0.8			0.13 (0.53)	0.4
	0.17 (0.69)	0.8			0.22 (0.77)	0.8
	0.24 (0.70)	1.1			0.21 (0.91)	0.8
	0.35 (0.68)	1.1			0.18 (1.00)	0.8
	0.24 (0.44)	1.2			0.20 (0.81)	0.9
					0.42 (0.78)	1.1
Average	0.23±0.03				0.19±0.03	
Bandintegral	0.21, 3.9 (2:1)		0.58, 2.2 and 6.6		0.3 and 0.8 (9:1)	
Dump-probe			(4:1:1)		0.35 and 0.8 (2:1)	

Table 4.1.2: Time coefficients (in ps) from precursor-successor fits to the transient spectra ("spectra") and fits to their integrated area ("bandintegral") in moderately polar solvents. Relative amplitude fractions are shown in brackets.

	Chloroform	hν/μJ	Toluene	hν/μJ	CCl4	hν/μJ
Spectra	0.34	0.4	0.14	0.4	0.16	0.3
Pump-probe	0.25	0.8	0.22	0.4	0.15	0.9
			0.21	0.9		
			0.25	1.4		
Average			0.21±0.02			
Bandintegral	0.13 (0.42)	0.4	0.11 (0.4)	0.4	0.16 (0.2)	0.3
Pump-probe	0.17 (0.43)	0.7			0.35 (0.7)	0.9
	0.21 (0.32)	0.7				
	0.25 (0.56)	0.8				
Average	0.19±0.04					

4.1.5 Precursor-successor modelling

The considerable changes in the form of the pump-probe and dump-probe spectra, the existence of isosbestic regions, and total area changes indicate population relaxation to be involved in the spectral relaxation of DCM after photoexcitation. The spectral dynamics in strongly dipolar solvents after 0.4 - 0.6 ps are attributed mainly to solvent reorientation (4.1.3). In consequence, the investigation of a possible photoreaction concentrates on the early time window. The time-resolved spectra were modelled by a *global fitting procedure* assuming a precursor-sucessor relationship between two spectrally distinct species. This kinetic model is rather simple; it was chosen because of its descriptive character rather than for any physical reason, as its parameter τ reveals information about the relevant timescale of the underlying population changes for each experiment.

Presuming spectral independence of the apparatus function, the bilinear structure of the time-dependent spectra can be used to model them as the product of a matrix $\underline{\underline{K}}$ containing

the kinetics and a matrix $\underline{\underline{A}}$ given by the wavelength-dependent amplitudes of the species associated with each kinetic trace [Ruth 98]:

$$M_{\lambda t} \cong A_{\lambda s} \cdot K_{st} \; . \qquad (4.3)$$

Here K_{st} is the convolution of the instrument response function R(t) with the time evolution E(t) of the species s :

$$K_{st} = R(t) \otimes E_s(t) \; , \qquad (4.4)$$

and $A_{\lambda s}$ is the spectrum of that species :

$$A_{\lambda s} = A_s(\lambda) \; . \qquad (4.5)$$

The matrix of the residuals $S_{\lambda t}$ depends linearly on the spectral amplitudes $\underline{\underline{A}}$:

$$S_{\lambda t} = M_{\lambda t} - A_{\lambda s} \cdot K_{st} \; . \qquad (4.6)$$

For any given matrix $\underline{\underline{K}}$ they can be determined by multiple linear regression. The nonlinear parameters defining the time evolution $E_s(t)$ may be obtained independently of the amplitudes by a Simplex optimization [Press 92], whereas a gradient-based nonlinear fitting algorithm such as the Levenberg-Marquardt algorithm implicitly takes the gradient dependence on the linear parameters into account.

Corresponding to precursor-sucessor kinetics, the functions $E_s(t)$ were set to be an exponential decay and exponential growth with the same time coefficient τ. This can be reduced to a constant and an exponential term, yielding two wavelength-dependent amplitudes which have to be combined to the spectrum of the precursor component:

$$A_1(\lambda) \exp(-t / \tau) + A_2(\lambda)(1 - \exp(-t / \tau)) = A'_1(\lambda) \exp(-t / \tau) + A_2(\lambda)$$
$$\text{with} \quad A_1(\lambda) = A'_1(\lambda) + A_2(\lambda) \qquad (4.7 \text{ and } 4.8)$$

Exemplary fits to the dynamic isolated absorption spectra of DCM in acetonitrile are displayed in Figure 4.1-25 along with the data. Figure 4.1-26 contains the spectra for the precursor and successor components. It should be recognized that for the dump-probe as well as for the pump-probe measurements, the precursor spectra are structured and broader than the successor spectra. A comparison with precursor-successor modelling of the directly measured dump-probe spectra yielded a difference of 0.01 ps in the time coefficient and a spectral difference of the two amplitudes very close to those from fits to the isolated absorption spectra.

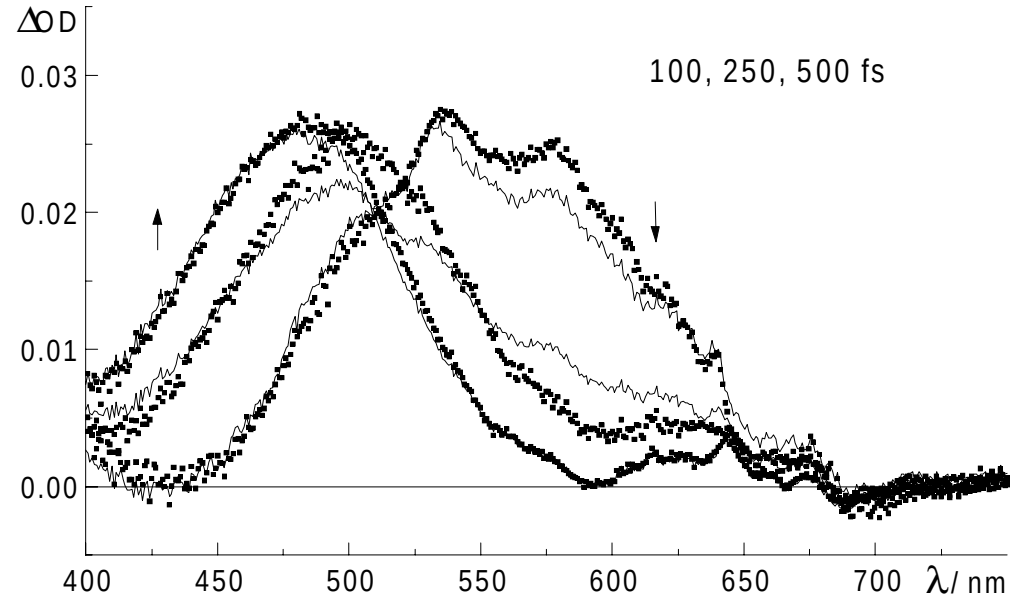

Figure 4.1-25 : Fit (solid lines) with precursor-successor modelling to isolated transient ground state absorption spectra (squares) of DCM in acetonitrile.

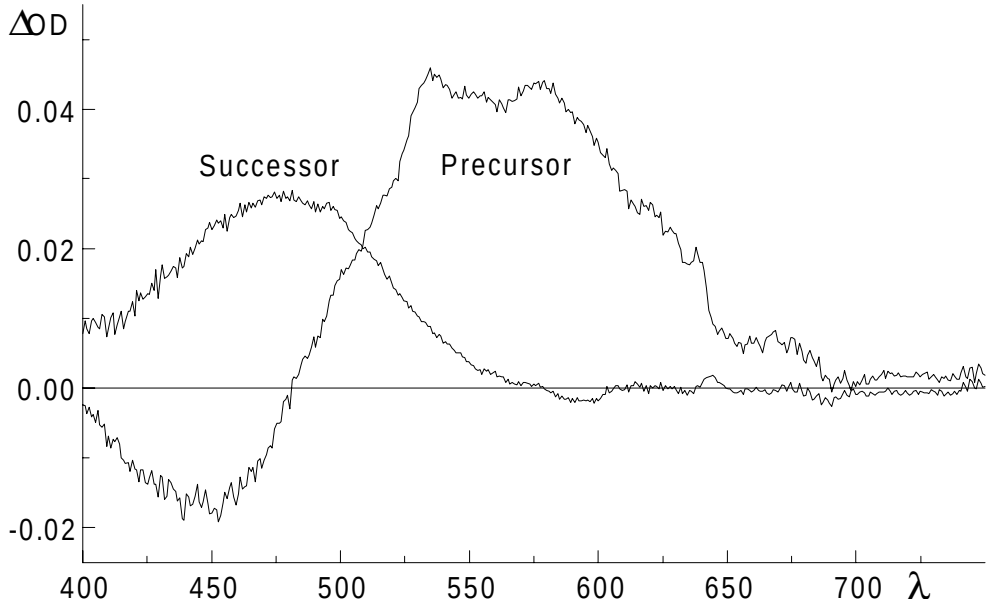

Figure 4.1-26 : Precursor and successor spectra from the analysis of isolated absorption spectra of DCM in acetonitrile of the previous figure.

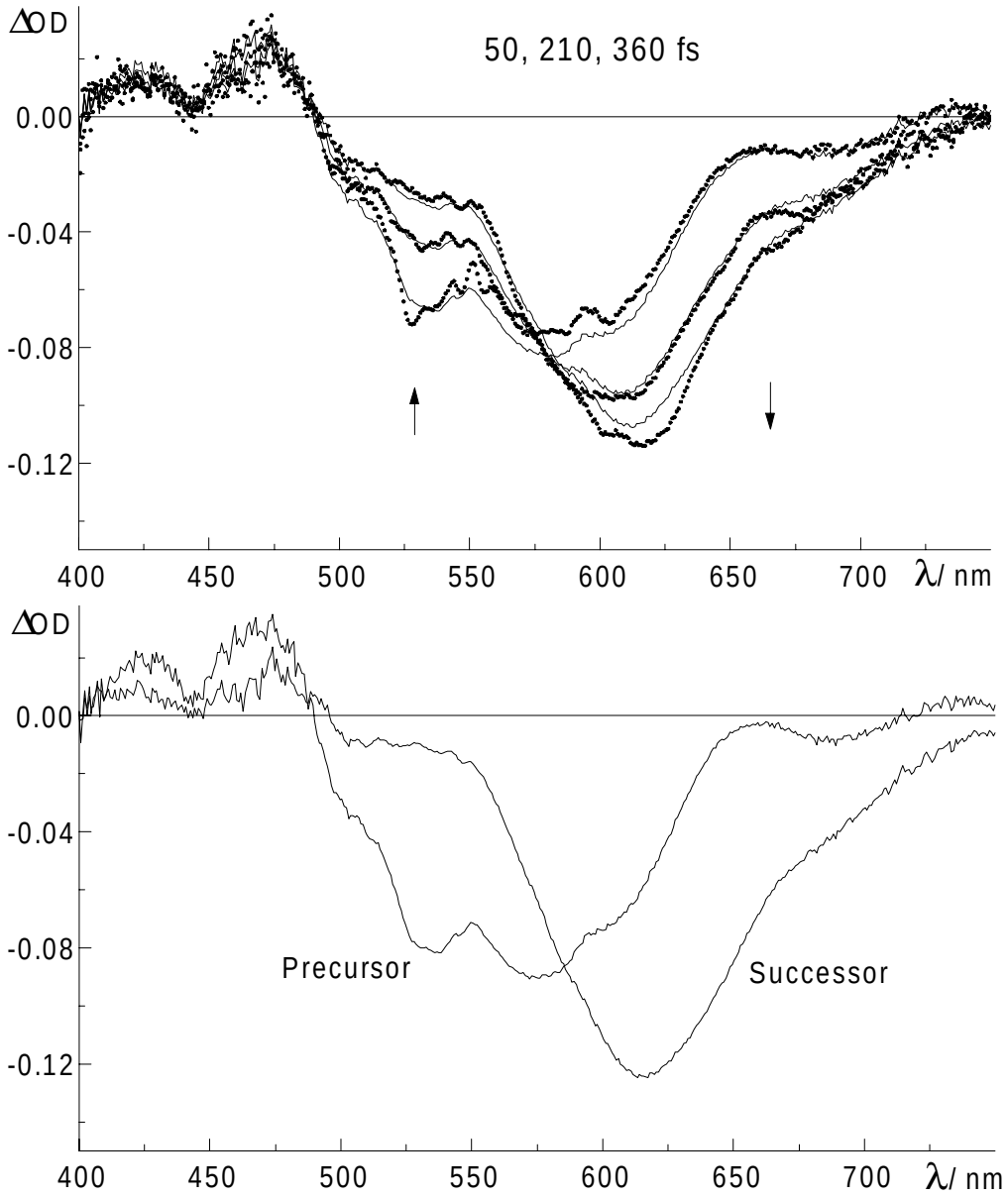

Figure 4.1-27 : a) Fit (solid lines) to isolated stimulated emission spectra of DCM in methanol (squares). b) Pecursor and successor spectra as obtained from analysis in a).

All optimizations were performed limiting the data to delays up to one picosecond, after which the continous spectral shift in strongly dipolar solvents demonstrated in 4.1.2 and 4.1.3 prevents the application of a kinetic model with species characterized by constant spectra. Precursor-successor modelling could also describe the time-dependent isolated emission spectra (Figure 4.1-27).

The time coefficients obtained from the precursor-successor modelling are compared in Table 4.1.1 and Table 4.1.2 for dump-probe and pump-probe measurements to the values

from exponential fits to the time-dependent bandintegral (see 4.1.4). For the pump-probe measurements, the variation of the relaxation times is less than for those from the integrated area. The mean values are in the range of 0.21 - 0.27 ps and close to the population dynamics indicated by the bandintegral evolution, except for tetrachloromethane, where $\tau \approx$ 0.16 ps. The relaxation times from modelling the isolated absorption spectra vary by 0.13 ps for different measurements, but are mostly around 0.3 ps for all solvents investigated.

In conclusion of section 4.1., the spectral response of DCM in strongly dipolar solvents after photoexcitation to the electronic excited state or to the ground state can be explained by solvent reorientation from 0.4 - 0.6 ps onwards.

For excited state relaxation, population changes of DCM were observed with time coefficients of approx. 0.2 ps from changes in the integrated intensity. The relative amplitude of the intensity changes grows with excitation energy. For acetonitrile, the characteristic time coefficient also increases with excitation energy. Modelling of the time-dependent spectra in the first picosecond with a precursor-successor kinetic scheme yielded a nearly solvent- and excitation energy-independent time coefficient of around 0.23 ($\pm$ 0.04) ps (averaged over all solvents). In the unpolar solvents, this relaxation of DCM seems to continue on a longer (picosecond) timescale.

The time-dependent intensity of the dump-probe spectra in strongly dipolar solvents exhibits solvent-dependent, multiple relaxation times, but the largest changes are within the first 0.2 - 0.6 ps. The latter are assigned to ground state population relaxation. The transient ground state absorption spectra within the first picosecond were modelled with a precursor-successor kinetic scheme as for the excited state, yielding also a nearly solvent-independent time coefficient of 0.28 ($\pm$ 0.07) ps (again, averaged over all solvents). The smaller intensity changes in the dump-probe spectra on a picosecond timescale are solvent-specific and follow the spectral response function, indicating transition moment or population changes with solvent reorientation.

4.2 Stationary spectroscopy

4.2.1 Absorption and fluorescence characteristics of DCM

To investigate the solvent dependence of the transition strength, the maximum extinction coefficient ε for the lowest energy optical transition of *trans*-DCM was determined in solvents of varying polarity. ε was found to be 30500 ± 3000 l mol^{-1} cm^{-1} in cyclohexane, 39700 ± 400 l mol^{-1} cm^{-1} in chloroform and 43300 ± 1300 l mol^{-1} cm^{-1} in strongly dipolar solvents, like acetonitrile, methanol and dimethyl sulfoxide. The value for ε given by [Lambda] for DCM in ethanol, 42500 l mol^{-1} cm^{-1}, falls in between the latter two values, as should be expected.

The quantum yield of *trans*-DCM fluorescence in cyclohexane was determined from a comparison of the relative intensities of the fluorescence bands in methanol and cyclohexane solutions. The solutions were of identical optical density at the excitation wavelength (455 nm) and subjected to identical fluorescence excitation and detection conditions. With a quantum yield of 0.43 in methanol, the fluorescence efficiency of *trans*-DCM in cyclohexane was found to be only $7.3\times10^{-3} \pm 5\times10^{-4}$.

Although the *cis*-isomers of substituted stilbenes are generally non-fluorescent, *cis*-DCM was investigated for fluorescence which might lead to unwelcome contributions to the dump-probe experiments. Transient absorption has been reported for *cis*-DCM in the wavelength range of 400 - 550 nm [Mey 90], so that this transition cannot interfere with *trans*-DCM stimulated emission pumping at 630 nm.

Solutions of *trans*-DCM in cyclohexane and chloroform were exposed to 308 nm XeCl excimer laser radiation (80 mJ, 10 Hz). The absorption spectrum was recorded in a 10 mm fused silica cell after every 500 shots (cyclohexane) and 135 shots (chloroform) and is presented for chloroform in Figure 4.2-1. The spectra show isosbestic points, the spectrum of the photo-generated component agreeing with that published for *cis*-DCM in solution [Mey 90]. In accordance with the high quantum yield for *trans*-cis isomerization of DCM in chloroform, only 500 shots were needed to obtain an equilibrium between the *trans*- and

cis-isomer populations. In *cyclohexane*, no absorption changes were found, obviously due to a *low quantum yield for photoisomerization* in this solvent.

The irradiated solution of DCM in chloroform was then excited at 375 nm, where the *cis*-isomer absorbs preferentially, and the fluorescence spectrum was compared to that of non-irradiated solutions (Figure 4.2-2). A weak fluorescence band appears only after irradiation in the region of 400 to 500 nm. The quantum yield for photoproduct fluorescence was estimated from the comparison of the relative intensity of the *trans*-DCM fluorescence band to the photoproduct fluorescence band to be $\approx 5\times10^{-4}$. The emission (Figure 4.2-2) is ascribed to the *cis*-isomer of DCM.

Nonwithstanding the low fluorescence quantum yield, care was taken to check for *cis*-DCM accumulation by recording stationary absorption spectra of the solution before and after time-resolved measurements, and no evidence for the presence of *cis*-DCM was found.

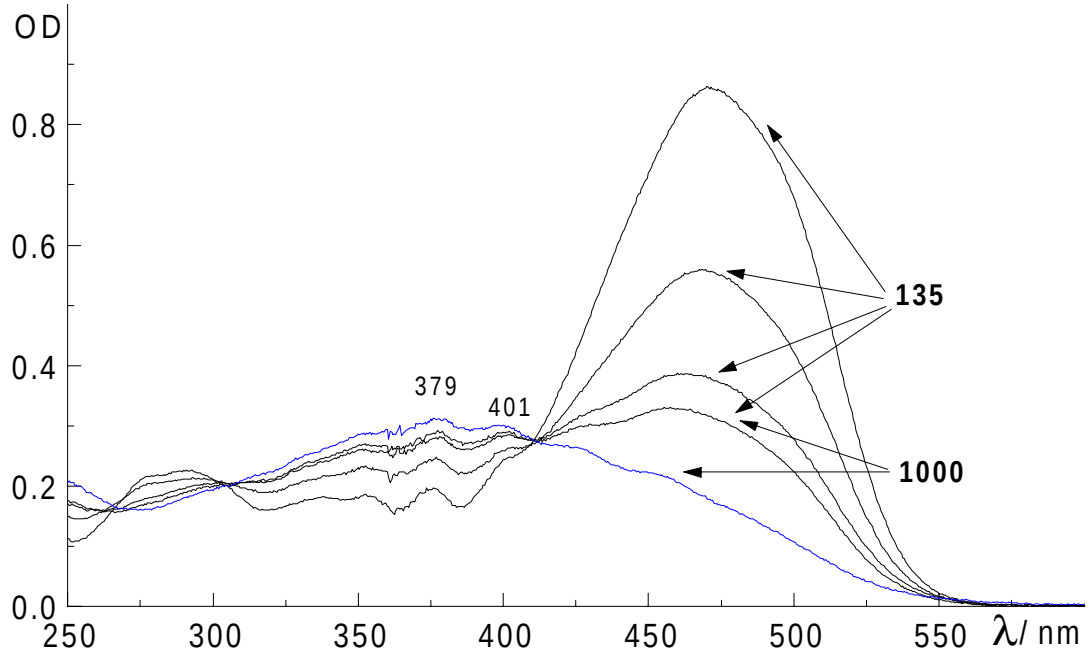

Figure 4.2-1: Absorption spectra of irradiated DCM in chloroform. The number of laser shots between subsequent spectra are indicated by arrows.

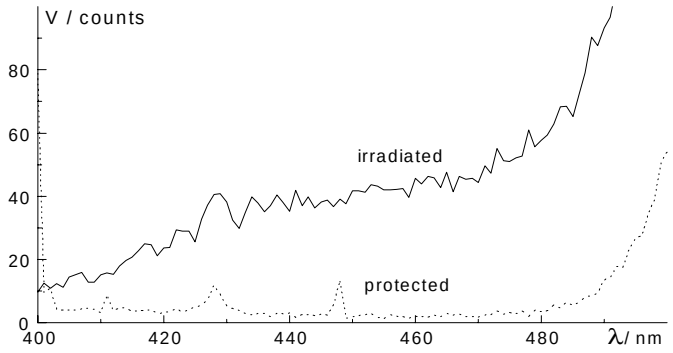

Figure 4.2-2: Fluorescence spectrum of photostationary DCM solution compared to that of a solution maintained in the dark. Excitation was at 375 nm. The new fluorescence band is assigned to *cis*-DCM.

4.2.2 Jet spectrum of DCM

The spectroscopy of isolated molecules permits information to be gained about their vibronic and electronic transitions, unimpeded by the line broadening and electronic coupling induced by the solvent environment.

Apart from the single peak visible in Figure 4.2-3, no further vibronic lines could be resolved in the *fluorescence excitation spectrum* of isolated DCM. The low signal-to-noise ratio for jet-cooled fluorescence excitation is ascribed to a very low fluorescence quantum yield of isolated DCM, coincident with the decrease of *trans*-DCM fluorescence efficiency with diminishing solvent polarity. The (0,0) transition energy for the lowest electronic transition was estimated from the peak in Figure 4.2-3 to 22416 cm^{-1}.

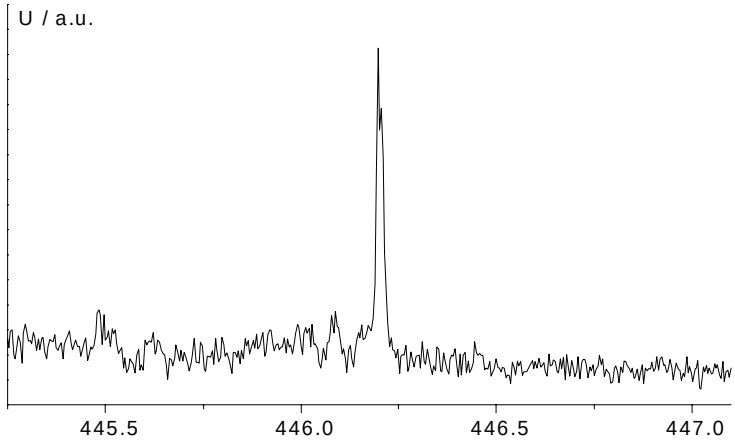

Figure 4.2-3 : Fluorescence excitation spectrum of isolated DCM, from [Mühl 99b].

4.2.3 Raman spectra

From the lines in resonance Raman (RR) spectra, the vibrational frequencies coupled to the optical transition can be obtained. Fast electronic dephasing presumed, their intensity in the RR spectrum scales with the dimensional equilibrium displacement of the vibrational mode upon excitation and its frequency: $I \propto \Delta^2\omega^2$ [Mye 87].

Due to the strong fluorescence of DCM, RR spectra could only be realized with excitation around 460 nm. For longer excitation wavelengths within the DCM absorption band, the large fluorescence background obscures any Raman lines. The RR spectrum of DCM in methanol is presented in Figure 4.2-4 a), while the RR spectrum of DCM crystals (after background subtraction) is shown on the same frequency scale in Figure 4.2-4 b).

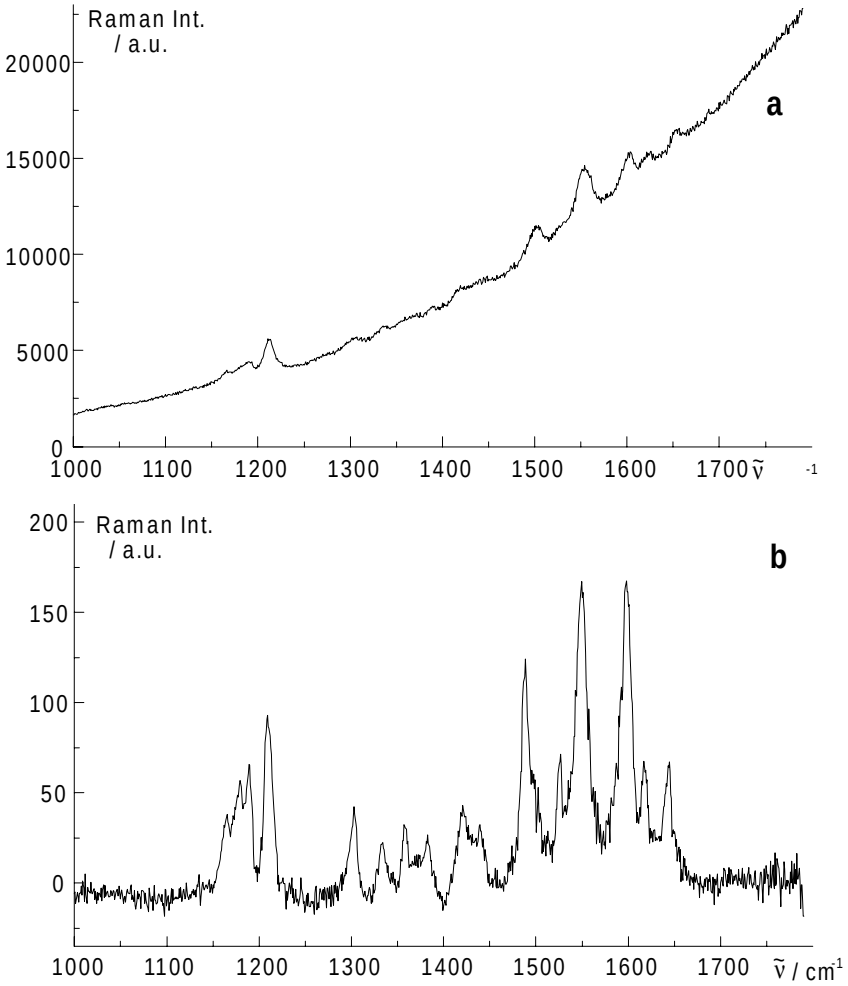

Figure 4.2-4: Resonance Raman spectra of DCM a) in methanol b) of DCM crystals. For the latter, the fluorescence background has been subtracted.

Table 4.2.1 : Resonance Raman frequencies (in cm^{-1}) for DCM from Stokes resonance Raman spectra in methanol and of DCM crystals. Also shown are relative displacements estimated from the intensities and frequencies of the peaks of the crystal spectrum.

Frequency / cm^{-1}	Frequency / cm^{-1}	rel. Displ.
DCM / Methanol	DCM / Crystal	DCM / Crystal
	1165	0.65
	1180	0.78
1189	1189	0.83
1213	1209	0.97
1308	1304	0.60
1339	1334	0.43
	1357	0.51
1387	1383	0.45
1420	1421	0.56
	1439	0.48
1503	1489	0.91
	1525	0.68
1554	1550	1.0
1603	1598	0.99
1624	1617	0.62
1655	1644	0.61

The RR bands are similar in relative intensity and close in frequency for DCM in crystallic form and dissolved in methanol, proving that indeed the lines in Figure 4.2-4 b) stem from DCM molecules. The frequencies of the RR bands are listed in Table 4.2.1. As the fluorescence background is very strong, an analysis of the intensities of the RR peaks was not performed for the methanol solution. Values for the relative displacements D of the modes in the crystal spectrum were calculated after $I \propto \Delta^2\omega^2$ and are also listed in Table 4.2.1. There is a notable shift towards higher frequencies between crystal and methanol surroundings for the modes around 1495, 1620 and 1650 cm^{-1}. The latter two can be

assigned to either the olefinic C=C stretch or the pyrane ring bond stretch, respectively [Colt 90]. The 1550 cm^{-1} band should correspond to the methylene bond stretch, in analogy to the shift of the ethylene vibration when substituted with chlorine (ethylene: 1670-1685 cm^{-1}, tetrachloroethylene 1560 cm^{-1} [Colt 90]). The phenyl C=C stretch is attributed to the 1598 cm^{-1} line. It is difficult to assign the lower frequency vibrations, as the dimethylamino group contributes in the range 1000-1300 cm^{-1} [Colt 90], as well as aromatic C-H bending and C-C stretching and phenyl-C stretching modes [Bar 90, Aren 95, Choi 97].

For *trans*-stilbene, the RR mode in the first singlet excited state at ≈1565 cm^{-1} has been assigned to the olefinic (ethylenic) C=C stretch [Qian 93]. It has been intensively studied to investigate vibrational relaxation in the excited state [see also Ham 92, Mat 95, Schultz 97]. Following the treatment of Qian et al. [Qian 93], a lower estimate for the vibrational energy relaxation time T_1 of DCM in methanol in the ground state can be deduced from the bandwidth Γ of the RR line at 1553 cm^{-1}. Γ was obtained to 17 cm^{-1} after background subtraction and fitting to a Gaussian (Figure 4.2-5 a), well above the frequency resolution of 4 cm^{-1}. The Gaussian lineshape of the Raman line implies inhomogeneous broadening from slow fluctuations of the solvent polarization not present for the crystal spectrum, where the same line has a Lorentzian shape (Figure 4.2-5 b). Ignoring the inhomogeneous broadening and pure dephasing (i.e. setting $T_2 \approx 2T_1$ in equation 2.37), $T_2 = (\pi c \Gamma)^{-1}$ yields a lower limit of 312 fs for ground state vibrational energy relaxation. If only the (unknown) linewidth in methanol due to homogeneous broadening was considered, the estimated limit for vibrational energy redistribution would be even larger.

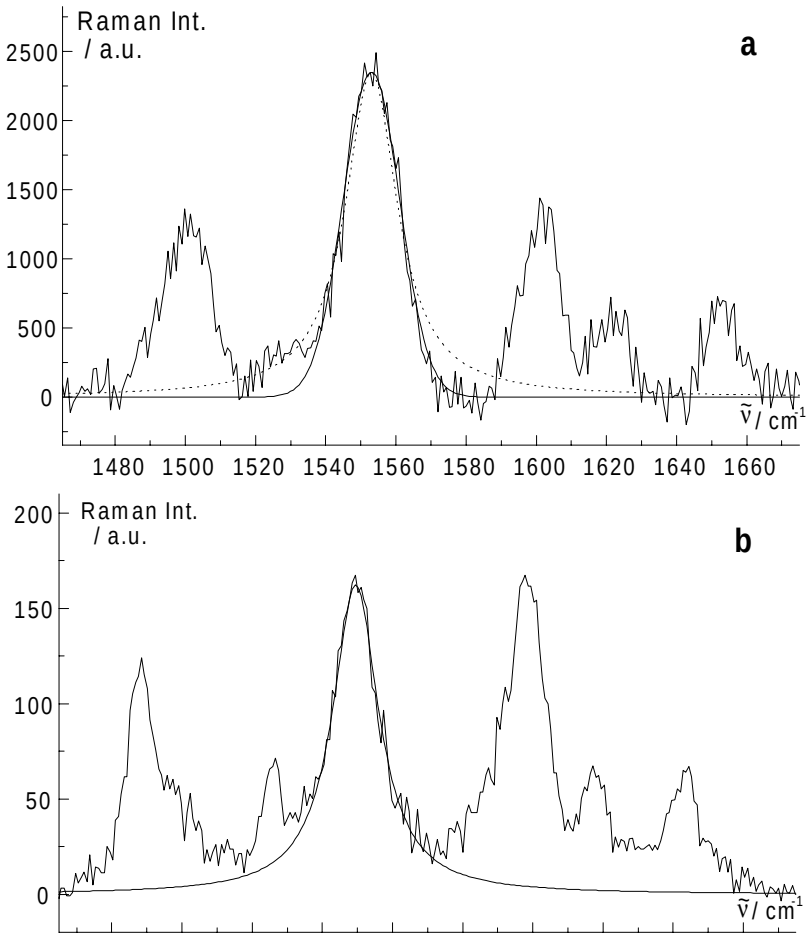

Figure 4.2-5: Fits to the profile of the C=C stretch around 1550 cm^{-1} in the resonance Raman spectrum of DCM. a) In methanol, shown are the adaptation of a Gaussian (solid) and a Lorentzian (dotted) lineshape. b) In crystallic form, shown is the adaptation of a Lorentzian lineshape.

Table 4.2.2 lists the RR frequencies obtained in [Kov 96] and frequencies extracted from the dump-probe spectra of DCM in methanol and acetonitrile. This was done by assignment of the structure observed in the early spectra to spectral hole burning in analogy to [Kov 96]. The frequencies of the particle (S_0) and hole (S_1) contributions were extracted via calculation of the second derivative spectrum [Pel 94] and calculating the frequency difference of the peaks to the dump frequency. It is evident that the transient spectra do not yield the Raman transitions dominanting the RR measurement. The physical origin of the structure observed in the early spectra should therefore be reconsidered.

Table 4.2.2 : Vibrational frequencies obtained from the structure of the early spectra in pump-probe and stimulated emission experiments. Values from the analysis of quantum beats (see 5.1.4) are denoted by asterisks.

	Frequencies / cm^{-1}		
Solvent	Dump-probe Methanol	Dump-probe Acetonitrile	Pump-probe Acetonitrile
			3450
			3130
	2337	2586	2560
	1861	1727	
	1496		
S_0			1430
		1209	
			1130
	768	772	
	460	452	
	3464	3869	3460
	2987	2958	2940
	2175	2247	2300
S_1	1502	1385	
	970	858	1090
	465	454	440
		322	410*
	130		150*
		77	70*

Non-resonant Raman spectra recorded in the larger range of 100-3600 cm^{-1} for DCM crystals are shown in Figure 4.2-6. They were also recorded in toluene, chloroform and methanol (not shown). The prominent lines of the non-resonant Raman spectra lie in the range 1000 - 1700 cm^{-1}, thereby justifying the choice of the detection range for the RR measurements. The frequencies of the crystal bands deviate slightly from those in the RR spectrum, possibly due to local heating by visible excitation, whereas the spectrum of DCM in methanol coincides in frequency with the RR spectrum. In chloroform, the solvent spectrum could be subtracted completely, whereas in methanol and toluene remaining solvent bands below 1200 cm^{-1} might indicate enhancement by solute-solvent mode coupling. The crystal lines at 2189 and 2202 cm^{-1} can be attributed to the in-phase and out-of-phase C≡N stretching modes of the two cyano groups [Lin 91]. A relative amplitude increase of the phenyl vibration (around 1600 cm^{-1}) and a decrease of the cyano stretch (at 2212 cm^{-1} in solution) and the band around 1418 cm^{-1} with polarity of the environment (crystal → toluene → chloroform → methanol) should be noted. It is interesting that the frequency shifts of the C=C stretching modes from 1545, 1645 and 1495 cm^{-1} in the crystal spectrum towards higher frequencies in solution scale with the polarizability of the solvent (methanol → chloroform → toluene) rather than with its polarity. The respective peaks can be found at 1561, 1656 and 1508 cm^{-1} in toluene. The lines at 1422 and 1215 cm^{-1} of the crystal spectrum shift in solution by approx. 6 and 3 cm^{-1} towards lower frequencies.

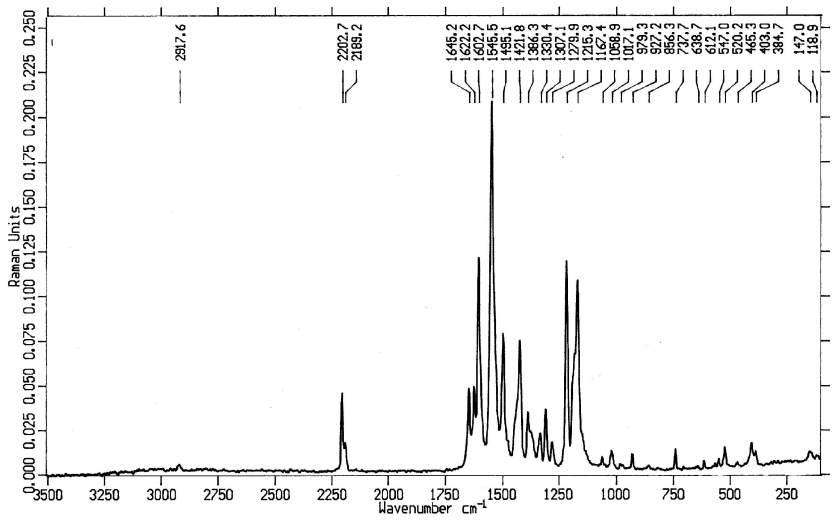

Figure 4.2-6: Raman spectrum of DCM crystals.

4.2.4 Solvatochromic analysis

Its large Stokes shift, increasing with solvent polarity, renders DCM a particularly suitable molecule for a solvatochromic analysis. Assuming the validity of the continuum model for solvation (see 2.3), the maxima of the absorption and fluorescence spectra of DCM in solvents of various polarities (Table 4.2.3) were plotted against the Debye reaction field factor F (= $(\varepsilon_{\square} - 1) /(\varepsilon_{\square} + 2) - (n^2 - 1)/(n^2 + 2)$). These data were modelled with the transition frequency ν as a function of F, as determined by the solvent nuclear polarization (middle terms in the right-hand side of equations 2.29 and 2.30). The dipole moment μ_e in the excited state, the peak frequency $\nu_{\square}$ of the isolated molecule and its Onsager radius R_o were treated as fit parameters. The dipole moment in the electronic ground state μ_g was set to 9 D obtained from the semiempirical calculations (4.3). Since ν in the middle terms of equ. 2.29, 2.30 depends linearly on F, the three parameters are correlated. From the various sets of parameters yielding similar ν(F)'s, only μ_e = 21 - 26 Debye went along with physically meaningful Onsager radii for both sets of data. The excited state dipole moment was therefore fixed at 23 D. Good convergence of the fits to the absorption / emission maxima was reached for values of 11.3 Å / 10.6 Å for R_o and 21875 cm^{-1} / 17673 cm^{-1} for $\nu_{\square}$ (Figure 4.2-7).

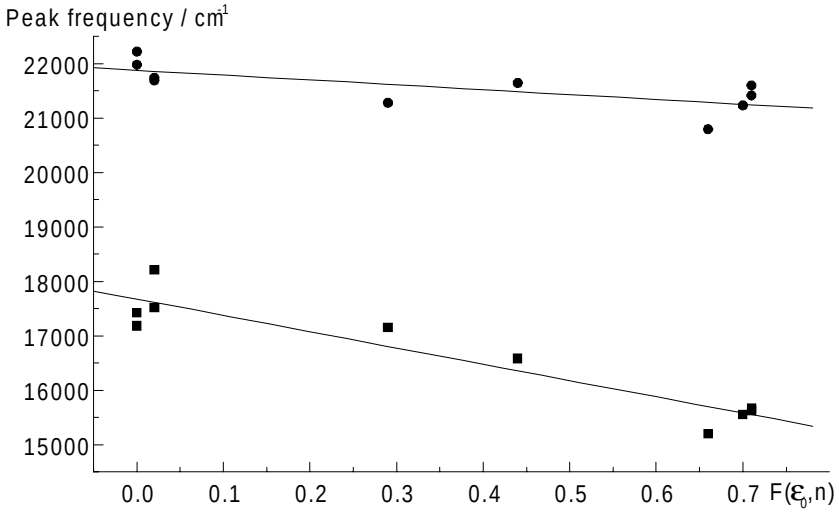

Figure 4.2-7 : Absorption (circles) and emission peak frequencies (squares) of DCM against the Debye reaction field factor F in different solvents. Also shown is modelling according to a reaction field treatment with μ_g = 9 D and μ_e = 23 D.

Consideration of the solvent reorganization energy due to electronic polarization (last term in the right-hand side of equations 2.29 and 2.30) improved the fit to the absorption maxima, reducing the residuals by 1.25, but did not change the quality of the fit to the emission maxima. The fit to the absorption maxima according to the full equ. 2.30 yielded 10.3 Å for R_o and 22402 cm^{-1} for $\nu_{\square}$. The latter value agrees well with the 22416 cm^{-1} for the (0,0) transition energy of isolated DCM obtained by fluorescence excitation in the jet experiment.

Table 4.2.3 : Solvent dielectric properties [Horng 95], peak maxima and widths of DCM stationary absorption and fluorescence spectra.

Solvent	ε_0	n	$F(\varepsilon_0,n)$	Max_{Abs} / nm	Max_{Fls} / nm	$Fwhm_{Abs}$/ cm^{-1}	$Fwhm_{Fls}$/ cm^{-1}
Cyclohexane	2.02	1.424	0.0	455	582	4302	5061
2-Meth. Butane	1.83	1.351	0.0	450	574	4395	5483
Toluene	2.38	1.494	0.02	460	571	4136	3471
Tetrachl.meth.	2.25	1.460	0.02	461	549	4170	4182
Chloroform	4.81	1.443	0.29	470	583	4092	2739
THF	7.58	1.405	0.44	462	603	4333	2633
Methanol	32.66	1.327	0.71	467	640	4545	2391
Acetonitrile	35.94	1.342	0.71	463	638	4587	2391
Prop. Carb.	64.92	1.420	0.7	471	643	4373	2361
DMSO	46.45	1.478	0.66	481	658	4335	2295

4.2.5 Simulation of stationary UV/VIS absorption and fluorescence spectra

Stationary absorption and fluorescence spectra of DCM in several solvents of low polarity are presented in Figure 4.2-8. The fluorescence spectra of *trans*-DCM in solvents of low polarity show a drastic reduction in width with increasing solvent polarity (Table 4.2.3). A prominent vibrational progression can be observed in the absorption and in the fluorescence spectra. The relative amplitudes of the bands due to this progression also change when increasing the solvent polarity.

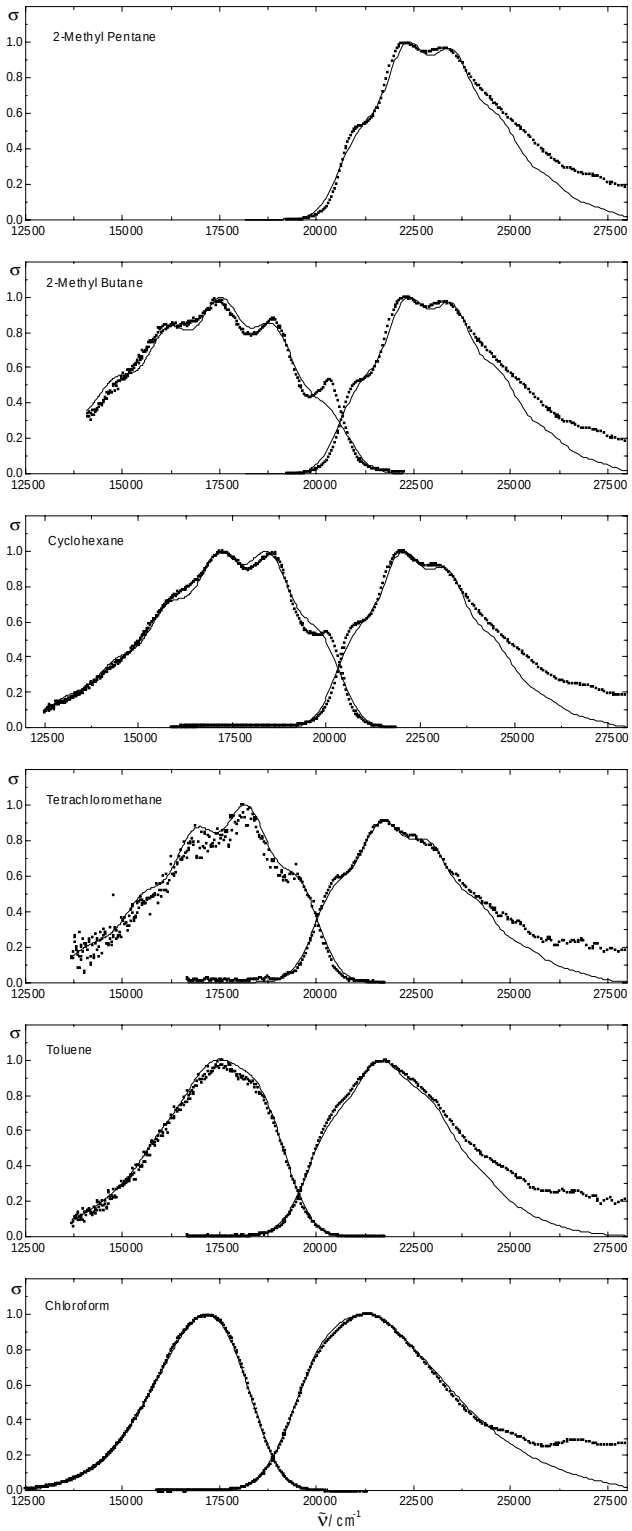

Figure 4.2-8 : Stationary emission (left) and absorption (right) spectra of DCM in various solvents of low polarity (dots) and modelling (lines) with a progression of an effective harmonic vibrational mode. Fluorescence quantum distributions have been converted to cross sections; all spectra are normalized.

To quantify this observation, a model of the electronic transition as coupled to one (effective) harmonic intramolecular vibrational mode was employed. In order to limit the number of parameters, all other intra- and intermolecular vibrations were treated as a bath broadening the transition. The vibrational frequencies were allowed to differ in the ground and electronically excited state. The wavefunctions of the eigenstates of an harmonic oscillator are given by Hermite polynomials.

Franck-Condon factors giving the probability for any transition (n', m'') were obtained by numerically calculating the overlap of the corresponding Hermite polynomials up to values of nine for n and m. The resulting line spectrum was convoluted with a Gaussian lineshape to achieve a simulation of the absorption / emission spectrum. The broadening σ, that means the width of the Gaussian, as well as the (0,0) transition energy E and the vibrational level spacing ω were adapted by a nonlinear fitting procedure to the absorption or fluorescence spectra. It should be noted, however, that the effective vibrational frequencies together with the displacement of the vibrational equilibrium position Δ had been presumed for the calculation of the Franck-Condon factors. Therefore, if the vibrational spacing resulting from the fits deviated by more than 70 cm^{-1} from the assumed value for the vibrational frequency, the vibrational frequency was changed and the Franck-Condon factors were recalculated. The procedure was thus iterated until coincidence was achieved. Table 4.2.4 lists the values for the displacement Δ (in units of $(\hbar / m\,\omega_{vib})^{1/2}$ and hence dimensionless), the broadening σ and the effective vibrational frequencies in the ground and excited states, ω_{ground} and ω_{exc}, for DCM in different solvents of low polarity. Missing structure of the stationary spectra in strongly dipolar solvents prevented them from being subjected to the same analysis. The fits to the stationary absorption and emission spectra are also shown in Figure 4.2-8. They reproduce the spectral features well, if somewhat underestimating the contribution from the (0,0) transition, probably due to the contribution of low-frequency modes not accounted for. The dimensionless displacement decreases with solvent polarity from approx. 2.0 for methyl butane to 1.3 (emission) and 1.55 (absorption) for chloroform. The effective vibrational frequencies also differ between solvents, the ground state effective vibrational frequency declining from 1360 to 1150 cm^{-1}, whereas the excited state effective vibrational frequency shifts with increasing polarity from 1200 to 1270 cm^{-1}. In the resonance Raman spectrum of DCM, the modes around 1550 cm^{-1} and 1210 cm^{-1} are dominating. Although this is partly reflected in the above analysis, the frequency shifts cannot be interpreted as such, but

should be viewed as a consequence of varying intensities of several vibrational modes coupled to the transition.

Table 4.2.4 : Dimensionless displacement Δ, (0,0)-transition energy $E_{(0,0)}$, width σ and frequencies ω_{exc} respective ω_{ground} of an effective harmonic vibrational mode as obtained from fits to the stationary absorption and fluorescence spectra of DCM.

Absorption

Solvent	Δ	$E_{(0,0)}$ / cm^{-1}	σ / cm^{-1}	ω_{exc} / cm^{-1}
2-Methyl Pentane	1.99	20942	552	1200
2-Methyl Butane	2.02	21104	530	1200
Cyclohexane	1.95	20775	545	1200
Tetrachl.meth.	1.85	20460	552	1270
Toluene	1.7	20410	658	1270
Chloroform	1.55	20112	784	1270

Fluorescence

	Δ	$E_{(0,0)}$ / cm^{-1}	σ / cm^{-1}	ω_{ground} / cm^{-1}
2-Methyl Butane	2.25	20231	572	1360
Cyclohexane	2.05	19805	582	1360
Tetrachl.meth.	1.85	19511	560	1270
Toluene	1.5	18553	672	1270
Chloroform	1.3	17696	719	1150

The difference between the values of the displacement between the absorption and emission can be explained by different coupling strengths of the vibrational mode to the electronic transition due to different geometries in the ground and excited states. This might be a change in bond angles or lengths as well as differences in the planarity of molecular

subunits. It is remarkable that the decline of the equilibrium displacement occurs gradually with increasing solvent polarity, being slightly more pronounced for the fluorescence.

4.3 Semiempirical calculations

To investigate the influence of dimethylamino bond angle rotation on the properties of isolated DCM in the electronic ground state (S_0), semiempirical calculations were carried out. A complete geometry optimization was performed employing the AM1 Hamiltonian and a modification of the Davidson-Fletcher-Powell algorithm for energy minimization from the program package AMPAC 5.0 (Semichem). The resulting geometry of *trans*-DCM in the ground state was nearly planar, with both methyl groups symmetrically tilted by 17° out of the plane containing the nitrogen atom and the phenyl ring, and the dimethylamino group rotated by approx. 4° around the phenyl-nitrogen bond. The dimethylamino group was then rotated by varying the dihedral angle ϕ of the methyl group closer to the oxygen in steps of 10°; all other bond angles and bond lengths were optimized using the Eigenvector Following algorithm. The dimethylamino group rotation angle θ was calculated afterwards from ϕ and the angle δ between the methyl–nitrogen-carbon planes of the two methyl groups by $\theta = \phi + \delta / 2 - 90°$. The heat of formation as a function of dimethylamino group torsion (Figure 4.3-1) shows a second, very shallow minimum slightly above $\theta = 30°$ and increases to a maximum for $\theta = \pm 90°$. A rotation of the dimethylamino group by $\theta = \pm 34°$ corresponds to a position where one of the methyl groups is in plane with the phenyl ring, leading to an energetic stabilization. The assymmetry in the $E(\theta)$ curve is due to the fact that only one methyl group was rotated, while the other was allowed to relax. When the free methyl group is supposed to pass through the plane with the phenyl ring, it tries to stay in plane with it instead. The main and the shallow minimum are energetically spaced by 0.41 kcal / mol, corresponding to 1.43 cm^{-1}, which is within the accuracy of calculation for the heat of formation. It should be remarked that a slight torsion of the neighbouring phenyl ring was induced by the dimethylamino group rotation. At the energetic minimum, with $\theta = 4°$, the dipole moment amounts to 9.1 D. For $\theta = 90°$, it exhibits a minimum of 6.8 D.

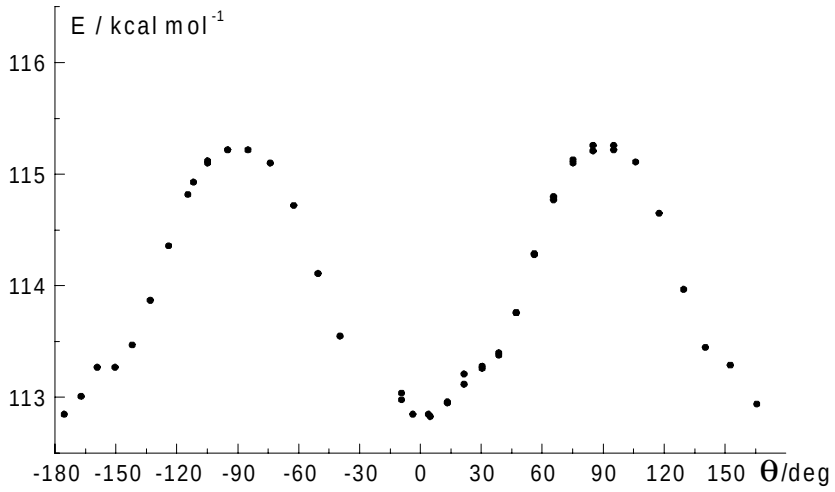

Figure 4.3-1: Heat of formation of DCM as a function of dimethylamino group rotation.

Transition energies to the next four excited electronic singlet states (S_1 - S_3) were obtained by configuration interaction with 20 electronic configurations to 23700, 29370, 30840 and 33620 cm^{-1}. The geometry in the S_3 was similar to that in S_0, while in S_1 both methyl groups of the dimethylamino group were tilted by 11.5° symmetrically out of the plane with the nitrogen and the phenyl ring, and *trans*-DCM in S_2 was found to be planar. Compared to the value of 22416 cm^{-1} for the (0,0)-transition energy from the jet spectrum, the transition energy to S_1 is overestimated by nearly 1300 cm^{-1}. There are further transitions around 40000 cm^{-1}, and several more between 45000 and 50000 cm^{-1} (Figure 4.3-2).

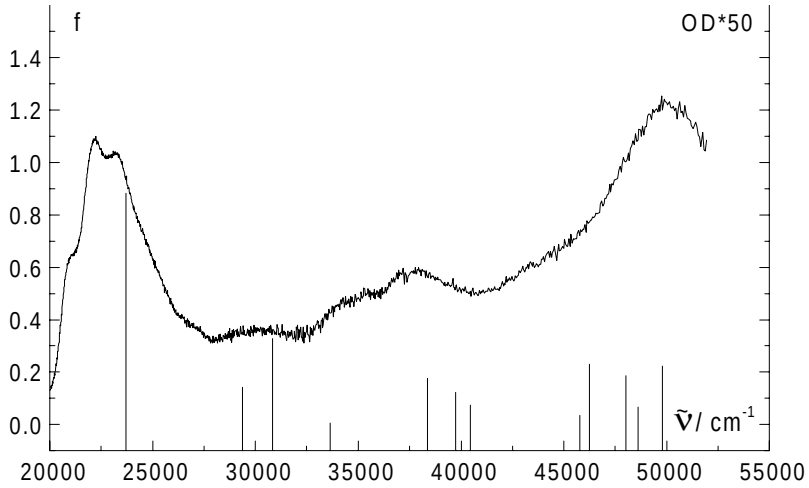

Figure 4.3-2 : Oscillator strength of transitions from trans-DCM electronic ground state. For comparison, the stationary absorption spectrum in 2-methyl pentane is also shown.

The changes in dipole moment upon excitation into S_1 or S_2 and subsequent transfer to S_0 were studied also employing configuration interaction with CI = 12. First, the molecular properties after Franck-Condon excitation were calculated by performing a self-consistent field calculation in the ground state geometry for S_1 or S_2. The molecule was then allowed to relax, that means a complete geometry optimization was carried out in the excited state. Finally, the ground state molecular properties were calculated by performing a self-consistent field calculation in the optimized geometry of the excited states for S_0. The resulting changes in dipole moment are visualized in the scheme of Figure 4.3-3. The differences in dipole moment between the Franck-Condon and the relaxed states were at the maximum 2 D.

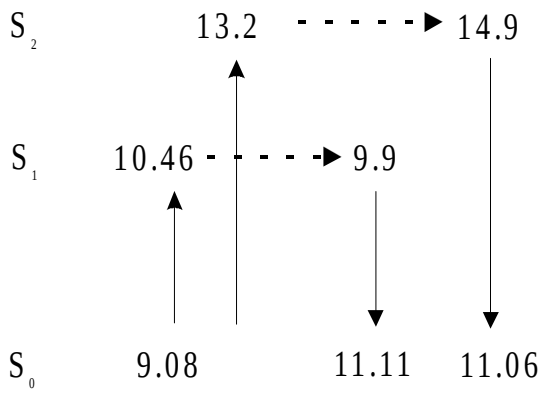

Figure 4.3-3: Dipole moments of DCM (in Debye) for Franck-Condon and relaxed electronic ground and excited states.

To check for the influence of rotation of other moieties, the dipole moment in S_1 and in S_2 was calculated after geometry optimization with configuration interaction for a fixed 90° rotation of the bonds connecting the pyrane ring or the anilino group to the central ethylenic part or for 90° rotation of the dimethylamino group. For all of these torsions, the dipole moment in S_1 and in S_2 decreased or did not increase by more than one Debye relative to the values obtained in the full optimization.

4.4 Simulation of solvation and vibrational relaxation dynamics

Calculations of time-dependent fluorescence spectra were performed based on the theoretical treatment of [Lor 87], where only effects of solvent and intramolecular vibrational relaxation were considered, with the aim of assessing whether these processes suffice to explain the observed spectral dynamics. The solute was described by a two-state model with a single harmonic vibrational mode coupled to the optical transition.

[Lor 87] solved the Liouville equation for the density matrix $\rho(t)$ of the solute-solvent system in the presence of an external electric field :

$$\frac{\partial \rho}{\partial t} = (-i/\hbar)\{[H,\rho] + [H_{rad},\rho] + [H_{int}(t),\rho]\} + \Gamma\rho \qquad (4.9)$$

Here H is the sum of the Hamiltonians governing the nuclear degrees of freedom of the solute and of the solvent in absence of each other, and the interaction of the solute with the nuclear and electronical degrees of freedom of the solvent for the electronic ground and excited state. H_{rad} is the Hamiltonian of the radiation field, and H_{int} is given by the transition dipole operator multiplied by the electric field E(t). Γ is a matrix operator representing vibrational relaxation.

The time-dependent fluorescence spectrum at the excitation frequency ω_1 and the emission frequency ω_2 is proportional to :

$$S(\omega_1,\omega_2,t) = Tr[\hat{S}\rho(t)] \quad , \qquad (4.10)$$

where the operator $\hat{S}$ denotes the time derivative of the number of photons in the emitted mode. The result for $S(\omega_1,\omega_2,t)$ is expressed in dependency of the solvent coordinate U. U is the difference in interaction energy of the solvent nuclear degrees of freedom with the solute in its ground and in the electronically excited state: $U \equiv W_e - W_g$.

The calculations have been performed using the following expression for $S(\omega_1,\omega_2,t)$:

$$S(\omega_1,\omega_2,t) = (2^{1/2}\pi^{3/2}\,E_1^{\,2}\,E_2^{\,2}) / [\hbar^4\Delta_g\omega A_e(t)] \sum_{a,b,c,d}|V_{ab}|^2 P(a)\exp\left[\frac{-(\omega_1 - \omega_{eg} - \omega_{ba})^2}{2(\Delta_g^2 + \omega^2)}\right]$$

$$\cdot|V_{cd}|^2\,\phi_{dd,bb}\exp\left\{-\left[2BA_e^2(t)\right]^{-1}\left[\omega_2 - \omega_{eg} - \omega_{dc} + (\sigma_g - \sigma_e)\left[1 - Z_e(t)\right]\right.\right.$$

$$\left.\left. - B\,Z_e(t)(\omega_1 - \omega_{eg} - \omega_{ba})\right]^2\right\} \qquad \text{[Lor 87]}$$

(4.11)

E_i denotes the amplitude of the pump- respective emission field. The excitation pulse envelope is assumed to be Gaussian in time with $E_1(t) = E_1 \exp(-\omega^2 t^2)$. V_{nm} is the transition matrix element between vibrational level n in the electronic ground state and m in the excited state, and ω_{eg} is the (0,0) absorption frequency of the fully soluted chromophore. P(a) is the probability that the solute occupies vibrational level a in the electronic ground state at thermal equilibrium; it is determined by the Boltzmann factor $P(a) = \exp(-W_a / k_B T)$.

Δ_g and Δ_e characterize the inhomogeneous broadening in the ground and excited state of the solute. In the following, $\Delta_g = \Delta_e$ has been assumed. The values for Δ, the ground and excitated state vibrational frequencies and the transition matrix elements V_{ab} and V_{cd} were taken from the simulation of the stationary emission and absorption spectra (see 4.2.5), neglecting homogeneous broadening. The total solvent reorganization energy $\sigma_e - \sigma_g$ was extracted from the (0,0)-transition energy difference for emission and absorption (4.2.5). For acetonitrile, where the stationary spectra have not been simulated, the difference between the Stokes shift calculated for chloroform from the (0,0) transition energies and the peak difference of the absorption and emission spectra was subtracted from the peak frequency difference for DCM absorption and emission in acetonitrile. The reorganization energy was thus calculated to be 970 cm^{-1} for cyclohexane, 2440 cm^{-1} for chloroform and 4320 cm^{-1} for acetonitrile.

The variables related to the solvation coordinate have been expressed in [Lor 87] as

functions of the dielectric properties of the solvent, using a Debye continuum model for the liquid. The normalized solvation coordinate correlation function Z(t), equivalent to the solvent fluctuation correlation function C(t) in 2.3., is then given by:

$$Z(t) = \exp(-t / \tau_L). \qquad (4.12)$$

(see 2.3). The longitudinal relaxation time τ_L of the solvent was set here to the weighted averaged time coefficient from exponential fits to the Stokes shift of coumarin 153 for the respective solvent as presented in [Horng 95], that is 0.25 ps for acetonitrile and 2.08 ps for chloroform.

B and $A_e(t)$ in the notation of [Lor 87] are defined by :

$$B = \Delta_g^2 / (\Delta_g^2 + \omega^2) \text{ and } A_e(t) = \left\{ \Delta_g^2 [\, 1 - Z_e^2(t) \,] + \omega^2 \right\}^{1/2} \qquad (4.13) \text{ and } (4.14)$$

and were calculated accordingly.

$\phi_{dd,bb}$ denotes the conditional probability that the solute occupies state d at time t, given that it occupied b at time zero. The conditional probabilities were obtained as in [Lor 87] using the model of Montroll and Shuler for vibrational relaxation of a harmonic oscillator of frequency ω coupled to a bath of harmonic oscillators of the same frequency (see 2.4). The formula for $\phi_{dd,bb}$ can easily be obtained by exchanging d for n and b for m in equation 2.41.

Calculations were performed for the solvents cyclohexane, chloroform and acetonitrile with γ_{vr} equal to $(200 \text{ fs})^{-1}$ and for acetonitrile with $\gamma_{vr} = (20 \text{ fs})^{-1}$. τ_L for cyclohexane was set to 0.25 ps, deduced from the spectral relaxation of photogenerated thiyl radicals [Loch 99]. The excess energy $\omega_{\square} - \omega_{eg}$ was 3620 cm^{-1} for all solvents. The pulselength was 50 fs, and the temperature 298 K.

As expected, the vibronic lines undergo a redshift equal to $\sigma_e - \sigma_g$ and broaden from the excitation pulse-length determined spectral width to Δ. When vibrational relaxation is much faster than solvent reorientation (such as for $\gamma_{vr} = (20 \text{ fs})^{-1}$, cf. Figure 4.4-1), the vibrational structure disappears within the first 100 fs. The subsequent relaxation consists only of the redshift, and the spectral width and form remain unaltered.

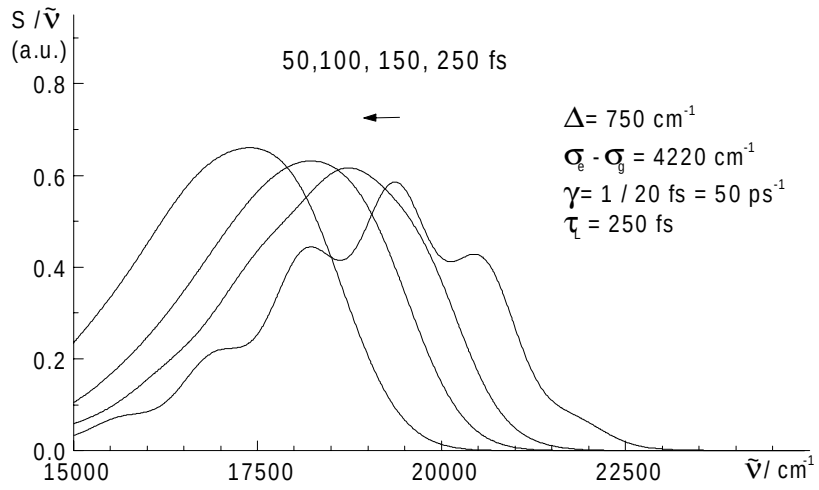

Figure 4.4-1: Time-dependent fluorescence lineshapes of DCM in acetonitrile after eq. 4.11 for a fast vibrational relaxation rate.

For a smaller vibrational relaxation rate coefficient of $(200\ fs)^{-1}$, simulations for acetonitrile are presented in figure Figure 4.4-2 along with the isolated emission spectra of DCM in that solvent. The decay of a structured emission in the 18000-24000 cm^{-1} region and the rise of a lower-frequency, nonstructured emission can be observed in both simulation and experiment. The lower-frequency emission in the simulations experiences a frequency shift about double of that in the empirical spectra, which in the simulations prevents the isosbestic region observed for delay times >300 fs around 17000 cm^{-1} in the empirical spectra.

Simulations and isolated emission spectra for DCM in chloroform are shown in Figure 4.4-3. The early simulated spectra are structured and dominated by vibrational relaxation. The smaller Stokes shift and longer reorientation time of chloroform compared to acetonitrile prevent large broadening of the spectra at intermediate times such as in the acetonitrile simulations. Therefore, the emission spectra in chloroform remain structured up to more than 500 fs. The main dynamic features only reflect those of the experiment if calculations for t > 300 fs are compared to earlier empirical spectra. This could partly be explained by faster solvent reorientation than represented by the average reorientation time.

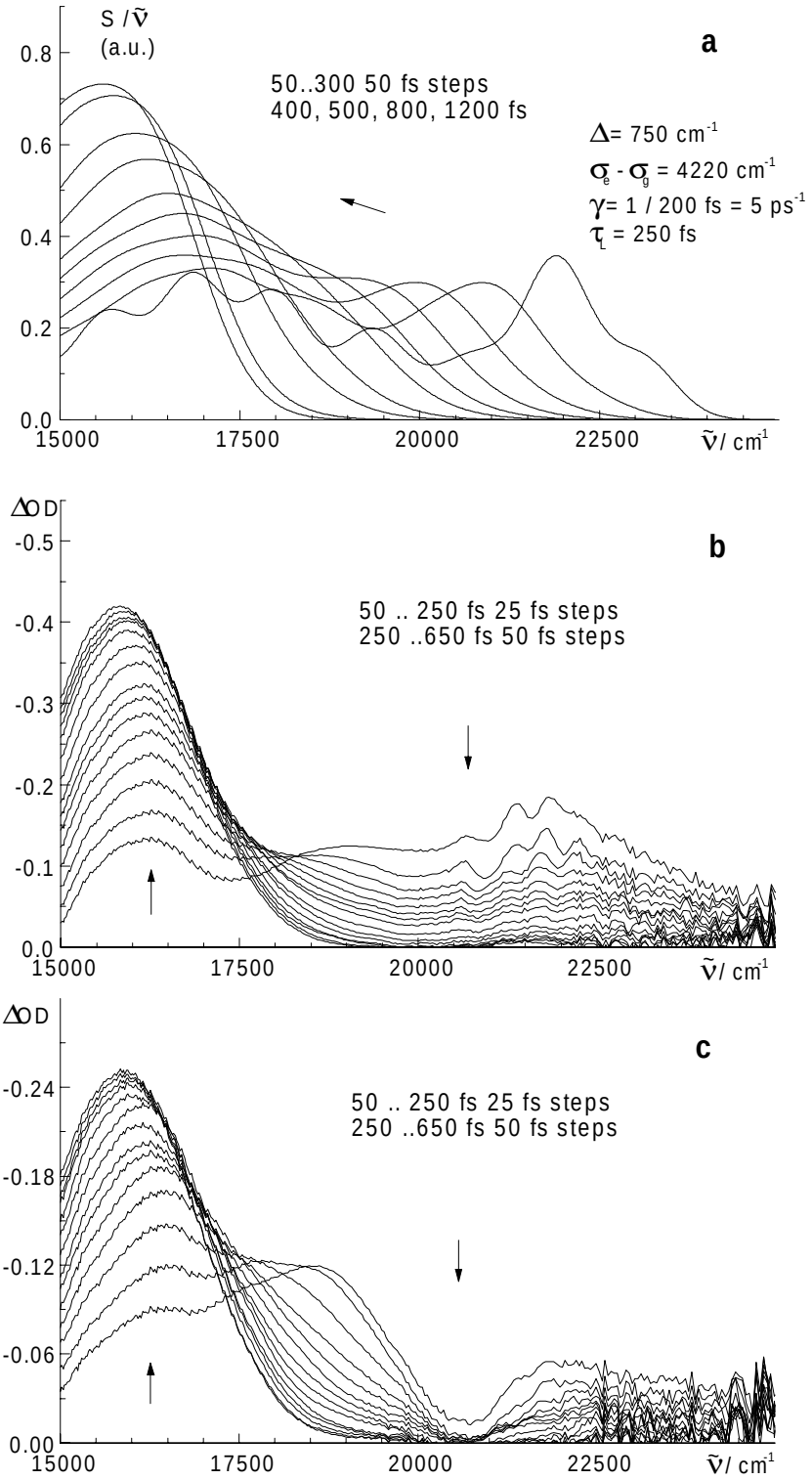

Figure 4.4-2: a) Time-dependent fluorescence lineshapes of DCM in acetonitrile after eq. 4.11 for a vibrational relaxation rate of $(200\ fs)^{-1}$. Also shown are isolated stimulated emission spectra in the same solvent after 470 nm excitation for an excitation pulse energy of a) 0.4 µJ and b) 0.9 µJ.

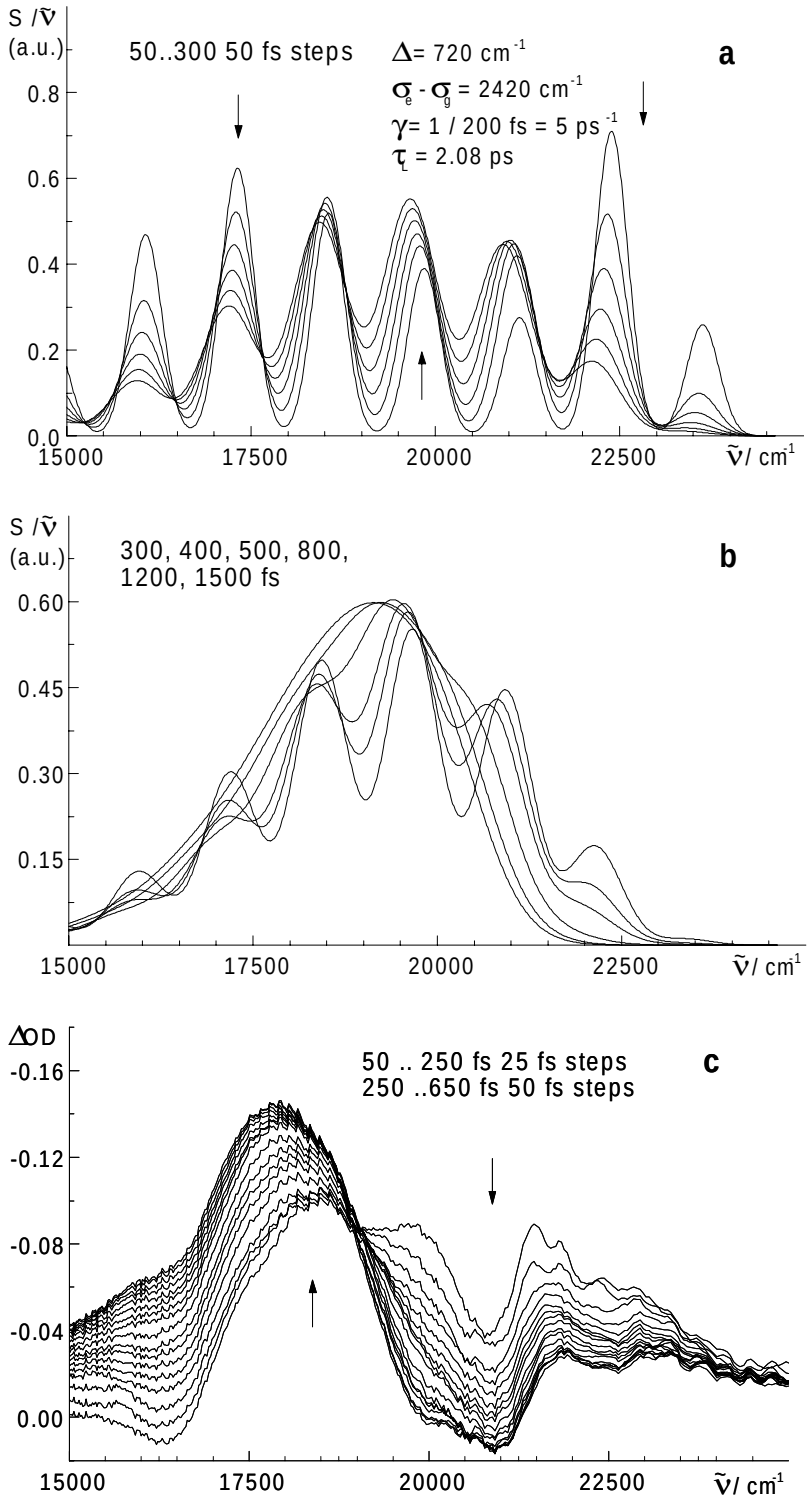

Figure 4.4-3: a) and b) Time-dependent fluorescence lineshapes of DCM in chloroform after eq. 4.11 for a vibrational relaxation rate of $(200\ \text{fs})^{-1}$ on different timescales. c) Isolated stimulated emission spectra in the same solvent after 450 nm excitation for an excitation pulse energy of 0.8 µJ.

The spectral dynamics in cyclohexane are better reproduced by the simulations (Figure 4.4-4), although the isosbestic region is shifted for about 1000 cm^{-1} to higher energies in the calculations. The spectral structure of the early empirical spectra is hidden by noise, so that no comparison of the scale of spectral broadening can be made. The Franck-Condon factors for vibronically excited DCM do not yield the large transition strength initially observed in the region 19000 - 22000 cm^{-1}, but the spectral amplitudes of the empirical fluorescence spectra are subject to a systematic uncertainty due to the spectral decomposition procedure.

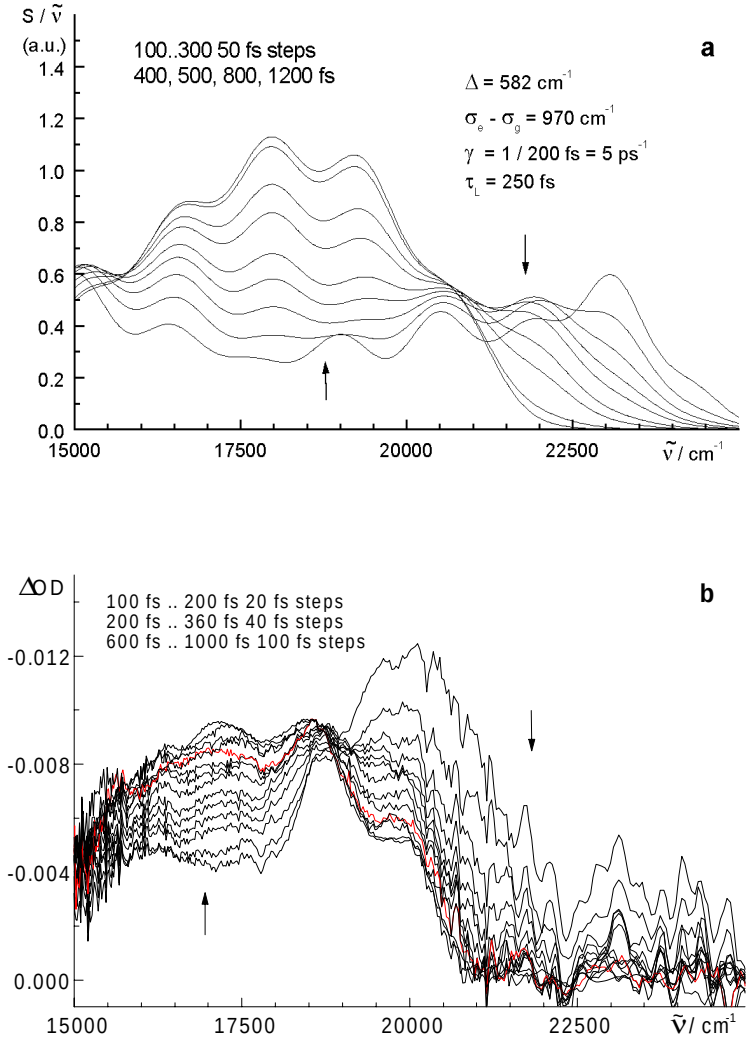

Figure 4.4-4: a) Time-dependent fluorescence lineshapes of DCM in cyclohexane after eq. 4.11. b) Isolated stimulated emission spectra in the same solvent after 450 nm excitation.

The values for the inhomogeneous broadening taken directly from the simulations of the stationary spectra are surely too large, considering that the line broadening in 2-methyl butane already amounts to approx. 550 cm^{-1}. It was necessary to include such large inhomogeneous broadening to model the observed spectral structure, since the frequency broadening in the frame of the continuum model as applied by Loring et al. is determined by equation 4.14 and much faster than the Stokes shift. So even when assuming 720 cm^{-1} for the inhomogeneous broadening in the slowly relaxing solvent chloroform, the spectral lines at t = 50 fs are already broadened to about 500 cm^{-1}.

4.5 LDS 750

Stationary absorption and emission spectra of LDS-750 are displayed in Figure 4.5-1. The width of the absorption band is larger in acetonitrile than in chloroform (4220 versus 3580 cm^{-1}), whereas the emission bandwidth is larger for chloroform (1580 versus 1390 cm^{-1}). With increasing solvent polarity, the absorption spectrum shifts to higher frequencies. The emission spectrum remains nearly unaltered, exhibiting only a small red shift of 150 cm^{-1} when going from chloroform to acetonitrile. The large width of the stationary absorption spectra of LDS-750 compared to the smaller width of the fluorescence spectra led to the assumption of several ground state conformers or isomers [Cast 87, Blanch 91, Smith 99]. Excitation of LDS-750 at 280, 332, 562 and 633 nm in acetonitrile did not change the stationary fluorescence spectrum, so that either the conformational relaxation in the excited state is fast or the conformers apart from one are non-fluorescent. The fact that the stationary absorption spectrum changes mainly its frequency position and not its shape argues against a distribution of different ground state conformers. Since they would be likely to show distinct dipole moments in the ground and excited state, their absorption spectra should exhibit different frequency shifts and the width of the total absorption spectrum should change.

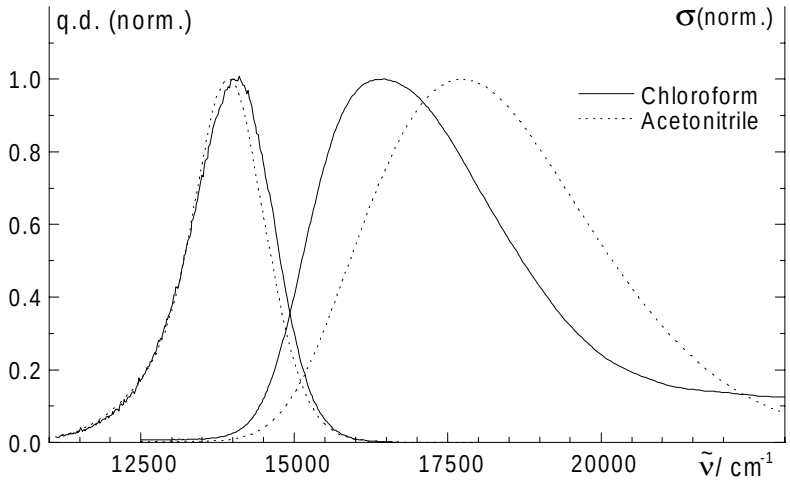

Figure 4.5-1: Stationary emission (left) and absorption (right) spectra of LDS-750 in chloroform and in acetonitrile.

Pump-probe measurements were carried out on LDS-750 with the pump pulse centered at 630 nm in chloroform, methanol, acetonitrile and propylene carbonate. The spectral dynamics were found independent of the excitation energy in the range between 0.4 and 1.2 µJ. Transient spectra for LDS-750 in acetonitrile are shown in Figure 4.5-2. Their overall composition from overlap of excited state absorption, ground state bleach and stimulated emission bands is essentially the same as for DCM (see 4.1.1). Due to pronounced changes of the excited state absorption band with delay time, spectral decomposition would be possible only by a global fitting procedure. The overall differential optical density rises for wavelengths higher than 693 nm and decreases below this isosbestic point on a longer timescale of about 600 fs. This is accompanied by the shift of the center of a broad stimulated emission band from about 700 to 723 nm.

In propylene carbonate, the initial emission band centered at 638 nm broadens and in part decays during the first 250 fs (Figure 4.5-3 a). Its decline continues up to 5 ps, going along with a rise of a lower-frequency emission band. An isosbestic point appears correspondingly around 693 nm. The rising emission is centered at 723 nm; its amplitude changes parallelly to that of the higher-frequency emission from 250 fs to about one picosecond. Afterwards, its increase proceeds up to 11 ps in spite of only small simultaneous changes in the higher-frequency emission amplitude (Figure 4.5-3 b).

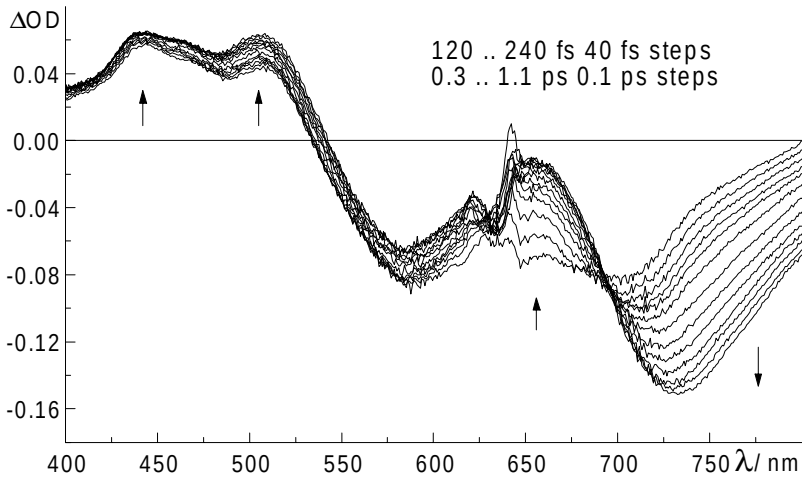

Figure 4.5-2: Pump-probe spectra of LDS-750 in acetonitrile after excitation at 630 nm.

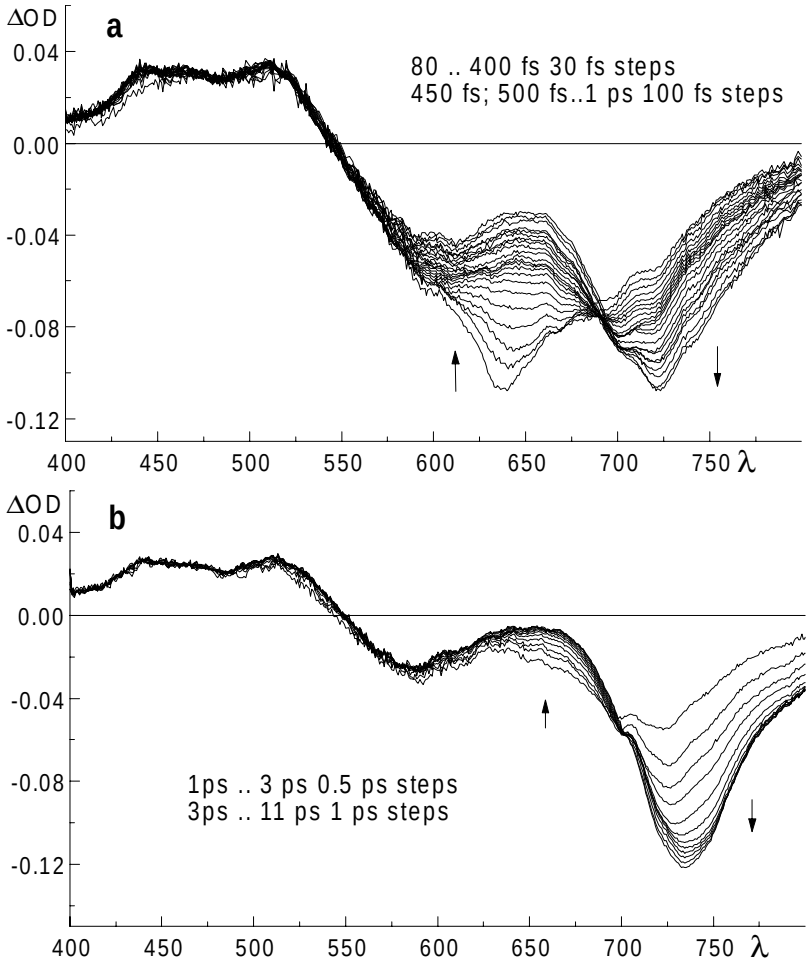

Figure 4.5-3: Pump-probe spectra of LDS-750 in propylene carbonate for different delays after excitation at 630 nm.

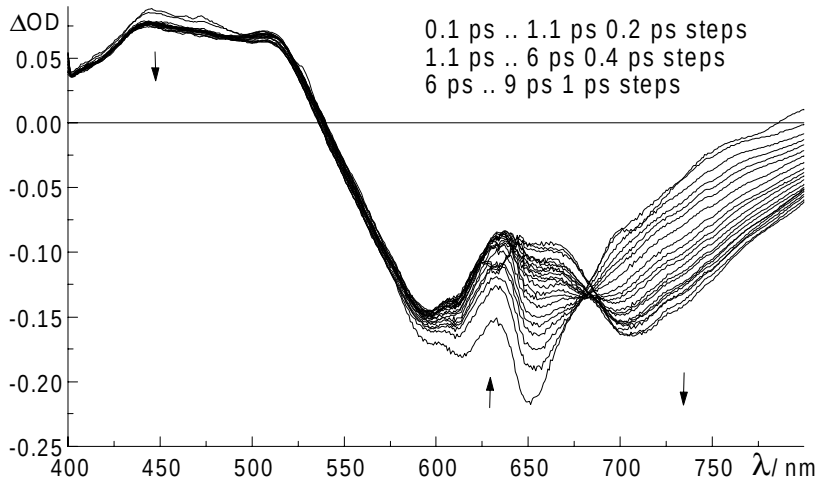

Figure 4.5-4: Pump-probe spectra of LDS-750 in chloroform after excitation at 630 nm.

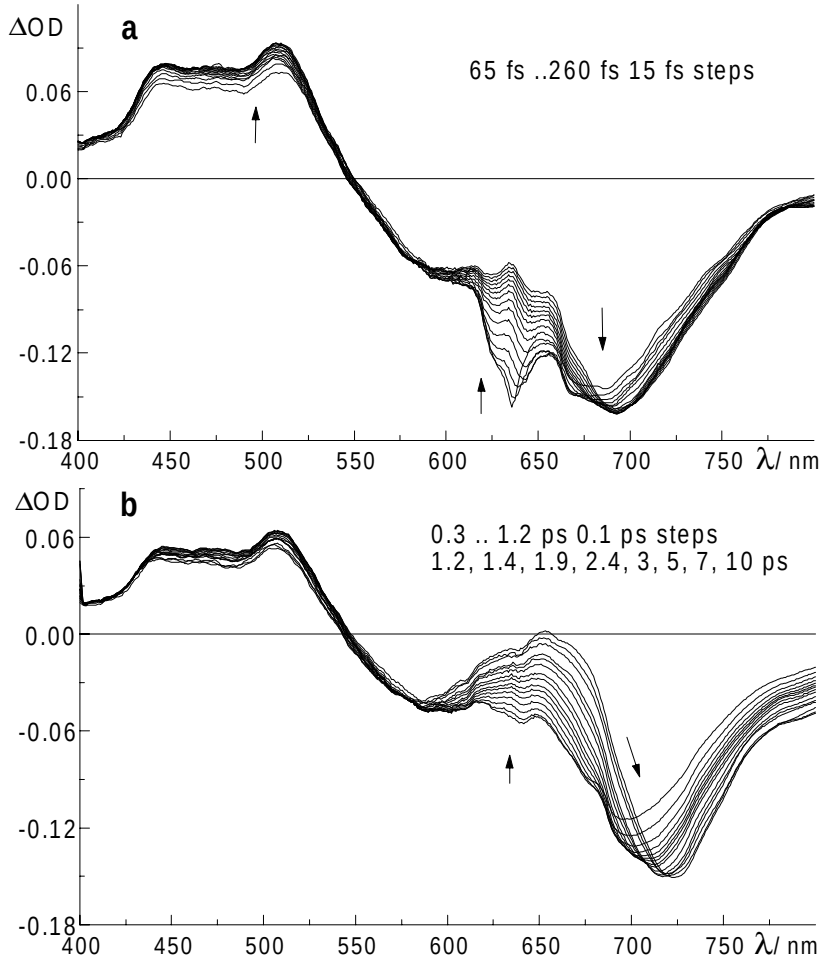

Figure 4.5-5: Pump-probe spectra of LDS-750 in methanol for different delays after excitation at 630 nm.

After photoexcitation of LDS-750 in chloroform (Figure 4.5-4), an emission band centered at 655 nm with a shoulder at 614 nm partly decays in the first 400 fs. For delay times from a few hundred femtoseconds until about 10 ps, these emission bands continue to decline in amplitude, and a broader emission band rises, shifting from around 695 to 707 nm. An isosbestic point is found at 683 nm.

In methanol, the spectral dynamics (Figure 4.5-5) are similar to the features in chloroform. The initial fast (within instrumental resolution) decay and broadening of a small emission band centered at 635 nm is accompanied by a rise of the excited state absorption. From about 120 fs up to several picoseconds, the broadened emission band decays further in the region 590 - 660 nm, while another emission band rises in the red spectral region. The latter shifts during its rise from approx. 685 nm to a final peak wavelength of 718 nm, leading to the appearance of several consecutive "temporary" isosbestic points.

Instead of a global analysis, which is often deranged by high parameter correlation, fits to selected kinetic traces were performed using sums of exponentials and effectively instanteneous contributions convoluted with the instrumental response function. Results for wavelengths representative of the species associated with the two emission bands are listed in table 4.5 and compared to characteristic time coefficients for solvent relaxation [Horng 95]. For all solvents, the fast disappearance of high-frequency emission is reflected in a large instanteneous or fast decay, whereas a large fraction (> 0.5) of low-frequency emission rises with time coefficients >0.53 ps. This indicates the involvement of more than two states in the dynamics. The time coefficients for fast decay of the high-frequency emission are close to those for inertial solvent motion, whereas the time coefficients of the slower decay / rise component change with solvent as the timescale for diffusive solvent motion. Apart from the values for methanol, the latter agreement is also quantitative.

Table 4.5.1: Decay and rise times (in ps) from fits of sums of exponential functions to wavelength traces of LDS 750 in different solvents. Solvent relaxation times from [Horng 95] are also given.

	τ / ps		
Solvent	Decay 645 nm	Solvent Rel.	Rise 722 nm
Acetonitrile	0.08 (0.86)	0.089 (0.686)	inst. (0.35)
	0.56 (0.14)	0.63 (0.314)	0.53 (0.65)
Methanol	inst. (0.6)	inst. (0.101)	inst. (0.47)
	0.99 (0.25)	0.28 (0.340)	0.66 (0.53)
	7.7 (0.15)	3.2 (0.298)	
		15.3 (0.261)	
Propylen	0.13 (0.74)	inst. (0.116)	0.19 (0.45)
Carbonate	1.82 (0.26)	0.180 (0.429)	0.99 (0.38)
		2.03 (0.237)	2.6 (0.17)
		6.57 (0.218)	
Chloroform	0.48 (0.53)	0.289 (0.356)	inst. (0.3)
	4.4 (0.47)	4.15 (0.644)	4.6 (0.7)

5 Discussion

Overview:

The results of section 4. are discussed and critically reflected, starting with DCM and continuing with LDS-750. An outlook on future investigations concludes this section.

5.1 DCM

5.1.1 Excited-state dynamics

The spectral dynamics of DCM after photoexcitation from the electronic ground state are characterized by strong excitation intensity dependence for all excitation wavelengths and solvents investigated. This is manifested in the pump-probe spectra, especially in the time evolution of their total spectral intensity. With increasing excitation energy the amplitude fraction of a non-instantaneous contribution to the decay of the total spectral intensity increases (Figure 4.1-22). This decay is ascribed to the rise and decay of stimulated emission in the ranges above and below approx. 575 nm in acetonitrile and methanol or approx. 525 nm in chloroform, toluene, tetrachloromethane and cyclohexane (4.1.2.2.). The spectral dynamics could be described by precursor-successor kinetics (4.1.5.), the analysis yielding a time coefficient τ of 0.23 ($\pm$ 0.04) ps averaged over the dynamics in all solvents investigated. This initial relaxation is followed by a red shift and further rise of the emission band in acetonitrile and in methanol, whereas in chloroform and in toluene the continued rise of the emission above 525 nm is accompanied by a further decay of emission below this wavelength.

The excitation energy dependence cannot be explained by saturation; it is interpreted as due to resonant two-photon absorption of DCM. Feeding of the S_1 from higher electronic states has been proposed before for DCM [Kov 96, Ruth]. Very high effective non-resonant two-photon absorption coefficients have been reported for bis-donor substituted stilbenes in

acetone and toluene by Ehrlich et al. [Ehr 97]. From a comparison of measurements with the same excitation energy, but different pump wavelengths of 530 and 470 nm in Figures 4.1-1 c) and 4.1-10 b), the larger relative amplitude of the blue shifted emission in the data for 470 nm excitation indicates a wavelength selectivity of the two-photon absorption process. The excited state absorption, as obtained from the spectral decomposition (fig. 4.1-1 b), has its maximum at 465 nm in acetonitrile. The two-photon absorption process may therefore be pictured to be resonant, with the first singlet excited state as an intermediate level. The transition strength for the excited state absorption can be roughly estimated from the spectral decomposition to about 1.4 x the transition strength for $S_0 \rightarrow S_1$ absorption. The maximum extinction coefficient for ground state absorption has been determined (cf. 4.2.1) as ≈ 43300 l mol^{-1} cm^{-1} in acetonitrile, so that the maximum exctinction coefficient for the excited state absorption is ≈ 61500 l mol^{-1} cm^{-1}. The absorption cross section σ can be calculated from the extinction coefficient after $\sigma = \varepsilon \cdot 1000 \ln(10)/N_A$ to maximum values of $\sigma_{\square\square} = 1.66 \times 10^{-16}$ cm^2 for the $S_0 \rightarrow S_1$ transition and $\sigma_{\square\square} = 2.36 \times 10^{-16}$ cm^2 for the $S_1 \rightarrow S_N$ transition.

The transition moment d is related to the absorption spectrum according to [Lip 68] by:

$$|d|^2 = \frac{3h \ln(10)\, 1000\, c}{8\pi^3 N_A} \int_{band} \frac{\varepsilon(\tilde{\nu})}{\tilde{\nu}} d\tilde{\nu} \quad . \tag{5.1}$$

From the intensity of a lognormal approximation to the ground and excited state absorption bands, the transition moments d_{01} and d_{1N} were calculated after equation 5.1 to 2.95 x 10^{-29} and 3.02 x 10^{-29} Asm, respectively.

A cross section of two-photon absorption $\tilde{\sigma}$ may be defined which is normalized by the photon flux per unit area $I = P / A\hbar\omega$:

$$\tilde{\sigma} = \sigma / I \quad . \tag{5.2}$$

Schubert and Wilhelmi [Schub] deduced the following expression for $\tilde{\sigma}$:

$$\tilde{\sigma}_{0N}(\omega) = \frac{\pi\omega_{0N}^2}{8(n^{(L)})^2 \varepsilon_0^2 c^2} g(2\omega - \omega_0) |\alpha_{0N}|^2 \quad . \tag{5.3}$$

Here $n^{(L)} \approx 1$, ε_0 is the vacuum dielectric constant, ω_0 is the (angular) transition frequency and $g(\omega - \omega_0)$ is the absorption line shape function. For simplicity, a Lorentzian lineshape is assumed, with

$$g(\omega-\omega_0) = \frac{1}{\pi}\frac{1/\tau_0}{(\omega-\omega_0)^2+(1/\tau_0)^2} \qquad (5.4)$$

where τ_0 is the dephasing time of the electronic transition and estimated to $\tau_0 \approx 10^{-13}$ s.

$\alpha_{\square\square\square}$is the polarizability matrix element for the transition between levels 0 and N. If the intermediate level 1 between the ground state and the state N reached by two-photon absorption is far from resonance, the polarizability can be approximated by [Schub] :

$$\alpha_{0N} \approx \frac{2}{\hbar}\frac{d_{01}d_{1N}}{\omega_{01}} \qquad (5.5)$$

so that for non-resonant two-photon absorption here α_{0N} would be $\approx 4.21 \times 10^{-39}$ Asm^2 / V and $\tilde{\sigma}_{0N} \approx 2.0 \times 10^{-54}$ m^4 s. A photon flux of $\approx 10^{33}$ m^{-2} would therefore be enough to achieve effective non-resonant two-photon absorption. The 50 fs, 470 nm-centered pulse with a diameter of 150 µm on the sample and 1 µJ pulse energy such as employed in the pump-probe experiments corresponds to an intensity of 1.1×10^{15} J/m^2s and a photon flux of $\approx 2.7 \times 10^{33}$ $m^{-2}s^{-1}$. This yields $\approx 0.54 \times 10^{-16}$ cm^2 for the two photon cross section and thus raises it to about one third of the cross section $\sigma_{\square\square\square}$for the one-photon transition to the first singlet excited state. In the case of resonant two-photon absorption, the interaction cross section may increase by up to 10^7-10^8 [Letok]. Unfortunately, the excitation energy could only be varied in a range from 0.2–1.4 µJ, the lower limit determined by the signal-to-noise ratio and the higher limit imposed by saturation of the $S_0 \rightarrow S_1$ transition. Therefore, and because of the overlap of the excited state absorption band, a more thorough study of the excitation intensity dependence of the blue shifted emission could not be carried out. The shift of the early emission bands in the pump-probe spectra of DCM in chloroform when changing from a 470 nm excitation wavelength to 530 nm excitation (figures 4.1-12 b) and 4.1-13), leads to the assumption that at least in chloroform, several higher-lying electronic states may be reached by two-photon absorption. This is roughly confirmed by the semiempirical calculations yielding three transitions between 38000 and 41000 cm^{-1}.

In the limit of zero excitation energy, the time coefficient τ for the decay of the integrated spectral intensity reduces to approx. 0.09 ps in acetonitrile (4.1.4.), close to the timescale of inertial motion for acetonitrile molecules of ≈ 100 fs [Cho 92, Horng 95, Ruth 98]. A

similar tendency towards lower values for τ in chloroform and tetrachloromethane cannot be relied on, because the large scattering of values from different days of experiment would require a larger data set. The trend in acetonitrile can be interpreted in two ways: either a very fast reaction takes place or is observed only for low excitation energy, or solvent relaxation gradually alters the transition strength for $S_1 \rightarrow S_0$ fluorescence. The lack of excitation energy dependence of the time coefficients from the precursor-successor fits and the fact that there is no fast decay of the emission in the blue and green spectral region support the second assumption. It may also explain the absence of a decrease of τ with excitation energy for methanol, where most of the energy relaxation from solvent reorientation is slower than 0.2 ps (see discussion of LDS-750 results). The solvent-dependent continued rise of the emission band in acetonitrile and methanol on a picosecond timescale would also be in line with a transition strength dependence on solvent orientation. It could not be examined whether these amplitude changes are reflected in the total intensity on a picosecond timescale, because the noise level is too high to detect a small decay component of the integrated spectral intensity. The amplitude rise could also be due to emission band narrowing as observed by Glasbeek et al. and Gustavsson et al. [vdMeul 98, Gust 95].

On the other hand, the appearance of a second band around 460 nm in addition to that at 540 nm (fig 4.1-10) with higher excitation energy indicates a three-state scheme such as proposed by Ruthmann [Ruth], who found evidence for a charge transfer reaction of DCM in S_1 in methanol with τ = 246 fs and feeding of the reactant state from an emissive higher-lying electronic state with τ = 120 fs.

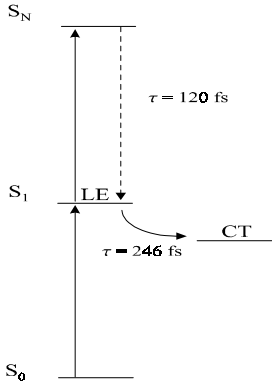

Figure 5.1-1: Three-state scheme for DCM relaxation in methanol as proposed by Ruthmann.

This cannot be corroborated here, as no indication of a decay as fast as 120 fs resulted from the precursor-successor modelling at high excitation energies. If there are three states involved in the relaxation, the reaction rate appears not to be influenced by the reaction path. It is also nearly independent of the solvent (table 4.1). The absence of dielectric relaxation effects on electron transfer have been reported for porphyrine-dichloroquinone cyclophanes [Pöll 92], so that a charge transfer reaction from two precursor states, the population of which depends on excitation energy, might be thought of.

5.1.2 Ground state dynamics

In the first 400-600 fs the evolution of the dump-probe spectra is determined by a decay of a structured absorption band at wavelengths larger than 519, 537 or 558 nm in acetonitrile, methanol and propylene carbonate, respectively, and the rise of another absorption to the blue of this temporary isosbestic point. The dynamics can also be modelled by precursor-successor kinetics with a time coefficient of 0.28 ($\pm$ 0.07) ps, averaged over similar dynamics in acetonitrile, methanol and propylene carbonate. After 400-600 fs, the absorption band shifts continously to the blue, accompanied by a decrease of the integrated spectral intensity on a solvent-dependent, picosecond time scale. From the empirical comparison of the dynamical Stokes-shift of DCM with that of coumarin 153 (4.1.3.), the relaxation of DCM after 0.6 ps in the ground and excited electronic states in dipolar solvents is assigned mainly to solvation dynamics. The decrease of the integrated intensity on the same timescale is attributed to a decline in amplitude of the absorption band, corresponding to a modification of the transition strength to the S_1 state by solvent reorientation. The dynamics before 0.6 ps are governed by a state-to-state transition, which could be either intramolecular vibrational redistribution or a conformational relaxation of DCM, possibly connected with a charge redistribution.

5.1.3 Charge transfer reaction

Possible evidence for a charge transfer reaction from the analysis of the stationary spectra and from quantum chemical calculations is discussed next. The solvatochromic analysis (4.2.4.) does not give evidence for a sizeable change in dipole moment after optical transition to the electronic excited or ground state, since the polarity dependence of the

peaks of the absorption and emission spectra could be described with nearly the same set of parameters, only differing by 0.3 Å in the Onsager cavity radius. Usually the molecular radius is not treated as a parameter but estimated from the van-der-Waals radius of the molecule. The value obtained here for r_0 (≈ 10 Å) is large compared to 5.7 Å for DCS from a similar analysis of [Il'ich 96]. It is closer to the 8 Å assumed for DCM by Marguet et al. [Marg 92] from extrapolated literature data of the subunits forming the DCM molecule. A crystallographic structure analysis would be necessary to clarify these differences. The deviations from the fit in Figure 4.2-7 are not due to measurement errors, but signify the shortcomings of the continuum model which does not account for microscopic solvent structure.

The excited state dipole moment of 23 Debye used in the solvatochromic analysis could not be reproduced in the quantum chemical calculations (9.9 D and 14.9 D for S_0 and S_1), which limits their reliability or at least their transferability to the description of the excited state in solution. The calculated dipole moment changes after excitation into S_1 or S_2 were very small (-0.44 D for S_1 and + 1.7 D for S_2) so that a large charge alteration after photoexcitation seems not very probable for DCM. Also, the small changes in dipole moment with torsion of the anilino, dimethylamino or dicyanomethylene-methyl-pyran subunits in S_0, S_1 or S_2 are not in favour of a TICT mechanism. This differs from the result of Marguet et al. concerning the dimethylamino group, which at a 90° twist in S_2 led to marked charge transfer character of the configuration and a dipole moment of 22.45 D. For the other single bond rotations, the results are in line with the findings in [Marg 92].

The simulation of the stationary absorption spectra (4.2.5.) would be more exact if carried out using the frequencies from the resonance Raman spectrum (4.2.3.). Since the transition strenghts could not be estimated from the spectrum in methanol, but only of the crystallic form, and the amplitudes as well as the frequencies of the non-resonant Raman spectrum were found to be influenced by the environment, this could not be done. Especially the Raman peaks corresponding to vibrations of the ethylene bonds involving π electrons were subject to solvent polarizabilitiy and polarity depending variations. Also, the analysis would not have permitted a comparison of the absorption and fluorescence bands. In the frame of the simplified picture of one effective harmonic mode coupled to the optical transition, the simulation of fluorescence and absorption spectra gave evidence for gradual changes in the equilibrium position and frequencies of the S_1 and S_0 vibrations with polarity of the solvent.

The same tendency towards a smaller equilibrium displacement with increasing polarity was found for the fluorescence and absorption bands. This can be attributed rather to a static modification of the energy hypersurface of a single excited or ground state than to a polarity-dependent barrier height for the transition between two discrete conformer states.
In summary of this subsection, configurational changes after Franck-Condon projection into the electronic ground and excited states cannot be ruled out and would be even expected from the different effective harmonic frequencies and mode displacements found in the analysis of the absorption and fluorescence bands. There is no evidence, though, of the existence of several stable conformers, or of a sizeable charge separation or large alteration of electronic structure connected with those changes.

5.1.4 Vibrational relaxation and solvent dynamics

After two-photon absorption and internal conversion to S_1, the molecules should be highly vibrationally excited. A lower limit for the vibrational energy relaxation time in the electronic ground state was derived from the width of the resonance Raman line at 1552 cm^{-1} to 310 fs (4.2.3.). A fit of the lineshape of the other dominant mode at 1213 cm^{-1} to a Gaussian gives a fwhm of 11 cm^{-1} , corresponding to $T_1 > 480$ fs. Vibrational relaxation in the excited state may be faster than in the ground state, but it is unlikely that its rate should increase by a factor of 10, as would be necessary for it to remain unobserved in the pump-probe experiment. For S_N, a much larger rate for intramolecular vibrational redistribution can be assumed from the higher density of vibronic states. Vibrational coherences due to impulsive excitation of low-frequency modes for DCM observed at probe wavelengths around 470 nm (Figure 5.1-2) persist for longer than a picosecond, implying small rates for vibrational dephasing and energy transfer also for low-frequency modes. This is important, because vibrational relaxation by energy transfer to low-frequency solvent modes via low-frequency "exchange" solute modes has been proposed [Shelby 79]. Vibrational dephasing time coefficients as large as 440-1330 fs have been found from the analysis of vibrational coherences in the time-resolved pump-probe spectra of a cyanine dye, HDITC, in ethylene glycol [Yang 99]. It is concluded that for high excitation energies, the dynamics observed in the pump-probe spectra of DCM with an average time coefficient 0.23 ($\pm$ 0.04) ps can be attributed to intramolecular vibrational energy redistribution in S_1 after fast internal

conversion from a higher-lying electronic state S_N. The approximate independence of the reaction rate from solvent polarity supports this assumption, as IVR for *trans*-stilbene has been found to take place in about 2 ps in methanol and in hexane [Schultz 97]. This can be explained by the presence of a large number of intramolecular low-frequency modes in molecules of the size of stilbene, which permit the redistribution of energy independently of the solvent low frequency modes and therefore render IVR insensitive to the solvent spectral density for such modes.

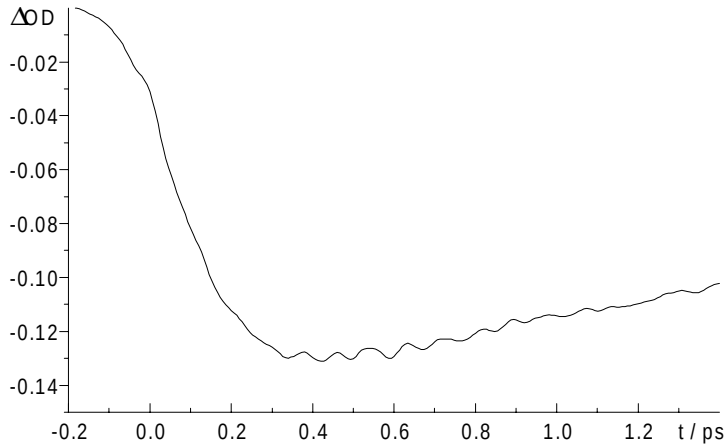

Figure 5.1-2: Quantum beats in the kinetic trace at 577 nm of DCM in methanol from pump-probe measurement with excitation at 470 nm and an excitation pulse energy of 0.4∴µJ.

The simulations of vibrational relaxation and solvent reorientation (4.4.) reflect the principal dynamic features of the stimulated emission spectra at high and intermediate pump energies, but can neither account for the exact frequency spacing of the emission bands, nor for the correct timescale of the spectral dynamics in chloroform. There are several reasons to consider: the simplest, that several optically bright excited (electronic) states are involved (see 5.1.1.). The dielectric relaxation times τ_L were set to the average time coefficient of the coumarin 153 Stokes shift dynamics, which may have led to an overestimation of the relevant τ_L in chloroform. For example, fast translational motion of the chloroform molecules might be the relevant movement here for energetic stabilization of the excited state. Furthermore, the value of 3620 cm^{-1} for the excess energy was rather arbitrarily selected from the energetic spacing of the emission bands in the early pump-probe spectra of DCM in methanol and might be too low, if following the quantum chemical calculations. On the other hand, vibrational relaxation could be faster for higher vibrational states than

determined by the quadratic dependency on excess energy in the model of Montroll and Shuler (2.4.). A bottleneck for vibrational relaxation at low excess energies has been proposed for *trans*-stilbene by Nakabayashi et al. [Nak 98]. Nevertheless, the simulations demonstrate why *spectral changes appear more pronounced in chloroform* (thanks to the relatively long reorientation time of the large chloroform molecules) not only for DCM, but also for LDS-750. Another interesting feature is the observation of *isosbestic points* in the cyclohexane and chloroform simulations, which is usually interpreted as a sign of direct inter(electronic)-state relaxation and here is due to intramolecular vibrational energy redistribution.

Cyclohexane has been treated analogously to the dipolar solvents, which at first view is justified by the observation of nonpolar solvation dynamics for other molecules [Loch 99, Gard 95, Yam 97], see also 2.3., and by the large Stokes shift of DCM in liquids with small $\varepsilon_{\square}$. At a closer look, this process has been explained by [Gard 95] as being due to quadrupol and higer order electrostatic moments of non-dipolar solvent molecules which are not present for 2-methyl butane. The Stokes-shift of DCM in 2-methyl butane is as large as 870 cm^{-1}, though (4.2.5.). Dispersive forces, which should then be responsible for the Stokes shift, are characterized by a $1/r^6$ potential, whereas Coulombic interaction energy decreases with distance as 1/r. Therefore, a treatment of non-dipolar solvation dynamics by a Debye model may seem inappropriate, and mechanical relaxation theory would be more suitable [Berg 94, Ma 95]. Ladanyi and Klein [Lad 96b] have shown in molecular dynamics simulations that in spite of the more translational character of non-dipolar solvation dynamics most of the solvation process arises from the innermost region of the solvent shell, as with dipolar solvation, and may therefore be as fast as the latter, only missing the Gaussian inertial component. The continuum model in the form used here only roughly approximates the dipolar solvation dynamics, since multiple timescales and Gaussian inertial behaviour are ignored, so that it serves as an approximation to both dipolar and non-dipolar solvation. A model describing both solvation processes in more detail and on a physical foundation would be more appropriate and might give results closer to the data.

5.1.5 Overall reaction scheme

The optical properties and the reaction dynamics of DCM as could be elucidated in this work are summarized and discussed in conclusion.

Franck-Condon excited state

The larger instantaneous relative amplitude of the excited state absorption in the pump-probe spectra of DCM in non-dipolar solvents implies a solvent-dependent transition strength to higher electronic states or to the ground state. It exceeds by far the solvent-dependence of the transition strength for the $S_0 \rightarrow S_1$ transition as reflected in the maximum extinction coefficients for the stationary absorption in 5.2.1. Therefore, it is mainly ascribed to a variation of the transition strength to higher electronic states. This is explained by *different instantaneous electron density distributions of the S_1 state in non-dipolar and dipolar solvents*. It should be interesting to check on this conclusion by performing semiempirical calculations under consideration of the solvent environment. The altered charge distribution implies a variation of the equilibrium displacement of the vibrational modes coupled to the electronic transition. Indeed, a gradual variation of the displacement of an effective harmonic vibrational mode with solvent polarity has been noted (4.2.5).

Competing reaction channels

The large dipole moment of DCM in S_1 implies a notable stabilization of the first singlet excited state by dipolar solvation. It is manifested in the spectral shift of the stimulated emission spectra, and also in the "Anti-Stokes" shift of the time-dependent ground state absorption spectra after 400-600 fs in dipolar solvents. Thus, the spectral evolution *after 400-600 fs in dipolar solvents* in the electronic ground and in the excited state is found to be determined mainly by diffusive *solvation dynamics*. Stabilization of the excited state by dipolar solvation would be coincident with an increased barrier height for isomerization in dipolar solvents, if the latter proceeded via an intermediate state of a moderate dipole moment. A *lack of evidence for photoisomerization in cyclohexane* together with the low fluorescence quantum yield in that solvent hint at the importance of *another desactivation channel apart from isomerization*, though, e.g. inter-system crossing to a close-lying triplet state.

The spectral evolution after 400-600 fs in dipolar solvents is attributed primarily to

solvation dynamics in the electronic ground and in the excited state. But what is the nature of the relaxation observed in the first half of a picosecond, and how to explain the changes in bandshape or (for dipolar solvents) in transition strength observed on a picosecond timescale?

Sub-picosecond dynamics

For *high excitation intensities* (>0.5x10^{15} J/m^2s) , *vibrational energy redistribution after fast internal conversion* from one or more higher-lying electronic state(s) S_N is likely to be the dominant process observed in the pump-probe measurements (see 5.1.1., 5.1.4.). In contrast to the findings of Ruthmann [Ruth], no differences were observed between the relaxed pump-probe spectra at 20-40 ps measured with high and low excitation intensities in methanol, acetonitrile and toluene. It is concluded that from any populated state S_N, internal conversion to S_1 is the only accessible reaction channel.

Low excitation intensities are difficult to realize, and even if present, vibrational excess energy may be conferred upon the molecules depending on the choice of the excitation wavelength. In the stimulated emission pumping experiments, the dump pulse was centered to the blue of the fluorescence maximum of DCM in the solvents investigated. *If the total Stokes shift* of DCM is attributed to dipolar, multipolar or nonpolar *solvent reorganization*, as presumed in 4.2.5., no excess energy is expected for the molecules after stimulated emission pumping. The same argumentation applies to optical excitation at 530 nm of DCM in methanol and acetonitrile with low excitation intensity. Resonant two-photon excitation can be more easily evaded here, as this wavelength is far from the excited state absorption maximum. The excitation wavelength 530 nm is also situated on the red edge of the absorption spectrum in methanol and acetonitrile. Unfortunately, the larger excited state absorption in non-dipolar solvents and its proximity to the ground state absorption band prevent similar measurement conditions for these solvents. But for dipolar solvents, in the frame of the stated assumption, *vibrational relaxation can be excluded* from the causes of the ground state dynamics and excited state dynamics for low-intensity 530 nm excitation.

Conformational relaxation

Under these experimental conditions, the decaying and rising bands are very close, the maxima spaced by approximately 900-1100 cm^{-1} (fig. 4.1-1 c) and 4.1-8 a). In the isolated ground state absorption spectra, the frequency difference between the maxima of the

precursor and successor species is 2100-2300 cm^{-1}. This is reflected in the precursor / successor spectral amplitudes as presented in figures 4.24 b) and 4.25 b). An assignment of the structured precursor spectra to a locally excited (LE) state as in [Kov 96] is not possible, because the ground state precursor spectra should then belong to the charge transfer conformation and be broad and without structure. A *conformational relaxation* is tentatively assigned to the observed relaxation in the electronic ground state and for low-intensity excitation conditions, also in the excited state.

The maximum dipole moment differences corresponding to the energetical spacing of the precursor and successor species can be estimated as follows. The solvent reorganization energy was estimated to 4320 cm^{-1} in acetonitrile (see 4.4.). The dipole moments of the relaxed ground state and excited state conformations were assumed as 9 and 23 Debye, and their absorption and fluorescence spectrum were assumed to be coincident with the stationary absorption and emission spectrum. The dipole moments of the precursor conformations in the ground and excited states were then calculated via equation 2.31, substituting $\Delta\nu - \Delta\nu_{\square}$ in equation 2.31 by 4320-2300 cm^{-1} and 4320 -1100 cm^{-1}, respectively. The dipole moment of the precursor conformation was thus estimated to <13.4 D in the ground state and to > 21.1 D in the excited state, so that the maximum dipole moment variation between reactant and product state would be 2 D in the electronic excited state and 4.4 D in the electronic ground state. The observed reaction therefore *cannot be characterized as a charge transfer reaction*, as it could be expected from 5.1.3. Since the reaction rate is nearly the same in the highly viscous propylene carbonate and in methanol ($\approx (0.3\ ps)^{-1}$), large amplitude motion such as a 90° single bond twist does not seem probable. Such a conformational relaxation was attributed to the reaction of DCS after photoexcitation by comparison with the bridged compound DCS-B24 [Abr 97]. Bicimer formation should also be ruled out for the DCM concentrations utilized.

The fact that the rate coefficient for relaxation in the excited state in most solvents ($\approx (0.23\ ps)^{-1}$) is found independent of the excitation intensity indicates a similar reaction mechanism for the conformational and the vibrational relaxation. Electron-transfer has been reported to proceed via higher vibrational levels of the product state. With only approximately 1000 cm^{-1} energy difference between the reactant and product states and no excess energy provided by photoexcitation, this reaction mechanism can be once more

excluded. *If some part of the Stokes shift* of DCM was due to *intramolecular vibrational reorganization*, though, the observed conformational relaxation in the excited and in the ground state *could simply reflect the redistribution of vibrational excess energy*.

Picosecond dynamics

The changes of the pump-probe spectra on a *picosecond timescale* may be explained *by vibrational cooling*, if the short-time dynamics are assigned to IVR. The manifestation of vibrational cooling should be more prominent for higher excitation intensity, when a large fraction of molecules is highly vibrationally excited. The fact that the observed spectral changes on a picosecond timescale are independent of excitation energy (figures 4.1-9, 4.1-11 and 4.1-12) renders vibrational cooling unlikely as their cause, and favours *(continued) conformational changes* on a picosecond timescale as an explanation. This is similar to the findings of [Mart 95, 97] and also accounts for the observation of an isosbestic region in the pump-probe experiments in chloroform and toluene on a picosecond timescale. In dipolar solvents, the conformational relaxation is held responsible for the decrease in transition strength with solvent reorientation in the electronic ground state, and for the amplitude growth of the stimulated emission spectra on the same timescale. An increase of transition strength in the excited state and a decrease in the ground state correspond to forward and backward reaction, respectively. The slightly different equilibrium displacements of an effective harmonic mode in the absorption and fluorescence spectra are attributed to this conformational relaxation. No charge transfer reaction as in [Mart 95, 97] is concluded. In contrast to the short-time dynamics, the characteristic timescale of this relaxation depends strongly on the solvent. For dipolar solvents, the nature of this reaction can be characterized as highly adiabatic, since no change in spectral bandshape occurs. This leads to the impression of a gradual variation of transition strength with solvent reorientation. It should be kept in mind, though, that for the excited state the small picosecond rise of the emission band in dipolar solvents might also be due to emission band narrowing by nonlinear solvation [Mat 97, vdMeul 98].

5.2 LDS-750

In contrast to DCM, LDS-750 shows a solvent-dependence of the dynamic changes in its stimulated emission band on a very short (sub-80 fs until 500 fs) timescale as well as in the picosecond range. The initial fast decay of an emission band centered around 635-655 nm is most pronounced in chloroform and propylene carbonate, whereas in methanol and acetonitrile it is harder to detect, taking place nearly within the instrumental time resolution. It is followed by a further decay of this band within 0.6 - 1.8 ps and the simultaneous rise of a red shifted emission band centered around 700-720 nm in all solvents except acetonitrile. Here the lower-frequency emission band rises with a time coefficient of approximately 0.5 ps with only small changes in differential optical density in the region of the higher-frequency emission. This is paralleled by the spectral evolution in propylene carbonate for long delay times, when the red shifted emission also grows with a time coefficient of 4.4 ps with only a very small corresponding decay of the higher-frequency emission band.

The time coefficients have been deduced from an analysis of the kinetic traces at prominent wavelengths and are subject to errors especially in methanol, where the observed frequency shift of the slowly rising emission band is large. The multiple timescales of the rise and decay of emission cannot be extracted from the integrated spectral intensity, as here the simultaneous rise and decay components partly compensate and therefore the other components are overweighted. In addition, the time coefficients for fits with sums of more than two exponential functions are often correlated if they do not differ by at least a factor of five, which naturally also limits the reliability of the analysis of the kinetic traces. The estimated error for the given time coefficients from different fits and measurements is about 20%.

The initial, fast decay of the higher-frequency emission is attributed to a fast depopulation of the Franck-Condon excited state. Since there is no simultaneous growth of the lower-frequency emission, the optical transition from the product state to the ground state should be forbidden. The reaction rate is close to the inverse time for inertial solvent motion (see 4.5.) and explains, why these motions were first claimed to have been observed in the spectroscopy of LDS-750. In chloroform, where the fastest solvent reorientation time is in the range of hundreds of femtoseconds and the spectral broadening and the decay is

therefore slower than for the other solvents (see 5.1.4.), the initial higher-frequency emission still exhibits some substructure with bands spaced by approximately 1000 cm^{-1}.

The Franck-Condon excited state is depopulated nearly completely by this fast reaction in acetonitrile, as the emission around 650 nm is found drastically reduced after 240 fs. This is not the case for the other solvents; especially in chloroform the amplitude of the lower-frequency emission band is still larger than that of the lower-frequency emission band after 1.3 ps. In methanol, propylene carbonate and chloroform population is transferred from the Franck-Condon excited state to the final emissive state on a 0.6 - 5 ps scale depending on solvent. Finally, in acetonitrile and propylene carbonate, the population of the final emissive state grows by feeding from an optically quasi-dark state, as now the higher-frequency emission rises accompanied only by small changes of differential optical density in the spectrum below 680 nm. The reaction rates for the population of the final emissive state vary with the relaxation times for diffusive solvent reorientation and agree with these apart from methanol (see 4.5.).

The reaction scheme thus involves *three electronic states or conformers in the first electronic excited state* (Figure 5.2-1), namely the Franck-Condon excited state A, a second state with a quasi-forbidden optical transition to the electronic ground state B, and the state from which the emission around 720 nm occurs (C). Since the transition $S_0 \rightarrow S_2$ was found at 9460 cm^{-1} higher energy than the $S_0 \rightarrow S_1$ transition [Ruth], the states A, B and C must correspond to conformers of LDS-750 in the first excited singlet state. The larger amplitude of the excited state absorption and bleach bands relative to the emission band in the relaxed spectrum of LDS-750 in chloroform compared to the more strongly dipolar solvents indicates a solvent-dependent population distribution between these conformers. The equilibrium population of the quasi-dark state appears to be significant in chloroform. It could not be checked if in consequence the fluorescence quantum yield in chloroform is lower than in the other solvents, since the fluorescence lifetime in chloroform was not known. For several dipolar solvents, [Cast 87] found an inverse proportionality between the fluorescence lifetime (160 ps in acetonitrile and 230 ps in methanol) and solvent visosity. It was concluded that the fluorescence lifetime of LDS-750 is shortened by some non-radiative process, most likely an excited state isomerization around one of the butadiene bonds.

The small red shift of the stationary emission spectra of LDS-750 with solvent polarity signifies a small dipole moment difference between state C and the (Franck-Condon) ground state. On the other hand, the blue shift of the stationary absorption band indicates a stabilization of the electronic ground state relative to the Franck-Condon excited state A, so that state A is expected to posess a smaller dipole moment than the ground state. This argumentation ignores possible differences in the dipole moment of the Franck-Condon and relaxed ground state configuration. An absolute dipole moment for ionic molecules can be specified only relative to a reference position, but the relative difference in dipole moment of different configurations could be estimated from semiempirical calculations as in [Ruth].
An analysis of the stationary spectra similar to that in 4.2.5 was performed by [Kov 97] yielding a dimensionless displacement of 1.4 for a harmonic 1500 cm^{-1} mode from the absorption and around 0.6 from the emission spectrum in acetonitrile. The observed dynamics after photoexcitation at 530 nm were explained by an ultrafast isomerization followed by a solvent-dependent process with a time coefficient of 0.6 ps in acetonitrile. Later, the latter mechanism was assigned to feeding from higher excited states after two-photon absorption [Ruth]. Due to the missing excitation intensity dependence observed in the experiments here, the quasi-dark state B cannot be populated by two-photon absorption, but instead is thought to be fed directly from the Franck-Condon excited state A (Figure 5.2-1 a). The further reaction mechanism is pictured as follows: The *diffusive reorientation of the solvent* molecules leads to an *energetic stabilization of state C* relative to state A (Figure 5.2-1 b). On the timescale of slow solvent motion, therefore population is transferred from A to C in all solvents except acetonitrile, where the inertial component of solvent reorientation is dominant and leads to depletion of state A. The stabilization of state C in strongly dipolar solvents finally leads to a lowering of state C beneath state B and causes additional feeding of state C from state B (Figure 5.2-1 c). Why this feeding is not observed in methanol, which is of comparable polarity to acetonitrile and propylene carbonate, can only be explained by the smaller relative influence of inertial motion in the solvent reorganization and consequently smaller population of the quasi-dark state B. The reaction mechanism A$\rightarrow$B is not clear, nor is the meaning of the connection between the reaction rate and inertial solvent reorientation understood. The isomerization of the retinal chromophore bacteriorhodopsin was reported by [Du 93] with nonexponential dynamics to proceed on various timescales, the fastest components lying in the range of 90-240 fs. The

conformer B might be an intermediate in an isomerization reaction of LDS-750, in conformity with the interpretation of [Kov 97]. Since the viscosity of propylene carbonate (2.53 cP) is large compared to methanol (0.55 cP) and acetonitrile (0.34 cP), the next step in isomerization might be hindered by solvent friction. This would acount for the elevated amplitude of the slow feeding of state C from B in propylene carbonate. The inversion of state C relative to A and B by dipolar solvation implies a markedly increase in dipole moment for the transitions A→C and B→C, so that in contrast to DCM LDS-750 is considered to be subject to a charge transfer reaction. Until a confirmation of the existence of such conformers from quantum chemical calculations can be given, the proposed scheme of Figure 5.2-1 should be regarded as preliminary.

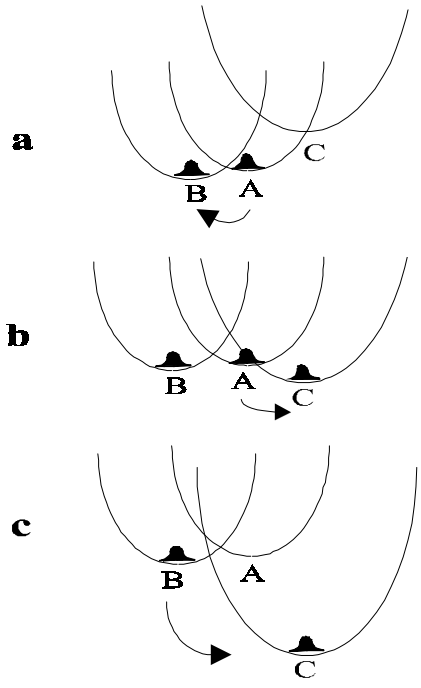

Figure 5.2-1: Proposed reaction scheme for LDS-750 relaxation after excitation into the first excited electronic singlet state. In the course from a) to c), an inversion of state C relative to states A and B occurs, due to larger energetic stabilization of state C by solvent reorientation.

5.3 Outlook

The interpretation of the pump-probe spectra is based on assumptions about or ignorance of possible changes of the spectral bands overlapping with the stimulated emission. A global analysis taking into account the excited state absorption kinetics would involve the unknown properties of at least one more higher excited electronic state. To reduce the information gained by the experiment to the $S_1 \rightarrow S_0$ transition, the *fluorescence upconversion technique* could be used instead. The spectral and temporal resolution of fluorescence upconversion experiments has up to now been limited by the nonlinear gating process of the spontaneously emitted photons, requiring a bandwidth-limiting phase-matching condition of the fluorescence and gating fields in the nonlinear crystal. An extension of this technique to the broadband, sub-100 fs regime is currently under way in our laboratory. The dump-probe technique combines high spectral and temporal resolution with the investigation of only the lowest optical transition and is therefore an extremely valuable tool to study reactions in the electronic ground state. It would be instructive to carry out these experiments on LDS-750, too, to see how the conformational back-reaction is reflected in the ground state absorption spectra. Unfortunately, the limited tunability of the CPM system did not allow for enough energy in amplified pulses above 700 nm, and below that wavelength ground state absorption was found to impede effective stimulated emission pumping of LDS-750.

The high two-photon absorbance of DCM and, as has been shown in [Kov 97, Eil 98], also of LDS-750 suggests the necessity to *reduce the pump pulse intensity to values well below* $10^{15}\ J/m^2 s$ in the investigations of large chromophores in solution. An absolute noise of $< 10^{-3}$ ΔOD is required to maintain the signal-to-noise ratio of 20-100 of the measurements demonstrated here. The further reduction of noise requires a still deeper understanding of the continuum generation process, since the spatial fluctuations of the probe continuum were found here to be the main source of noise.

Slow *intramolecular vibrational energy redistribution* has been proposed rarely up to now for complex dyes (see 2.4.) and should be considered in the interpretation also of other donor-acceptor substituted stilbenes' dynamics. It would be interesting to perform

stimulated emission pumping experiments with various excess energies or IR pump-probe experiments to study the vibrational relaxation process in the ground state. Time-resolved Anti-Stokes resonance Raman scattering investigations could also provide information on the excited state vibrational energy relaxation, but they are limited by the necessary frequency resolution of 10-15 cm^{-1} to about one picosecond in time resolution.

Finally, reliable *semiempirical calculations including solvent polarization or ab-initio calculations* (now also available for large chromophores [Schol 98, Krueg 98]) would be extremely useful to find out about possible pathways of photoexcited dyes on the multidimensional intra- and intermolecular energy hypersurface and design tailor-made experiments for the chromophore and problem under investigation.

References

[Abr 97] Abraham, E., Oberlé, J., Jonusauskas, G., Lapouyade, R., Rullière, C., J. Photochem Photobiol. A: Chemistry 105, 101-107, 1997.

[Alf 70] Alfano, R.R., Shapiro, S.L., Phys. Rev. Lett. 24, 584, 592, 1217, 1970.

[Amos 73] Amos, A.T., Burrows, B.L., in: Advances in Quantum Chemistry, Adv. Quant. Chem. 7, Ed. Löwdin, P.O., Ac. Press, New York, 1973, p 289.

[Ang 89] Angel, G., Gagel, R., Laubereau, A., Chem. Phys. Lett. 156, 169-174, 1989.

[Aren 95] Arenas, J.F., Tocon, I.L., Otero, J.C., Marcos, J.I., J. Phys. Chem. 99, 11392-11398, 1995.

[Bag 83] Bagchi, B., Fleming, G.R., Oxtoby, D.W., J. Chem. Phys. 78, 7375-7385, 1983.

[Bag 84] Bagchi, B., Oxtoby, D.W., Fleming, G.R., Chem. Phys. 86, 257-267, 1984.

[Bag 94] Bagchi, B., Roy, S., in: Ultrafast Dynamics and Solvent effects, Eds. Gauduel, Y., Rossky, P.J., Am. Inst. of Physics, New York, 1994, pp 296-309.

[Bar 90] Baranovic, G., Meic, Z., Güsten, H., Mink, J., Keresztury, G., J., Phys. Chem. 94, 2833-2843, 1990.

[Bard 97] Bardeen, C.J., Cerullo, G., Shank, C.V., Chem. Phys. Lett. 280, 127-133, 1997.

[Bau 77] Baumann, W., Deckers, H., Loosen, K.-D., Petzke, F., Ber. Bunsenges. Phys. Chem. 81, 799-804, 1977.

[Bau 92] Baumann, W., Nay, Z., Maiti, A.K., Reis, ., Rodrigues, S.V., Detzer,N., in: Dynamics and Mechanisms of Photoinduced Transfer and Related Phenomena, Eds. Mataga, N., Okada, T., Masuhara, H., Elsevier Science Publishers B.V., pp 211-229, 1992.

[Berg] Bergmann Schaefer, Lehrbuch der Experimentalphysik, Optik, Walter de Gruyter, Berlin 1993.

[Berg 94] Berg, M., Chem. Phys. Lett. 228, 317, 1994.

[Bern 73] Bernstein, J., Spectrochim. Acta 29A, 147, 1973.

[Bing 95] Bingemann, D., Ernsting, N.P., J. Chem. Phys. 102, 2691, 1995.

[Bing] Bingemann, D., Dissertation, Göttingen 1994.

[Blanch 91] Blanchard, G.J., J. Chem. Phys. 95, 6317-6324, 1991.

[Bor 84] Bor, Z., Rácz, B., Opt. Commun. 54, 165-170, 1984.

[Braun] Braun, D. Dissertation, Berlin 1995 and citations therein.

[Bult] Bultmann, T., Dissertation, Göttingen 1994.

[Cal 83] Calef, D.F., Wolynes, P.G., J. Phys. Chem. 87, 3387, 1983.

[Cast 87] Castner, E.W., Maroncelli, M., Fleming, G.R., J. Chem. Phys. 86, 1090-1097, 1987.

[Cheng 91] Cheng, L.-P., Tam, W., Stevenson, S.H., Meredith, G.R., Rikken, G., Marder, S.R., J. Phys. Chem. 95, 10631-10643, 1991.

[Cho 92] Cho, M., Rosenthal, S.J., Scherer, N.F., Ziegler, L.D., Fleming, G.R., J. Chem. Phys. 96, 5033-5038, 1992.

[Cho 96] Cho, M., J. Chem. Phys. 105, 10755-10765, 1996.

[Choi 97] Choi, C.H., Kertesz, M., J. Phys. Chem. A 101, 3823-3831, 1997.

[Colt 90] Colthup, N.B., Daly, L.H., Wiberley, S.E.: Introduction to IR and Raman Spectroscopy, Academic Press, 3rd edition, San Diego 1990.

[Cruz 88] Cruz, C.H., Becker, P.C., Fork, R.L., Shank, C.V., Opt. Lett 13, 123, 1988.

[DeLong 94] DeLong, K.W., Fittinghoff, D.N., Trebino, R., Sullivan, A., Hunter, J., White, W.E., Kane, D.J., in : Ultrafast Phenomena IX, Springer Series in Chem. Physics, Vol. 60, 127-131, Springer, Heidelberg 1994.

[Du 93] Du, M., Fleming, G.R., Biophys. Chem. 48, 101-111, 1993.

[East 93] Easter, D.C., Baronavski, A.P., Chem. Phys. Lett. 201, 153-158, 1993.

[Ehr 97] Ehrlich, J.E., Wu, X.L., Lee, L.-Y.S., Hu, Z.-Y., Röckel, H., Marder, S.R., Perry, J.W., Opt. Lett. 22, 1843-1845, 1997.

[Eil 96] Eilers-König, N., Kühne, T., Schwarzer, D., Vöhringer, P., Schroder, J., Chem. Phys. Lett. 253, 69-76, 1996.

[Eil 98] Eilers-König, N., Kovalenko, S., Ernsting, N.P., in: Ultrafast Phenomena XI, Springer Series in Chem. Physics, Vol. 63, 547-549, Springer, Heidelberg 1998.

[Els 91] Elsaesser, T., Kaiser, W., Ann. Rev. Phys. Chem. 42, 83, 1991.

[Eng 99] Engleitner, S., Seel, M., Zinth, W., J. Phys. Chem. A 103, 3013-3019, 1999.

[Ernst] Ernsting, N.P., Habilitation, Göttingen 1990.

[Farz 99] Farztdinov, V.M., private communication, Berlin 1999.

[Flem 96] Fleming, G.R., Cho, M., Ann. Rev. Phys. Chem. 47, 109-134, 1996.

[Fons 94] Fonseca, T., Kim, H.Y., Hynes, J.T., J. Mol. Liquids 60, 161-200, 1994.

[Fork 84] Fork, R.L., Martinez, O.E., Gordon, J.P., Opt. Lett. 9, 150-152, 1984.

[Four 93] Fourkas, J.T., Berg, M., J. Chem. Phys. 98, 7773, 1993.

[Frau 85] Frauenfelder,H., Wolynes, P.G., Science 229, 337-345, 1985, and citations therein.

[Fuchs 96] Fuchs, C., Schreiber, M., J. Chem. Phys. 105, 1023-1028, 1996.

[Gai 97] Gai, F., McDonald, J.C., Anfinrud, P.A., J. Am. Chem. Soc. 119, 6201-6202, 1997.

[Gard 95] Gardecki, J., Horng, M.L., Papazyan, A., Maroncelli, M., J. Mol. Liquids 65/66, 49-57, 1995.

[Ged 97] Gedeck, P., Schneider, S., J. Photochem. Photobiol. A: Chem. 105, 165-181, 1997.

[Gil 91] Gilabert, E., Lapouyade, R., Rullière, C., Chem. Phys. Lett. 185, 82-87, 1991.

[Gold 94] Goldberg, S.Y., Bart, E., Meltsin, A., Fainberg, B.D., Huppert, D., Chem. Phys.183, 217-233, 1994.

[Görn 78] Görner, H., Schulte-Frohlinde, D., J. Photochem. 8, 91-102, 1978.

[Görn 87] Görner, H., J. Photochem. Photobiol. A 40, 325, 1987.

[Görn 95] Görner, H., Kuhn, H.J., in : Advances in Photochem., Vol. 19, 1-117, John Wiley & Sons, New York 1995, and citations therein.

[Grab 79] Grabowski, Z.R., Rotkiewicz, K., Siemiarczuk, A., Cowley, D.J., Baumann, W., Nouv. J. Chim. 3, 443, 1979 and Lipinski, J., Chojnacki, H., Grabowski, Z.R., Rotkiewicz, K., Chem. Phys. Lett. 70, 449, 1980.

[Grot 80] Grote, R.F., Hynes, J.T., J. Chem. Phys. 73, 2715-2732, 1980.

[Gruen 83] Gruen, H., Görner, H., Z. Naturforsch. 38a, 928-936, 1983.

[Gruen 89] Gruen, H., Görner, H., J. Phys. Chem. 93, 7144-7152, 1989.

[Güst 68] Güsten, H., Klasinc, L., Tetrahedron 24, 5499, 1968.

[Gust 95] Gustavsson, T., Baldacchino, G., Miaolocq, J.-C., Pommeret, S., Chem. Phys. Lett. 236, 587-594, 1995.

[Ham 92] Hamaguchi, H., in : Time-resolved Vibrational Spectroscopy V, Ed. Takahashi, H., Springer Proceedings in Physics, Vol. 68, pp 206-208, Springer, Heidelberg, 1992.

[Harr 90] Harris, C.B., Smith, D.E., Russell, D.J., Chem. Rev. 90, 481, 1990.

[Hasch 95] Hasche, T., Ashworth, S.H., Riedle, E., Woerner, M, Elsaesser, T., Chem. Phys. Lett. 244, 164-170, 1995.

[Heit 93] Heitele, H., Angw. Chem. Int. Ed. Engl. 32, 359-377, 1993.

[Horng 95] Horng, M.L., Gardecki, J.A., Papazyan, A., Maroncelli, M., J. Phys. Chem. 99, 17311-17337, 1995.

[Hub 84] Hub, W., Schneider, S., Dörr, F., Oxman, J.D., Lewis, F.D., J. Am. Chem. Soc. 106, 708, 1984.

[Hüb 91] Hübner, H.-J., Wörner,M., Kaiser, W., Chem. Phys. Lett. 182, 315-320, 1991.

[Hynes 86] Hynes, J.T., J. Phys. Chem. 90, 3701-3706, 1986, and citations therein.

[Il'ich 96] Il'ichev Y.V., Kühnle, W., Zachariasse, K.A., Chem. Phys. 211, 441-453, 1996.

[Jort 88] Jortner, J., Bixon, M., J. Chem. Phys. 88, 167, 1988.

[Jung 68] Jungmann, H., Güsten, H., Schulte-Frohlinde, D., Chem. Ber. 101, 2690, 1968.

[Kang 90] Kang, T.J., Jarzeba, W., Barbara, P.F., Fonseca, T., Chemical Physics 149, 8195, 1990.

[Kaws 77] Kawski, A., Gryczynski, I., Jung, C., Heckner, K.-H., Z. Naturforsch.32a, 420-425, 1977.

[Kim 97] Kim, H..J., Hynes, J.T., J. Photochem. Photobiol. A: Chem. 105, 337-343, 1997.

[Kov 96] Kovalenko, S.A., Ernsting, N.P., Ruthmann, J., Chem. Phys. Lett. 258, 445-454, 1996.

[Kov 97] Kovalenko, S.A., Ernsting, N.P., Ruthmann, J., J. Chem. Phys. 106, 3504-3511, 1997.

[Kov 98] Kovalenko, S.A., Ruthmann, J., Ernsting, N.P., J. Chem. Phys. 109, 1894-1900, 1998.

[Kov 99a] Kovalenko, S.A., Dobryakov, A.L., Ruthmann, J., Ernsting, N.P., Phys. Rev. A 59, 2369-2384, 1999.

[Kov 99b] Kovalenko, S.A., Senyushkina, T.A., Farztdinov, V.M., Ruthmann, J., Ernsting, N.P., to be published.

[Kram 40] Kramers, H.A., Physica 7, 284, 1940.

[Krueg 98] Krueger, B.P., Scholes, G.D., Gould, I.R., Fleming, G.R., in: Ultrafast Phenomena XI, Springer Series in Chem. Physics, Vol. 63, 666-668, Springer, Heidelberg 1998.

[Kühn 96] Kühn, O., Renger, T., May, V., Chem. Phys. 204, 99, 1996.

[Lad 95] Ladanyi, B.M., Stratt, R.M., J. Phys. Chem. 99, 2502, 1995.

[Lad 96a] Ladanyi, B.M., Stratt, R.M., J. Phys. Chem. 100, 1266, 1996.

[Lad 96b] Ladanyi, B.M., Klein, S., J. Chem. Phys. 105, 1552-1561, 1996.

[Laerm 89] Laermer, F., Elsaesser, T., Kaiser, W., Chem. Phys. Lett. 156, 381-386, 1989.

[Lambda] Brackmann, U. : Laser Dyes, Lambda Physik GmbH, 2nd ed., Göttingen 1994.

[Lap 92] Lapouyade, R., Czeschka, K., Majenz, W., Rettig, W., Gilabert, E., Rullière, C., J. Phys. Chem. 96, 9643-9650, 1992.

[Lars 97] Larsen, R.E., David, E.F., Goodyear, G., Stratt, R.M., J. Chem. Phys. 107, 524-543, 1997.

[Laur] Laurent, T., Diploma thesis, Berlin, 1995.

[Les 84] Lesiecki, M., Asmar, F., Drake, J.M., Camaioni, D.M., J. Luminesc. 31&32, 546-548, 1984.

[Less 76] Lessing, H.E., von Jena, A., Chem. Phys. Lett. 42, 213, 1976.

[Letok] Letokhov, V.S. : Laser Photoionization Spectroscopy, Ac. Press, Orlando/Florida 1987.

[Lin 91] Lin-Vien, D., Colthup, N.B., Fateley, W.G., Graselli, J.G.: The Handbook of IR and Raman Characteristic Frequencies of Organic Molecules, Academic Press, San Diego 1991.

[Lip 63] Liptay, W., Z. Naturforsch. 18a, 705, 1963.

[Lip 66] Liptay, W., Z. Naturforsch. 21a, 1605-1618, 1966.

[Lip 68] Liptay, W., Schlosser, H.-J., Dumbacher, B., Hünig, S., Z. Naturforsch. 23a, 1613-1625, 1968.

[Lipp 57] Lippert, E. Z. Elektrochem. 61, 962-975, 1957.

[Lipp 87] Lippert, E., Rettig, W., Bonacic-Koutecky, V., Heisel, F., Miehe, A., Adv. Chem. Phys. 68, 1, 1987.

[Loch 99] Lochschmidt, A., Eilers-König, N., Heineking, N., Ernsting, N.P., J. Phys. Chem. A 103, 1776-1784, 1999.

[Loch] Lochschmidt, A., Dissertation, Berlin 1998.

[Lor 87] Loring, R.F., Yan, Y.J., Mukamel, S., J. Chem. Phys. 87, 5840-5857, 1987.

[Ma 95] Ma, J., Vanden Bout, D., Berg, M., J. Mol. Liquids 65/66, 301-304, 1995.

[Mar 87] Maroncelli, M., Fleming, G.R., J. Chem. Phys. 86, 6221, 1987.

[Mar 89] Maroncelli, M., MacInnis, J., Fleming, G., Science 243, 1674-1681, 1989.

[Mar 94] Maroncelli, M., Kumar, P.V., Papazyan, A., Horng, M.L., Rosenthal, S.J., Fleming, G.R., in : Ultrafast Dynamics and Solvent effects, Eds. Gauduel, Y.,

Rossky, P.J., Am. Inst. of Physics, New York, 1994, pp 310-333.

[Marc 85] Marcus, R.A., Sutin, N., Biochim. Biophys. Acta 811, 265, 1985.

[Marg 92] Marguet, S., Mialocq, J.C., Millie, P., Berthier, G., Momicchioli, F., Chem. Phys. 160, 265-279, 1992.

[Mart 84] Martinez, O.E., Fork, R.L., Gordon, J.P., Opt. Lett. 9, 156-158, 1984.

[Mart 95] Martin, M.M., Plaza, P., Meyer, Y.H., Chemical Physics 192, 367-377, 1995.

[Mart 97] Martin, M.M., Plaza, P., Changenet, P., Meyer, Y.H., J. Photochem. Photobiol. A: Chem. 105, 197-204, 1997.

[Mas 97] Masuda, A., Masuda, Y., Fukuda, Y., J. Phys. Chem. A 101, 2245-2253, 1997.

[Mat 95] Matousek, P., Parker, A.W., Toner, W.T., Towrie, M., de Faria, D.L.A., Hester, R.E., Moore, J.N., Chem. Phys. Lett. 237, 373-379, 1995.

[Mat 97] Matyushov, D.V., Ladanyi, B., J. Chem. Phys. 107, 1375-1387, 1997.

[McRae 57] McRae, E.G., J. Phys. Chem. 61, 562, 1957.

[Mey 87] Meyer, M., Mialocq, J.C., Opt. Commun. 64, 264-268, 1987.

[Mey 88] Meyer, M., Mialocq, J.C., Rougée, M., Chem. Phys. Lett. 150, 484-490, 1988.

[Mey 90] Meyer, M., Mialocq, J.-C., Perly, B., J. Phys. Chem. 94, 98-104, 1990.

[Mial 93] Mialocq, J.C., Armand, X., Marguet, S., J. Photochem. Photobiol. A Chem. 69, 351-356, 1993.

[Mindl 83] Mindl, T., Hefferle, P., Schneider, S., Dörr, F., Appl. Phys. B 31, 201-207, 1983, and references therein.

[Mok 89] Mokthari, A., Chesnoy, J., Lauberau, A., Chem. Phys. Lett. 155, 593, 1989.

[Mon 57] Montroll, E.W., Shuler, K.E:, J. Chem. Phys. 26, 454-465, 1957.

[Moy 96] Moylan, C.R., Ermer, S., Lovejoy, S.M., McComb, I.H., Leung, D.S., Wortmann, R., Krdmer, P., Twieg, R.J., J. Am. Chem. Soc. 118, 12950-12955, 1996.

[Mühl 99a] Mühlpfordt, A., Schanz, R., Ernsting, N.P., Farztdinov, V.M., Grimme, S., Phys. Chem. Chem. Phys. 1, 3209-3218, 1999.

[Mühl 99b] Mühlpfordt, A., Eilers-König, N., unpublished results.

[Mye 87] Myers, A.B., Mathies, R.A., in: Biological Applications of Raman Spectroscopy, Vol. 2, pp. 1-58, John Wiley & Sons, New York 1987.

[Nad 87] Nadler, W., Marcus, R.A., J. Chem. Phys. 86, 3906, 1987.

[Nak 98] Nakabayashi, T., Okamoto, H., Tasumi, M., J. Phys. Chem. A 102, 9686-9695, 1998.

[Ons 36] Onsager, L., J. Am. Chem. Soc. 58, 1486, 1936.

[Pel 94] Pélikan, P., Ceppan, M., Liska, M. : Applications of Numerical Methods in Molecular Spectroscopy, Ed. Brown, S., CRC Press, Boca Raton / Florida 1994.

[Penz 93] Penzkofer, A., Beidoun, A., Lehmeier, H.-J., Opt. and Quant. Electron. 25, 317-349, 1993.

[Per 95] Pérez, V., González-Lafont, A., Lluch, J.M., Bertrán, J., J. Chem. Soc. Faraday Trans. 91, 1451-1455, 1995, and citations therein.

[Pol 94] Polimeno, A., Barbon, A., Nordio, P.L., Rettig, W., J. Phys. Chem. 98, 12158-12168, 1994.

[Pöll 92] Pöllinger, F., Heitele, H., Michel-Beyerle, M.E., Anders, C., Futscher, M., Staab, H.A., Chem. Phys. Lett. 198, 645-652, 1992.

[Press 92] Press, W.H., Teukolsky, S.A., Vetterling, W.T., Flannery, B.P., in: Numerical recipes, Cambridge University Press, Cambridge 1992.

[Qian 93] Qian, J., Schultz, S.L., Bradburn, G.R., Jean, J.M., J. Phys. Chem. 97, 10638-10644, 1993, and references therein.

[Qian 95] Qian, J., Schultz, S.L., Jean, J.M., Chem. Phys. Lett. 233, 9-15, 1995.

[Rain 94] Raineri, F.O., Friedman, H.L., J. Chem. Phys. 101, 6111, 1994.

[Ras 93] Rasaiah, J.C., Zhu, J., J. Chem. Phys. 98, 1213-1227, 1993.

[Ras 94] Rasaiah, J.C., Zhu, J., in: Ultrafast Dynamics and Solvent effects, Eds. Gauduel, Y., Rossky, P.J., Am. Inst. of Physics, New York, 1994, pp 421-434.

[Recht 96] Rechthaler, K., Köhler, G., Chem. Phys. Lett., 250, 152-158, 1996.

[Reid 94] Reid, P.J., Alex, S., Jarzeba, W., Schlief, R.E., Johnson, A.E., Barbara, P.F., Chem. Phys. Lett. 229, 93-100, 1994.

[Rett 86] Rettig, W., Angew. Chem. Int. Ed. Engl. 25, 971-988, 1986.

[Rett 89] Rettig, W., Majenz, W., Chem. Phys. Lett. 154, 335-341, 1989.

[Rett 92] Rettig, W., in : Dynamics and Mechanisms of Photoinduced Transfer and Related Phenomena, Elsevier, B.V., 1992.

[Rett 94] Rettig, W., Gilabert, E., Rullière, C., Chem. Phys. Lett. 229, 127-133, 1994.

[Rips 87] Rips, I., Jortner, J., J. Chem. Phys. 87, 2090-2104, 1987.

[Ros 91] Rosenthal, S.J., Xie, X., Du, M., Fleming, G.R., J. Chem. Phys. 95, 4715-4718, 1991.

[Ros 94] Rosenthal, S.J., Jimenez, R., Fleming, G.R., J. Mol. Liquids 60, 25-56, 1994.

[Ruth 98] Ruthmann, J., Kovalenko, S.A., Ernsting, N.P., Ouw, D., J. Chem. Phys. 109, 5466-5468, 1998.

[Ruth] Ruthmann, J., Dissertation, Göttingen, 1998, and citations therein.

[Sala 80] Sala, K.L., Kenney-Wallace, G.A., Hall, IEEE J. Quant. Electron. QE-16 (9), 990-996, 1980.

[Salin 87] Salin, F. and Brun, A., J. Appl. Phys. 61 (10), 4736-4739, 1987.

[Salt 92] Saltiel, J., Waller, A.S., Sears, D.F., Jr., J. Photochem. Photobiol. A: Chem. 65, 29, 1992.

[Salt 93] Saltiel, J., Waller, A.S., Sears, D.F., Jr., Garrett, C.Z., J. Phys. Chem. 97, 2516, 1993.

[Schent 91] Schenter, G.K., Duke, C.B., Chem. Phys. Lett. 176, 563-570, 1991.

[Schol 98] Scholes, G.D., Yu, J.-Y., Nagasawa, Y., Gould, I.R., Fleming, G.R., in: Ultrafast Phenomena XI, Springer Series in Chem. Physics, Vol. 63, 658-662, Springer, Heidelberg 1998.

[Schub] Schubert, M., Wilhelmi, B., : Nonlinear Optics and Quantum Electronics, J. Wiley & Sons, New York, 1986.

[Schultz 97] Schultz, S.L., Qian, J., Jean, J.M., J. Phys. Chem. A 101, 1000-1006, 1997.

[Schwarz 96] Schwarzer, D., Troe, J., Votsmeier, M., Zerezke, M., J. Chem. Phys. 105, 3121-3131, 1996.

[Sens 93] Sension, R.J., Repinec, S.T., Szarka, A.Z., Hochstrasser, R.M., J. Chem. Phys. 98, 6291, 1993.

[Shank 82] Shank, C.V., Yen, R., Fork, R.L., Orenstein, J., Baker, G.L., Phys. Rev. Lett. 49, 1660, 1982.

[Shelby 79] Shelby, R.M., Harris, C.B., Cornelius, P.A., J. Chem. Phys 70, 34, 1979.

[Shen 84] Shen, Y.R., The Principles of Nonlinear Optics, John Wiley and Sons, NY 1984.

[Shor 58] Shorygin, P.P., Ivanova, T.M., Sov. Phys. Dokl. 3, 764, 1958.

[Sian 69] Siano, D.B., Metzler, D.E., J. Chem. Phys. 51, 1856-1861, 1969.

[Sieg] Siegman, A.E., Lasers, University Science Books, Mill Valley (California) 1986.

[Sim 91] Simon, P., Szatmari, S., Schäfer, F.P., Opt. Lett. 16, 1569-1571, 1991.

[Smith 99] Smith, N.A., Meech, S.R., Rubtsov, I.V., Yoshihara, K., Chem. Phys. Lett. 303, 209-217, 1999.

[Sob 96] Sobolewski, A.L., Domcke, W., Chem. Phys. Lett. 250, 428-436, 1996.

[Stratt 94] Stratt, R.M., Cho, M., J. Chem. Phys 100, 6700, 1994.

[Strick 62] Strickler, S.J., Berg, R.A., J. Chem. Phys. 37, 814-822, 1962.

[Su 88] Su, S.-G., Simon, J.D., J. Chem. Phys. 89, 908, 1988.

[Suk 90] Sukowski, U., Seilmeier, A., Elsaesser, T., Fischer, S.F., J. Chem. Phys. 93, 4094-4101, 1990.

[Sum 86] Sumi, H., Marcus, R.A., J. Chem. Phys. 84, 4894-4914, 1986.

[Szabo 88] Szabó, G., Bor, Z., Müller, A., Opt. Lett. 13 (9), 746-748, 1988.

[Szip 94] Szipöcs, R., Ferencz, K., Spielmann, C., Krausz, F., Opt. Lett. 19, 201-203, 1994.

[Tayl 84] Taylor, A.J., Erskine, D.J., Tang, C.L., Chem. Phys. Lett. 103, 430-435, 1984.

[Tok 94] Tokmakoff, A., Sauter, B., Fayer, M.D., J. Chem. Phys. 100, 9035-9043, 1994.

[Tom 91] Tominaga, K., Walker, G.C., Jarzeba, W., Barbara, P.F., J. Phys. Chem. 95, 10475-10485, 1991, and Tominaga, K., Walker, G.C., Kang, T.J., Barbara, P.F., Fonseca, T., ibid, 10485-10492.

[Treacy 69] Treacy, E.D., IEEE J. Quant. Electron. QE-5, 454-458, 1969.

[Vald 86] Valdmanis, J.A., Fork, R.L., IEEE J. Quant. Electr. QE-22, 112, 1968.

[Vald 86] Valdmanis, J.A., Fork, R.L., IEEE J. Quant. Electron. QE-22, 112, 1986.

[vdMeul 96] van der Meulen, P., Zhang, H., Jonkman, A.M., Glasbeek, M., J. Phys. Chem. 100, 5367-5373, 1996.

[vdMeul 98] van der Meulen, P., Jonkman, A.M., Glasbeek, M., J. Phys. Chem. A 102, 1906-1911, 1998.

[vdZwan 85] Van der Zwan, g., Hynes, J.T., J. Phys. Chem. 89, 4181-4188, 1985.

[Walk 92] Walker, G.C., Akesson, E., Johnson, A.E., Levinger, N.E., Barbara, P.F., J. Phys. Chem. 96, 3728-3736, 1992.

[Wang 89] Wang, Q.Z., Ho, P.P., Alfano, R.R., in: The Supercontinuum Laser Source, Ed. Alfano, R.R., Springer, New York 1989.

[Wang 97] Wang, C., Akhremitchev, B., Walker, G.C., J. Phys. Chem. A 101, 2735-2738, 1997.

[Whit 92] Whitnell, R.M., Wilson, K.R., Hynes, J.T., J. Chem. Phys. 96, 5354-5369, 1992.

[Witt 96] Wittmann, M., Penzkofer, A., Opt. Commun. 126, 308-317, 1996.

[Wolf 98] Wolfseder, B., Seidner, L., Domcke, W., Stock, G., Seel, M., Engleitner, S.,

Zinth, W., Chem. Phys. 233, 323-334, 1998.

[Yam 97] Yamaguchi, T., Kimura, Y., Hirota, N., J. Phys. Chem. A 101, 9050-9060, 1997.

[Yang 95] Yang, T.-S., Vöhringer, P., Arnett, D.C., Scherer, N.F., J. Chem. Phys. 103, 8346-8359, 1995.

[Yang 99] Yang, T.-S., Chang, M.-S., Chang, R., Hayashi, M., Lin, S.H., Vöhringer, P., Dietz, W., Scherer, N.F., J. Chem. Phys. 110, 12070-12081, 1999.

[Yosh 95] Yoshihara, K., Tominaga, K., Nagasawa, Y., Bull. Chem. Soc. Jpn. 68, 696-712, 1995.

[Young] Young, M. : Optics and Lasers (including Fibers and Optical Waveguides), 4th rev. Ed., Springer, Heidelberg 1992.

[Zach 93] Zachariasse, K.A., von der Haar, T., Hebecker, A., Leinhos, U., Kühnle, W., Pure Appl. Chem. 65, 1745, 1993.

[Zhong 96] Zhong, Q., Wang, Z., Sun, Y., Zhu, Q., Kong, F., Chem. Phys. Lett. 248, 277-282, 1996.

[Zhu 92] Zhu, J., Rasaiah, J.C., J. Chem.Phys. 96, 1435-1443, 1992.

[Zong 97] Zong, Y., McHale, J.L., J. Chem. Phys. 106, 4963-4972, 1997.

[Zus 80] Zusman, L.D., Chem. Phys. 49, 295, 1980.

Annex

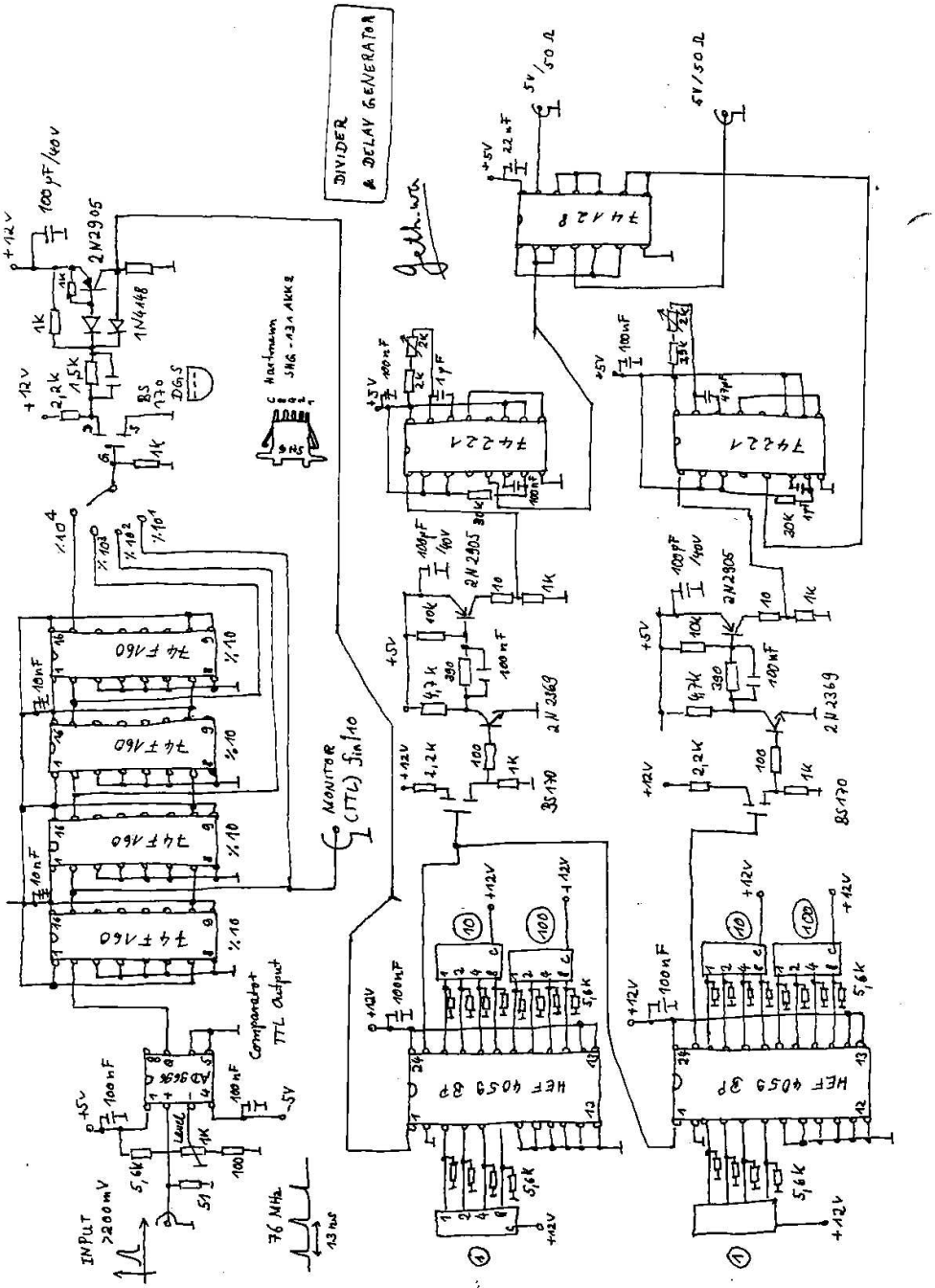

Figure A-1: Frequency divider and delay generator.

Danksagung

Prof. N.P. Ernsting danke ich für die großzügige Förderung dieser Arbeit und für die Gewährung der wissenschaftlichen Freiheit, die ein selbstständiges wissenschaftliches Arbeiten erst ermöglicht.

Bei Herrn J. Jethwa vom Max-Planck-Institut für biophysikalische Chemie in Göttingen möchte ich mich herzlich für die gute Zusammenarbeit beim Design der Elektronik für die Lasersynchronisation bedanken. Ohne seine große Erfahrung wäre auch die Behebung kleinerer Probleme und Fehler sehr viel mühseliger geraten.

Für die Überlassung der Pump-Probe Messungen am DCM in Lösung danke ich Dr. S. Kovalenko ebenso wie für interessante und lehrreiche Gespräche über die Kontinuumserzeugung und optische Breitbandspektroskopie. Dr. J. Ruthmann danke ich für seine hervorragende Vorarbeit zum DCM und LDS-750 und für die Möglichkeit, seinen reichhaltigen Fundus an MATLAB-Programmen zu nutzen.

Dr. K.-W. Brzezinka und Dr. K. Witke von der BAM haben die die Raman-spektroskopischen Untersuchungen durchgeführt und mir auch bei der Zuordnung der Peaks zur Seite gestanden.

Weiterhin möchte ich mich bei allen Kollegen, Kolleginnen und Freunden bedanken, ohne deren tatkräftige Unterstützung und Aufmunterung diese Arbeit nie zustande gekommen wäre, insbesondere bei Dr. Annette Mühlpfordt, Heiderose Steingräber und Beate Kießling.

Lebenslauf

Am 13.12.1968 wurde ich, Nina Christine Iris Eilers-König, als Kind von Dr. Christel Eilers-König, geb. König, und Hans Georg Eilers in Bielefeld geboren. Von September 1976 bis Dezember 1978 besuchte ich die Grundschule in Bonn-Buschdorf, anschließend bis Juli 1979 die Grundschule in Troisdorf. Das Gymnasium Zum Altenforst, Troisdorf, verließ ich im Juni 1987 mit dem Abitur. Im Herbst 1988 begann ich das Physikstudium an der Georg-August-Universität in Göttingen, wo ich im Oktober 1990 das Vordiplom ablegte. In meiner Diplomarbeit untersuchte ich im Arbeitskreis von Dr. D. Schwarzer unter der Leitung von Prof. J. Troe in der Abteilung Spektroskopie des Max-Planck-Institutes für biophysikalische Chemie die Reaktions- und Solvatationsdynamik von 4-Dimethylamino-4'-Cyano-Stilben in Alkoholen mittels zeitaufgelöster Pump-Probe-Spektroskopie. Im Oktober 1994 schloß ich das Physikstudium mit der Diplomprüfung ab. Nach einer Tätigkeit als wissenschaftliche Mitarbeiterin in den Abteilungen Spektroskopie und Laserphysik des Max-Planck-Institutes für biophysikalische Chemie wechselte ich im Oktober 1995 in den Arbeitskreis von Prof. N.P. Ernsting an die Humboldt-Universität zu Berlin. Dort beschäftigte ich mich zunächst mit dem Einfluß der Lösungsmittelumgebung auf die geminale Rekombination photodissoziierter organischer Disulfide. Seit Herbst 1997 untersuchte ich die schnelle Reaktionsdynamik von Styrylfarbstoffen in Flüssigkeiten im elektronischen Grund- und angeregten Zustand. Daraus enstand die vorliegende Arbeit.